

# SNE SIMULATION NOTES EUROPE

Modelling and Simulation in Physiology



SNE Special Issue

Volume 23 No.2 August 2013

doi: 10.11128/sne.23.2.1018



Journal on Developments and  
Trends in Modelling and Simulation

Membership Journal for Simulation  
Societies and Groups in EUROSIM

Print ISSN 2305-9974  
Online ISSN 2306-0271



## SNE Editorial Board

SNE - Simulation Notes Europe is advised and supervised by an international scientific editorial board. This board is taking care on peer reviewing and handling of *Technical Notes*, *Education Notes*, *Short Notes*, *Software Notes*, *Overview Notes*, and of *Benchmark Notes* (definitions and solutions). At present, the board is increasing:

- David Al-Dabass, [david.al-dabass@ntu.ac.uk](mailto:david.al-dabass@ntu.ac.uk)  
Nottingham Trent University, UK
- Felix Breitenecker, [Felix.Breitenecker@tuwien.ac.at](mailto:Felix.Breitenecker@tuwien.ac.at)  
Vienna Univ. of Technology, Austria, Editor-in-chief
- Maja Atanasijevic-Kunc, [maja.atanasijevic@fe.uni-lj.si](mailto:maja.atanasijevic@fe.uni-lj.si)  
Univ. of Ljubljana, Lab. Modelling & Control, Slovenia
- Aleš Belič, [ales.belic@sandoz.com](mailto:ales.belic@sandoz.com)  
*Sandoz / National Inst. f. Chemistry, Slovenia*
- Peter Breedveld, [P.C.Breedveld@el.utwente.nl](mailto:P.C.Breedveld@el.utwente.nl)  
University of Twente, Netherlands
- Agostino Bruzzone, [agostino@itim.unige.it](mailto:agostino@itim.unige.it)  
Università degli Studi di Genova, Italy
- Francois Cellier, [fcellier@inf.ethz.ch](mailto:fcellier@inf.ethz.ch)  
ETH Zurich, Switzerland
- Vlatko Čerić, [vceric@efzg.hr](mailto:vceric@efzg.hr)  
Univ. Zagreb, Croatia
- Russell Cheng, [rhc@maths.soton.ac.uk](mailto:rhc@maths.soton.ac.uk)  
University of Southampton, UK
- Eric Dahlquist, [erik.dahlquist@mdh.se](mailto:erik.dahlquist@mdh.se), Mälardalen Univ., Sweden
- Horst Ecker, [Horst.Ecker@tuwien.ac.at](mailto:Horst.Ecker@tuwien.ac.at)  
Vienna Univ. of Technology, Inst. f. Mechanics, Austria
- Vadim Engelson, [vadim.engelson@mathcore.com](mailto:vadim.engelson@mathcore.com)  
MathCore Engineering, Linköping, Sweden
- Edmond Hajrizi, [ehajrizi@ubt-uni.net](mailto:ehajrizi@ubt-uni.net)  
University for Business and Technology, Pristina, Kosovo
- András Jávör, [javor@eik.bme.hu](mailto:javor@eik.bme.hu),  
Budapest Univ. of Technology and Economics, Hungary
- Esko Juuso, [esko.juuso@oulu.fi](mailto:esko.juuso@oulu.fi)  
Univ. Oulu, Dept. Process/Environmental Eng., Finland
- Kaj Juslin, [kaj.juslin@vtt.fi](mailto:kaj.juslin@vtt.fi)  
VTT Technical Research Centre of Finland, Finland
- Francesco Longo, [f.longo@unical.it](mailto:f.longo@unical.it)  
Univ. of Calabria, Mechanical Department, Italy
- Yuri Merkuryev, [merkur@iit.rtu.lv](mailto:merkur@iit.rtu.lv), Riga Technical Univ.
- David Murray-Smith, [d.murray-smith@elec.gla.ac.uk](mailto:d.murray-smith@elec.gla.ac.uk)  
University of Glasgow, Fac. Electrical Engineering, UK
- Gasper Music, [gasper.music@fe.uni-lj.si](mailto:gasper.music@fe.uni-lj.si)  
Univ. of Ljubljana, Fac. Electrical Engineering, Slovenia
- Thorsten Pawletta, [pawel@mb.hs-wismar.de](mailto:pawel@mb.hs-wismar.de)  
Univ. Wismar, Dept. Computational Engineering,  
Wismar, Germany
- Niki Popper, [niki.popper@dwh.at](mailto:niki.popper@dwh.at)  
dwh Simulation Services, Vienna, Austria
- Thomas Schriber, [schriber@umich.edu](mailto:schriber@umich.edu)  
University of Michigan, Business School, USA
- Yuri Senichenkov, [sneyb@dcn.infos.ru](mailto:sneyb@dcn.infos.ru)  
St. Petersburg Technical University, Russia
- Sigrid Wenzel, [S.Wenzel@uni-kassel.de](mailto:S.Wenzel@uni-kassel.de)  
University Kassel, Inst. f. Production Technique, Germany

## Author's Info

Authors are invited to submit contributions which have not been published and have not been considered for publication elsewhere to the SNE Editorial Office. Furthermore, SNE invites organizers of EUROSIM conferences to provide post-conference publication for the authors of their conference (with peer review).

SNE distinguishes different types of contributions (*Notes*):

- *Overview Note* – State-of-the-Art report in a specific area, up to 14 pages, only upon invitation
- *Technical Note* – scientific publication on specific topic in modelling and simulation, 6 – 8 (10) pages
- *Education Note* – modelling and simulation in / for education and e-learning; max. 6 pages
- *Short Note* – recent development on specific topic, max. 4 p.
- *Software Note* – specific implementation with scientific analysis, max 4 pages
- *Benchmark Note* – Solution to an ARGEIM Benchmark; basic solution 2 pages, extended and commented solution 4 pages, comparative solutions 4-8 pages

Further info and templates (doc, tex) at SNE's website.

## SNE Contact & Info

→ [www.sne-journal.org](http://www.sne-journal.org)

✉ [office@sne-journal.org](mailto:office@sne-journal.org), [etc@sne-journal.org](mailto:etc@sne-journal.org)

✉ SNE Editorial Office, ARGESIM / dwh Simulation Services,  
Neustiftgasse 57-59, 1070 Vienna, Austria

### SNE SIMULATION NOTES EUROPE

ISSN SNE Print ISSN 2305-9974, SNE Online ISSN 2306-0271

WEB: → [www.sne-journal.org](http://www.sne-journal.org), DOI prefix 10.11128/sne

**Scope:** Technical Notes, Short Notes and Overview Notes on developments and trends in modelling and simulation in various areas and in application and theory; benchmarks and benchmark documentations of ARGESIM Benchmarks on modelling approaches and simulation implementations; modelling and simulation in and for education, simulation-based e-learning; society information and membership information for EUROSIM members (Federation of European Simulation Societies and Groups).

**Editor-in-Chief:** Felix Breitenecker, Vienna Univ. of Technology, Inst. f. Analysis and Scientific Computing, Div., Math. Modelling and Simulation, Wiedner Hauptstrasse 8-10, 1040 Vienna, Austria;  
✉ [Felix.Breitenecker@tuwien.ac.at](mailto:Felix.Breitenecker@tuwien.ac.at), ✉ [etc@sne-journal.org](mailto:etc@sne-journal.org)

**Layout / Administration:** J. Tanzler, F. Preyser, T. Wobruha;  
C. Wyrzens, R. Leskovar et al.; Math. Modelling and Simulation Group, Vienna Univ. of Technology, Wiedner Hauptstrasse 8-10, 1040 Vienna, ✉ [office@sne-journal.org](mailto:office@sne-journal.org)

**Print SNE:** Grafisches Zentrum, TU Vienna,  
Wiedner Hauptstrasse 8-10, 1040, Vienna, Austria

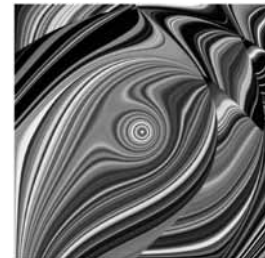
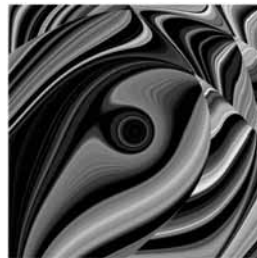
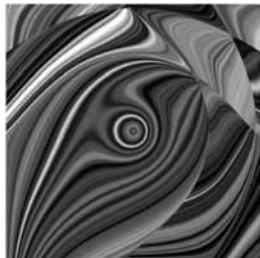
**Online SNE:** ARGESIM / ASIM, c.o. dwh Simulation Services,  
Neustiftgasse 57-59, 1070 Vienna, Austria

**Publisher:** ARGESIM ARBEITSGEMEINSCHAFT SIMULATION NEWS  
- WORKING COMMITTEE SIMULATION NEWS, Neustiftgasse 57-59,  
1070 Vienna, Austria; → [www.argesim.org](http://www.argesim.org), ✉ [info@argesim.org](mailto:info@argesim.org)  
on behalf of ASIM (→ [www.asim-gi.org](http://www.asim-gi.org) and EUROSIM  
→ [www.eurosim.info](http://www.eurosim.info))

© ARGESIM / EUROSIM / ASIM 2013

## Editorial

Dear Readers – Traditionally the second issue of each SNE Volume is a Special Issue – also in 2013 SNE continues this tradition, with a special issue on *Modeling and Simulation in Physiology*. – for details see the editorial of the guest editors. We are glad that for SNE Volume 23 Vlatko Cerić, past president of CROSSIM, is providing his algorithmic art as design for SNE cover page. The technique used for the picture series (covers pictures below? is alienation of ‘classic’ pictures by certain algorithms.



Special thanks to the guest editors of this special issue, to Maja Atanasijević-Kunc, Univ. Ljubljana, Faculty of Electrical Engineering, and to Xenia Descovich, AIT Austrian Institute of Technology and Manz Verlag, Vienna, Austria, for compiling this very interesting issue.

Felix Breitenecker, SNE Editor-in-Chief, [eic@sne-journal.org](mailto:eic@sne-journal.org); [felix.breitenecker@tuwien.ac.at](mailto:felix.breitenecker@tuwien.ac.at)

### Contents SNE 23(2)

Special Issue	SNE doi: 10.11128/sne.23.2.1018
<b>‘Modeling and Simulation in Physiology’</b>	
The Lattice Boltzmann Method and Multiscale Hemodynamics: Recent Advances and Perspectives. G. Pontrelli, I. Halliday, S. Melchionna, T. J. Spencer, S. Succi .....	59
Modelling Metabolic Pathways Involved in the Pathogenesis of Non-Alcoholic Fatty Liver Disease. A. Naik, A. Belic .....	71
Identification of the Long-Term Effects of Mild to Moderate Neonatal Cerebral Hypoxia Based on EEG Signals Analysis. A. Belic, M. Cukic, D. Neubauer, T. Bregant .....	77
Burdens of Obesity: Multi-Model Description. M. Atanasijević-Kunc, J. Drinovec, T. Sentočnik .....	85
Modeling Elastic Walls in Lattice Boltzmann Simulations of Arterial Blood Flow. X. Descovich, G. Pontrelli, S. Succi, S. Melchionna, M. Bammer .....	93
Simulating Aortic Blood Flow and Pressure by an Optimal Control Model. S. Parragh, B. Hametner, S. Wassertheurer ..	101
A Comparative Analysis of CA Model and ODE Model for SIR-type Epidemics. A. Gerstenmayer, F. Miksch .....	107
EUROSIM Societies Info & News .....	N1-N8

### Editorial SNE Special Issue

#### ‘Modelling and Simulation in Physiology’

Modelling and simulation have become established methodologies in explanation, analysis and prediction of systems operation and can therefore be met practically in all scientific disciplines, where medicine and other life sciences are no exceptions.

These ascertainments are proved by a huge number of excellent publications.

In spite of the fact that even in these areas the nature of problems can differ drastically, developed methodologies enable the usage of similar and systematically organised design techniques, where of course the cooperation with problem experts is of crucial importance.

This Special issue presents selected post publications of MATHMOD 2012, the 7th Vienna International Conference on Mathematical Modelling (Vienna, Austria, February 2012) and detailed observation proves that close cooperation of interdisciplinary teams can result in a very interesting and important observations which can help to promote both areas: medical research as well as modelling and simulation techniques.

The presented special issue comprises seven papers. In the first contribution (Giuseppe Pontrelli, Ian Halliday, Simone Melchionna, Timothy J. Spencer, Sauro Succi: The Lattice Boltzmann Method and Multiscale Hemodynamics - Recent Advances and Perspectives) the authors present recent advances and perspectives of the lattice Boltzmann method and multiscale hemodynamics. They point out the complexity of handling several concurrent actors when studying fluids of different types and at different scales and propose the lattice Boltzmann method as a powerful computational tool to combine the different aspects of blood flow simulation in a unified framework.

The next paper (Adviti Naik, Aleš Belič: Modelling Metabolic Pathways Involved in the Pathogenesis of Non-Alcoholic Fatty Liver Disease) addresses non-alcoholic fatty liver disease (NAFLD), a poorly understood complex disorder that occurs at a high frequency in Western populations with unhealthy dietary and life-

style habits. Authors are presenting a dynamic semi-quantitative model of the metabolic and signalling pathways which was generated using an object-oriented library of components based on differential equations. The model aims to identify novel mechanisms of NAFLD pathogenesis and regulatory components.

The third contribution (Aleš Belič, Milena Čukić, David Neubauer, Tina Bregant: Identification of the Long-Term Effects of Mild to Moderate Neonatal Cerebral Hypoxia Based on EEG Signals Analysis) is addressing hypoxic-ischemic encephalopathy (HIE) during perinatal period. It is the most common cause of neonatal seizures and is associated with an increased risk of epilepsy in later life. In the presented study EEG data are analysed with power spectra analysis of the principal components of the EEG signals, fractal dimension estimation and sample entropy estimation. Presented results indicate that the power density properties in the alpha frequency range correlate with learning difficulties of the patients.

In the fourth paper (Maja Atanasijević-Kunc, Jože Drinovec, Tina Sentočnik: Burdens of Obesity: Multi-Model Description) the modelling structure, which comprises and combines the results from different models, is proposed with which it is possible to evaluate the observed diseases' burdens important for certain country or population.

The fifth contribution (Xenia Descovich, Giuseppe Pontrelli, Sauro Succi, Simone Melchionna, Manfred Bammer : Modeling Elastic Walls in Lattice Boltzmann Simulations of Arterial Blood Flow) presents an accurate and computationally efficient approach for modelling elastic walls in lattice Boltzmann simulations of arterial blood flow. The described method acts strictly locally and can be used for simulations in two and three dimensions.

In the sixth contribution (Stephanie Parragh, Bernhard Hametner, Siegfried Wassertheurer: Simulating Aortic Blood Flow and Pressure by an Optimal Control Model) authors introduce an optimal control model for the simulation of aortic blood flow and pressure. The presented approach is a combination of the well-established three-element Windkessel model of the arterial system and an optimality criterion. Simulation results show the capability of the optimal control problem to generate pathophysiological flow and pressure patterns with meaningful parameter values and the potential for the simulation of blood flow based on pressure alone.

The last contribution (Anita Gerstenmayer, Florian Miksch: Simulation of an SIR-type epidemic with a cellular automaton and differential equations) proposes a solution to the comparison C17. Authors compare a classical SIR-type epidemic using two different modelling techniques, a continuous approach with ordinary

differential equations and a discrete Lattice Gas Cellular Automata.

The editors would like to express their sincere gratitude to all authors for their co-operation and efforts when preparing the revised versions of the papers and also to the ARGESIM SNE staff for helping to manage the administration work. We hope that the selected papers would contribute to further bridging and promoting similar interdisciplinary activities in the area of intriguing life sciences.

Xenia Descovich, AIT Austrian Inst. of Technology GmbH,  
and Manz Verlag, Vienna, Austria  
*xenia.descovich@tuwien.ac.at, xenia.descovich@wissenistmanz.at*  
Maja Atanasijević-Kunc, Univ. Ljubljana, Faculty of  
Electrical Engineering, Slovenia;  
*maja.atanasijevic@fe.uni-lj.si*

## SNE Reader's Info

Simulation Notes Europe publishes peer reviewed *Technical Notes*, *Short Notes* and *Overview Notes* on developments and trends in modelling and simulation in various areas and in application and theory, with main topics being simulation aspects and interdisciplinarity.

Individual submissions of scientific papers are welcome, as well as post-conference publications of contributions from conferences of EUROSIM societies.

Furthermore SNE documents the ARGESIM Benchmarks on *Modelling Approaches and Simulation Implementations* with publication of definitions, solutions and discussions (*Benchmark Notes*). Special *Educational Notes* present the use of modelling and simulation in and for education and for e-learning. SNE is the official membership journal of EUROSIM, the Federation of European Simulation Societies. A News Section in SNE provides information for EUROSIM Simulation Societies and Simulation Groups.

SNE is published in a printed version (Print ISSN 2305-9974) and in an online version (Online ISSN 2306-0271). With Online SNE the publisher ARGESIM follows the Open Access strategy, allowing download of published contributions for free. Since 2012 Online SNE contributions are identified by a DOI (Digital Object Identifier) assigned to the publisher ARGESIM (DOI prefix 10.11128). Print SNE, high-resolution Online SNE, full SNE Archive, and source codes of the *Benchmark Notes* are available for members of EUROSIM societies.

SNE Print ISSN 2305-9974, SNE Online ISSN 2306-0271  
SNE Issue 23(2) August 2013 doi: 10.11128/sne.23.2.1018  
→ [www.sne-journal.org](http://www.sne-journal.org)

✉ [office@sne-journal.org](mailto:office@sne-journal.org), [elic@sne-journal.org](mailto:elic@sne-journal.org)

✉ SNE Editorial Office, c/o ARGESIM / DWH,  
Neustiftgasse 57-59, 1070 Vienna, Austria

# The Lattice Boltzmann Method and Multiscale Hemodynamics: Recent Advances and Perspectives

Giuseppe Pontrelli<sup>1\*</sup>, Ian Halliday<sup>2</sup>, Simone Melchionna<sup>3</sup>,  
Timothy J. Spencer<sup>2</sup>, Sauro Succi<sup>1</sup>

<sup>1</sup>Istituto per le Applicazioni del Calcolo - CNR, Via dei Taurini 19, 00185 Roma, Italy; \*[giuseppe.pontrelli@gmail.com](mailto:giuseppe.pontrelli@gmail.com)

<sup>2</sup>MERI - Sheffield Hallam University, UK

<sup>3</sup>IPFC - CNR, Roma, Italy

Simulation Notes Europe SNE 23(2), 2013, 59 - 70  
DOI: 10.11128/sne.23.on.10181  
Received: Nov. 3, 2012 (Selected MATHMOD 2012 Postconf. Publ.); Revised Accepted: June 15, 2013;

**Abstract.** Large-scale simulations of blood flow allow for the optimal evaluation of endothelial shear stress for real-life case studies in cardiovascular pathologies. The procedure for anatomic data acquisition, geometry and mesh generation are particularly favorable if used in conjunction with the Lattice Boltzmann method and the underlying cartesian mesh. The methodology allows to accommodate red blood cells in order to take into account the corpuscular nature of blood in multi-scale scenarios and its complex rheological response, in particular, in proximity of the endothelium. Taken together, the Lattice Boltzmann framework has become a powerful computational tool for studying sections of the human circulatory system.

## Introduction

Mathematical models and numerical simulations of the cardiovascular system are one of the major challenges in applied sciences nowadays. The rapid development of computing power and the progress in numerical techniques for parallel computers have resulted in significant breakthroughs in vascular research and blood flow simulations constitute a rapidly growing field for the bioengineering and clinical communities. The study of blood in the macrovasculature, as much as in capillaries, has deep implications in understanding and prevention of the most common cardiovascular pathologies, with atherosclerosis being perhaps the best known example.

Atherosclerosis is responsible for ~ 35% of annual deaths in civilized countries and its development depends on the presence of systemic risk factors. The disease results from the accumulation of lipid molecules within the vessel walls, as well as from enhanced exposure to intramural penetration of nano-sized biological bodies [1]. The build up of the resultant soft tissue and the eventual changes in its consistency leads to serious atherosclerotic pathologies, including catastrophic events such as plaque rupture. Atherosclerotic plaques appear in regions of disturbed blood flow where the local wall shear stress (WSS) is low ( $< 1.0$  Pa) or of alternating direction [2]. Hence, plaques tend to form near arterial bifurcations where the flow is always altered compared to unbranched regions [3].

Atherosclerosis primarily affects the coronary arteries and the evidence that low average WSS has a key role in the disease localization and progression is widely accepted [4, 5, 6]. Predictions of where and how the illness is likely to develop can be obtained by fluid dynamics simulations as a routine methodology to study blood flow patterns in human arteries. As a matter of fact, the shape and the structure of endothelium plays a number of important roles in the vascular system and its dysfunction may lead to several pathological states, including early development of atherosclerosis [7]. The microscopic shape of the endothelium is defined by the presence of endothelial cells (EC's henceforth), making the arterial wall undulate. This effect becomes more pronounced in small-sized vessels, where the corrugation degree increases. The study of blood flow over a regularly undulating wall made of equally aligned and distributed EC's has been recently carried out in [8] where the variation of wall shear stress over the EC's

has been computed. Furthermore, the endothelium is coated by long-chained macromolecules and proteins which form a thin porous layer, called the glycocalyx [9]. The glycocalyx has a *brushlike* structure and a thickness which varies with the vessel diameter, but its average is 100 nm for arterioles. It has several roles: it serves as a transport barrier, to prevent ballistic red blood cell (RBC) interactions with the endothelium, and as a sensor and a transducer of mechanical forces, such as fluid shear stress, to the surface of EC's. Actually, it has been recognized that the glycocalyx responds to the flow environment and, in particular, to the fluid stress, but the mechanism by which these proteins sense the shearing forces and transduce mechanical into biochemical signals is still not fully understood [7].

The glycocalyx itself is remodeled by the shearing flow and by the compression exerted by the deformed erythrocytes in capillaries [10]. Flow induced mechanotransduction in EC's has been studied over the years with emphasis on correlation between disturbed flow and atherosclerosis. Recently, some mathematical modelling work has been carried out, using a porous medium to model the endothelial surface layer (ESL henceforth) [11, 12]. However, none of these works include the effect of the roughness, or wavy nature, of the wall, which should be incorporated for a more realistic description at the microscopic level. In the following sections we will present a coarse-grained model that attempts to include some of the basic physical microscale effects of the ESL attached to the EC's and hence, examine to what extent the wall shear stress may vary due to this layer in addition to the previously examined EC shape and particulate transport.

Simulations of blood flows based on the Lattice Boltzmann (LB) method provide a particularly efficient and exible framework in handling complex arterial geometries. In the past, the LB method has been applied to a broad range of fluid-dynamic problems, including turbulence and multiphase flows [13], as well as in blood flow simulations in steady and pulsatile regimes and with non-Newtonian flows through stenoses [14]. A direct benefit of the joint use of simulation and imaging techniques is to understand the connection between fluid-mechanical flow patterns and plaque formation and evolution, with important implications for predicting the course of atherosclerosis and possibly preventing or mitigating its effects, in particular by non-invasively and inexpensively screening large numbers of patients for incipient arterial disease, and to intervene

at clinical level prior to the occurrence of a catastrophic event. One option is to obtain the arterial wall shape, plaque morphology and lumen anatomy from the non-invasive Multi-Detector Computed Tomography (MDCT) imaging technique, as in the newest systems with 320-detector rows, a technology that enables 3D acquisition of the entire arterial tree in a single heart beat and high accuracy of nominal resolution of 0.1 mm [15].

The LB method is particularly suitable for handling such complex arterial geometries, since most of its simplicity stems from an underlying cartesian mesh over which fluid motion is represented. LB is based on moving information along straight-line trajectories, associated with the constant speed of fictitious molecules which characterize the state of the fluid at any instant and spatial location. This picture stands in sharp contrast with the fluid-dynamic representation, in which, by definition, information moves along the material lines defined by fluid velocity itself, usually a very complex space-time dependent vector field. This main asset has motivated the increasing use over the last decade of LB techniques for large-scale simulations of complex hemodynamic flows [16, 17, 18, 19].

The main aim of this paper is to show that the inclusion of crucial components such as RBC's, the corrugated wall and the glycocalyx, can be done within a single unified computational framework. This would allow us to reproduce blood rheology in complex flows and geometrical conditions, including the non-trivial interplay between erythrocytes and wall structure. The possibility of embedding suspended bodies in the surrounding plasma and the glycocalyx representation over an undulated endothelial wall addresses major steps forward to model blood from a bottom-up perspective, in order to avoid unnecessary and sometimes wrong assumptions in hemodynamics.

## 1 The Lattice Boltzmann Method and Hemodynamics

In the last decade, the LB method has captured increasing attention from the fluid dynamics community as a competitive computational alternative to the discretization of the Navier-Stokes equations of continuum mechanics. LB is a hydrokinetic approach and a minimal form of the Boltzmann kinetic equation, based on the collective dynamics of fictitious particles on the nodes of a regular lattice.

The dynamics of fluid particles is designed in such a way as to obey the basic conservation laws ensuring hydrodynamic behavior in the continuum limit, in which the molecular mean free path is much shorter than typical macroscopic scales [13]. This condition is clearly met in most blood flow regimes, together with the Newtonian rheological behavior of blood in large arterial systems. Non-Newtonian rheological models appropriate for simulating blood flow in medium or small-sized arteries, such as the Casson, Carreau or Carreau-Yasuda models, can be also incorporated within the LB approach [20, 21].

The LB method can be regarded as a mesoscopic (between microscopic and macroscopic) approach for modeling macroscopic hydrodynamics. Rather than following the position and velocity of each particle in the system, as is done in microscopic models (i.e. molecular dynamics), the fluid flow is described by tracking the evolution of the density distribution function (or population). In other words, the LB method is based on the collective dynamics of fictitious particles on the nodes of a regular lattice where the basic quantity is  $f_p(\mathbf{x}, t)$ , representing the probability of finding a ‘fluid particle  $p$ ’ at the mesh location  $\mathbf{x}$  and at time  $t$  and traveling with discrete speed  $\mathbf{c}_p$ . ‘Fluid particles’ represent the collective motion of a group of physical particles.

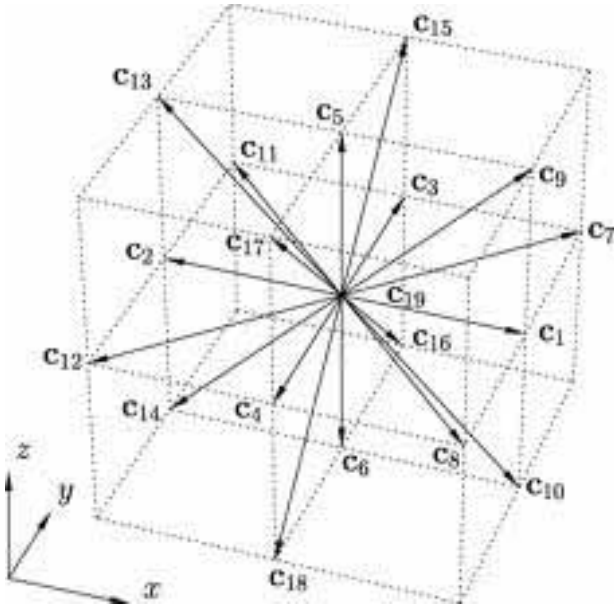


Figure 1: The D3Q19 cubic lattice.

The rate of change of the particle distribution function is given by the following discrete Boltzmann equation:

$$\partial_t f_p + \mathbf{c}_p \cdot \nabla f_p = -\frac{1}{\tau} (f_p - f_p^{eq}) \quad (1)$$

in which the left-hand side represents the molecular free streaming, whereas the right-hand side represents molecular collisions via a single-time relaxation towards local equilibrium  $f_p^{eq}$  on a typical timescale  $\tau$  [13]. The latter is called the relaxation time and, in macroscopic terms, it is related to the fluid viscosity.

To discretize the previous equation, we employ the common three-dimensional 19-speed cubic lattice (D3Q19) with mesh spacing  $\Delta x$ , where the discrete velocities  $\mathbf{c}_p$  connect mesh points to first and second neighbors (Fig. 1) [22]. The fluid populations are advanced in a timestep  $\Delta t = 1$  through the following evolution equation:

$$f_p(\mathbf{x} + \mathbf{c}_p \Delta t, t + \Delta t) = f_p(\mathbf{x}, t) - \omega (f_p - f_p^{eq})(\mathbf{x}, t) + F_p(\mathbf{x}, t) \quad (2)$$

The right hand side of Eq. (2) represents the effect of fluid-fluid molecular collisions, through a relaxation towards a local equilibrium, typically a second-order expansion in the fluid velocity of a local Maxwellian with speed  $\mathbf{u}$ ,

$$f_p^{eq} = w_p \rho \left[ 1 + \frac{\mathbf{u} \cdot \mathbf{c}_p}{c_s^2} + \frac{\mathbf{u} \mathbf{u} : (\mathbf{c}_p \mathbf{c}_p - c_s^2 \mathbf{I})}{2c_s^4} \right] \quad (3)$$

where  $c_s = 1/\sqrt{3}$  is the speed of sound,  $w_p$  is a set of weights normalized to unity, and  $\mathbf{I}$  is the unit tensor in Cartesian space. The relaxation frequency  $\omega = \frac{1}{\tau}$  controls the kinematic viscosity of the fluid. The kinetic moments of the discrete populations provide the local mass density  $\rho(\mathbf{x}, t) = \sum_p f_p(\mathbf{x}, t)$  and momentum  $\rho \mathbf{u}(\mathbf{x}, t) = \sum_p \mathbf{c}_p f_p(\mathbf{x}, t)$ . The last term  $F_p$  in eqn. (2) represents a momentum source, given by the presence of suspended bodies, if RBC's are included in the model, as discussed in the following sections. Through the Chapman-Enskog procedure, in the incompressible limit, the Navier-Stokes eqns:

$$\begin{aligned} \nabla \cdot \mathbf{u} &= 0 \\ \frac{\partial \mathbf{u}}{\partial t} + (\mathbf{u} \cdot \nabla) \mathbf{u} &= -\frac{1}{\rho} \nabla P + \nu \nabla^2 \mathbf{u} + \mathbf{F} \end{aligned} \quad (4)$$

are recovered from eqn. (2) [13], where  $P$  is the pressure,  $\nu = c_s^2 \Delta t \left( \frac{1}{\omega} - \frac{1}{2} \right)$  the kinematic viscosity and  $\mathbf{F}$  is any body force, corresponding to  $F_p$  in eqn. (2).

The LB is a low-Mach, weakly-compressible fluid solver and presents several major advantages for the practical implementation in complex geometries. In particular, in hemodynamic simulations, the curved blood vessels are shaped on the Cartesian mesh scheme via a staircase representation, in contrast to body-fitted grids that can be employed in direct Navier-Stokes simulations. This apparently crude representation of the vessel walls is sufficient at macroscopic level and can be systematically improved by increasing the mesh resolution. In addition, at the high mesh resolution required to sample low-noise WSS data, the LB method requires rather small time steps (of the order of  $10^{-6}$  s for a resolution of  $20\ \mu\text{m}$ ).

The wall shear stress, which is a crucial quantity in hemodynamic applications, can be computed via the deviatoric stress tensor  $\sigma(\mathbf{x}, t) \equiv \nu\rho(\partial_x\mathbf{u} + \partial_x\mathbf{u}^T)$ , evaluated via its kinetic representation:

$$\sigma(\mathbf{x}, t) = -\frac{3\nu\omega}{c_s^2} \sum_p \mathbf{c}_p \mathbf{c}_p (f_p - f_p^{eq})(\mathbf{x}, t) \quad (5)$$

The tensor second invariant is the Wall Shear Stress or WSS,

$$\mathcal{S}(\mathbf{x}_w, t) = \sqrt{\frac{1}{2}(\sigma:\sigma)(\mathbf{x}_w, t)} \quad (6)$$

where  $\mathbf{x}_w$  represents the position of sampling points in close proximity to the mesh wall nodes.  $\mathcal{S}(\mathbf{x}_w, t)$  provides a direct measure of the strength of the near-wall shear stress [23]. It is worth mentioning that the WSS evaluation via Eq. (5) is completely local and does not require any finite-differencing procedure. This is particularly advantageous near boundaries where the computation of gradients is very sensitive to morphological details. In order to sample high signal/noise WSS data, the LB mesh needs high spatial resolution, with mesh spacing being as small as  $\Delta x \cong 50\ \mu\text{m}$  for standard fluid dynamic simulations, or being as small as  $\Delta x \cong 10\ \mu\text{m}$  in order to account for the presence of RBC's. Simulations in extended arterial systems are based on the acquisition of MDCT data which are segmented into a stack of slices, followed by a mesh generation from the segmented slices. For a typical coronary artery system, the procedure to build the LB mesh from the MDCT raw data starts from a single vessel, formatted as stacked bidimensional contours (slices), with a nominal resolution of  $100\ \mu\text{m}$ .

In spite of recent technological progress, this resolution is still insufficient and the inherently noisy geometrical data pose a problem in the evaluation of WSS, a quantity that proves extremely sensitive to the details of the wall morphology. Raw MDCT data present a mild level of geometric irregularities that can affect the quality of the LB simulations. For the simulation, we resort to regularize the initial geometry by smoothing the sequence of surface points via a linear filter along the longitudinal direction. Similarly, one could filter out surface points along the azimuthal contour. We have shown that such smoothing is necessary in order to avoid strong artifacts in the simulation results [24]. Even if the precise shape of the vessel is unknown, as it falls within the instrumental indeterminacy, the numerical results converge to a common fluid dynamic pattern as the smoothing procedure reaches a given level. The regularized geometries are still of great interest because they obey the clinical perception of a smooth arterial system and, moreover, the smoothing procedure falls within the intrinsic flexibility of the arterial system.

When studying coronary arteries as a prototypical system for plaque formation and development, one issue regards the presence of deformable vessels. Whereas larger arteries undergo high deformations, a simple calculation shows that the distensibility index of a coronary artery of sectional area  $A$  is  $b^{-1} \cong 1.5\ \text{mmHg}$ . Therefore, the arterial section during a heartbeat has a maximal deformation of  $\delta A/A = b\Delta P$ , with  $\Delta P$  the maximal pressure variation over a cardiac cycle. For a pressure jump of  $40\ \text{mmHg}$ , the deformation is less than 3% and thus the rigid coronary systems do not introduce major artifacts in the computed flow and pressure distributions.

LB allows to impose no-slip boundary conditions at the endothelium by employing the bounce-back method; this consists of reversing at every time step the post-collisional populations pointing towards a wall node, providing first-order accuracy for irregular walls [13]. In the bounceback method the points corresponding to the exact no-slip hydrodynamic surface fall at intermediate positions between the external fluid mesh nodes and the nearby wall mesh nodes. Owing to its simplicity, the method handles irregular vessel boundaries in a seamless way, although more sophisticated alternatives with higher order accuracy are available [25, 26, 27].

In a branched portion of arteries, boundary conditions at the inlet and multiple outlets can be chosen in different ways, typically by following the flow-pressure, pressure-pressure or flow-flow prescriptions. The first two options are more popular in fluid dynamic models and pressure conditions at the outlets reflect the presence of a recipient medium. Even flow-flow conditions have found some applicability, as they can accommodate some type of metabolic autoregulation as encoded by Murray's law [28]. It is worth mentioning that flow-flow conditions can give rise to numerical instabilities in simple pipe flows, as long-living transients can develop. The absence of a peripheral system can be compensated by using an equivalent RCL circuit at each system outlet, where the auxiliary circuitry introduces an external viscous dissipation ( $R$ ), vessel compliance ( $C$ ) and fluid inertia ( $L$ ) and compensates for the missing components (lumped parameter model).

In the framework of the LB method, boundary conditions at the inlet and multiple outlets can be imposed as follows. A constant velocity (with plug or parabolic profile) is enforced at the entrance of the main artery, as a way to control the amplitude of the flow. Even if the inlet profiles are not the real ones for irregular geometries, they fulfill the purpose of imposing the total flow rate in the chosen region. The fluid flow spontaneously and rapidly develops the consistent profile already at a short distance downstream. A constant pressure is imposed on the several outlets of the main artery, as well as on the outlet of all secondary branches (of the order of 10 in typical coronary systems). This leaves the simulation with the freedom of creating an appropriate velocity profile in the outlet regions, and building up a pressure drop between the inlet and the several outlets. The Zou-He method [29] is used to implement both the velocity inlet and the pressure outlets. This method exploits information streamed from fluid bulk nodes onto boundary cells, and imposes a completion scheme for particle populations which are unknown because their neighboring nodes are not part of the fluid domain. The boundary cells are treated as normal fluid cells where the conventional LB scheme holds. Thanks to this natural integration of the boundary scheme, the method is second-order accurate in space, compatible with the overall accuracy of the LB method [30]. The method handles in a natural way time-dependent inflow conditions for pulsatile flows.

The algorithm requires that all nodes of a given inlet or outlet are aligned on a plane which is perpendicular to one of the three main axes, although the injected flow profile and direction can be arbitrary. However, since the inlet section is typically a critical region of simulation in terms of numerical stability due to the high fluid velocities, it is preferable to have an incoming flow direction aligned with one of the cartesian axes. This requirement can be fulfilled by rotating the artery in such a way as to align the inlet axis with one of the cartesian axes, which guarantees an exact control on the flow imposed at the inlet. Conversely, the outlet planes are not in general normal to the orientation of the blood vessels. However, this does not lead to noticeable problems, because the pressure drop along typical arterial systems is mild, and the error due to imposing a constant pressure along an inclined plane is negligible.

## 2 Blood as a Suspension

Blood is a complex fluid made of many corpuscular elements suspended in the plasma. Red blood cells (RBC's) or erythrocytes constitute an important component in blood because of their large number density and their crucial role in oxygen transport. Typically, a human RBC has a biconcave shape of  $\sim 8 \mu\text{m}$  in diameter and  $\sim 2 \mu\text{m}$  in thickness. The interior fluid has a viscosity of 6 cP, which is about 5 times of that of the suspending plasma. The cell membrane is highly deformable so the RBC's can pass through capillaries of as small as  $4 \mu\text{m}$  inner diameter with large deformation: they exhibit both rotational and orientational responses that effect and modulate blood rheology [1]. While blood flow is quasi-Newtonian away from the endothelial region, the presence of RBCs strongly affects flow in the proximity of the endothelium, where the interplay of RBC crowding for hematocrit levels up to 50% depletion due to hydrodynamic forces, and RBC's arrangement in rouleaux take place.

In order to consider these different factors, we have recently proposed a model that focuses on three independent components: the far-field hydrodynamic interaction of a RBC in a plasma solvent, the raise of viscosity of the suspension with the hematocrit level and the many-body collisional contributions to viscosity [31]. These three critical components conspire to produce large-scale hemorheology and the local structuring of RBCs.

The underlying idea is to represent the different responses of the suspended bodies, emerging from the rigid-body as much as the vesicular nature of the globule, by distinct coupling mechanisms. These mechanisms are entirely handled at kinetic level, that is, the dynamics of plasma and RBC's is governed by appropriate collisional terms that avoid to compute hydrodynamic forces and torques via the Green's function method, as employed in Stokesian dynamics [32]. The fundamental advantage of hydrokinetic modeling is to avoid such an expensive route and, at the same time, enabling to handle finite Reynolds conditions and complex or irregular boundaries within the simple collisional approach. At the macroscopic scale, the non-trivial rheological response emerges spontaneously as a result of the underlying microdynamics.

The presence of suspended RBCs is included via the following forcing term (see eqn. (2)):

$$F_p = w_p \left[ \frac{\mathbf{G} \cdot \mathbf{c}_p}{c_s^2} + \frac{(\mathbf{G} \cdot \mathbf{c}_p)(\mathbf{u} \cdot \mathbf{c}_p) - c_s^2 \mathbf{G} \cdot \mathbf{u}}{c_s^4} \right] \quad (7)$$

where  $\mathbf{G}(\mathbf{x}, t)$  is a local force-torque. This equation produces first-order accurate body forces within the LB scheme. Higher order methods, such that in [33], could be adopted. However, given the non-trivial dependence of the forces and torques on the fluid velocity and vorticity, Guo's method would require an implicit numerical scheme whereas it is preferable to employ an explicit, first-order accurate numerical scheme.

The fluid-body hydrodynamic interaction is constructed according to the transfer function  $\tilde{\delta}(\mathbf{r}_i)$  centered on the  $i$ -th particle position  $\mathbf{r}_i$  and having ellipsoidal symmetry and compact support. The shape of the suspended body can be smaller than the mesh spacing, allowing to simulate a ratio of order 1:1 between suspended bodies and mesh nodes. In addition, the body is scale-adaptive, since it is possible to reproduce from the near-field to the far-field hydrodynamic response with desired accuracy [34]. The fluid-particle coupling requires the computation of the following convolutions over the mesh points and for each configuration of the  $N$  suspended bodies:

$$\begin{aligned} \tilde{\mathbf{u}}_i &= \sum_{\mathbf{x}} \mathbf{u}(\mathbf{x}) \tilde{\delta}(\mathbf{x} - \mathbf{r}_i) \\ \tilde{\boldsymbol{\Omega}}_i &= \sum_{\mathbf{x}} \boldsymbol{\Omega}(\mathbf{x}) \tilde{\delta}(\mathbf{x} - \mathbf{r}_i) \\ \tilde{\mathbf{T}}_i &= \sum_{\mathbf{x}} \mathbf{t}(\mathbf{x}) \times (\mathbf{x} - \mathbf{r}_i) \tilde{\delta}(\mathbf{x} - \mathbf{r}_i) \end{aligned} \quad (8)$$

where  $\boldsymbol{\Omega}$  is the fluid vorticity and  $\mathbf{t}$  is the fluid traction vector, quantities that are directly obtained from the LB computational core. The three convolutions allow to compute the drag force and drag torque, inclusive of tank trading components. On the fluid side, the body-induced forces are encoded by the term

$$\mathbf{G}(\mathbf{x}) = - \sum_{i=1}^N \left[ \mathbf{D}_i \tilde{\delta}(\mathbf{x} - \mathbf{r}_i) + \frac{1}{2} \mathbf{T}_i \times \partial \tilde{\delta}(\mathbf{x} - \mathbf{r}_i) \right]$$

where  $\mathbf{D}_i$  and  $\mathbf{T}_i$  are the drag forces and torques acting on the particles, constructed from the quantities in eqs (8).

Besides hydrodynamic interactions, mechanical forces regulate the direct interactions and the packing attitude of suspended bodies. The interactions are modeled as pairwise by means of the Gay-Berne (GB) potential [35], the pairwise GB energy being a function of the relative distance between pairs of RBCs and their mutual orientation. In addition, their interaction depends on the eccentricity of each particle, so that, as for the hydrodynamic coupling, mixtures of particles of different shapes can be handled within a unified framework. Once the forces and torques standing from both hydrodynamics and direct mechanical forces are computed, the rigid body dynamics is propagated via a time second-order accurate algorithm [36, 37].

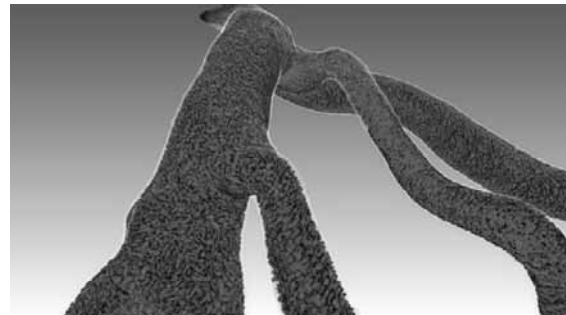


**Figure 2:** Snapshot of a multi-branched artery in presence of RBC's for 50% hematocrit.

Numerical results have shown that the particulate nature of blood cannot be omitted when studying the rheology of this biofluid and the shear stress distribution in complex geometries. Regions of low shear stress can appear as the hematocrit reaches physiological levels as a result of the non-trivial organization of RBC's and the irregular morphology of vessels, with far reaching consequences in real-life cardiovascular applications, where the organization of RBC's impacts both the local flow patterns and the large-scale flow distribution in vascular networks. A crucial advantage of the hydrokinetic mod-

el with the presence of realistic hematocrit is its reduced computational cost, thus enabling the investigation of systems of physiological relevance (Fig. 2).

### 3 The Corrugated Wall Surface

At a lower scale, new intriguing aspects come to light in hemodynamics. For example, the vessel wall surface is covered by endothelial cells (EC), that give a wavy structure, so far neglected (Fig. 3): this does not imply a significant variation in the flow field, but it can be relevant in computing WSS, which is constant in a flat-walled artery. Indeed, the EC's (a single EC has been estimated to be about  $15\ \mu\text{m}$  long by  $0.5\ \mu\text{m}$  high, see [38]) form a continuous, undulated wall layer above which blood is flowing. At such mesoscopic scale, the wall may be considered as a wavy surface constituted by a regular array of equal, repeated EC's. We consider a two-dimensional channel flow between two boundary surfaces located at  $y = \pm h(x)$ , with the x-axis in the direction of the mean flow. The shape of each internal wall appears as a smoothly corrugated surface: the channel semi-width is obtained as a perturbation around a reference constant value  $H$ :  $h(x) = H \pm \xi(x)$  where  $\xi(x)$  is given by repeating the profile of a single EC several times and subsequently smoothing it. The quantity  $\max \xi/H$  represents the corrugation degree.

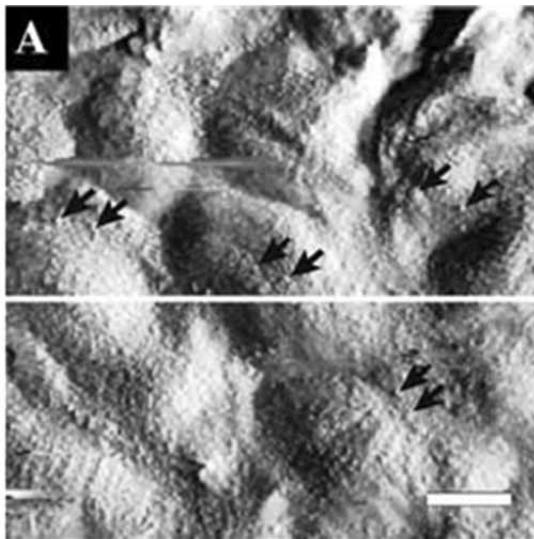


**Figure 3:** The rough surface of the endothelium as imaged using scanning force microscopy (from [38]). Arrows point to granular structures on EC's surfaces, white line marks scanning line for height profile evaluation, scale bar corresponds to  $5\ \mu\text{m}$ .

For such complex geometries, the original LB method, designed to be used over a uniform Cartesian grid, would represent a severe limitation for high resolutions near the walls. Recent advances in LB have led to a substantial enhancement for handling irregular shapes, and a particularly interesting option is represented by finite-volume formulations on fully unstructured grids (ULBE) [39]. The pressure-driven axi-symmetric flow of a continuum fluid through a plane channel having a corrugated surface where the grid is locally refined (Fig. 4) has been recently modeled with ULBE by [8].

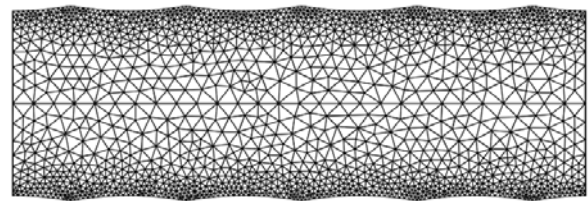


**Figure 4:** A 2D arterial segment having a corrugated wall, covered by a near-wall refined triangular unstructured mesh.

At small Reynolds number and with moderate corrugation degree, the velocity profiles preserve the parabolic shape (Fig. 5). However, the wall corrugation causes a local change of the velocity derivative and hence a variation on the WSS values which match the undulation of the wall: in particular, the minimum and maximum of WSS correspond to the wall throat and peak, respectively. Their values depend on the vessel diameter and on the flow rate, but their ratio remains almost constant. As Fig. 5 shows, the shear stress rises linearly in the transverse direction, except near the wall. Here, the variation in cross-sectional width generates a substantial local difference in the shear rates and stresses, and the consequence is a local variation of these quantities in a boundary layer close to the wall and an oscillation of the shear rates and WSS along the endothelium.

We have further investigated the dependence and the sensitivity on the corrugation degree, and quantified the WSS differences with the variation of vessel diameter and flow rates. It was shown a significant WSS variations between the EC's wall peaks and throats, especially in small-sized arteries [8].

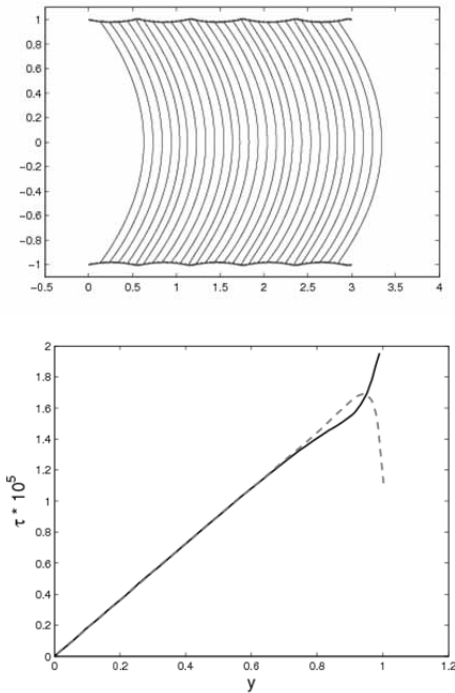


**Figure 5:** Parabolic velocity profiles along the wavy channel: its wall is constituted by a uniform sequence of peaks and throats (top). Cross-stream variation of shear stress in half-channel: continuous line - peak of EC; dashed line - valley of EC (LB units) (bottom).

### 4 The Endothelial Surface Layer

The endothelial surface is not only wavy in its geometry, but, at a smaller scale, it is covered by fibrous filaments and long protein chains forming a thin layer called the endothelial surface layer (ESL) or glycocalyx [9]. From a fluid dynamics point of view, the ESL can be modelled as a porous layer of constant thickness (50–100 nm) which suits the wall undulation, through which the flow of the continuous phase (plasma) is possible. This would alter the boundary condition of the problem, specifically the classical no-slip condition at the vessel wall may have to be replaced to allow for plasma penetration through the ESL. The LB method readily accommodates a model of the glycocalyx itself, as it is particularly well suited to address what would now become a multiscale model. Furthermore, and differently than in sect. 2, the mesoscopic particulate nature of the blood is now addressed in the context of a bi-component fluid model: RBC are here deformable, neutrally buoyant liquid drops constrained by a uniform interfacial tension and suspended in the plasma.

Conceptually, the idea is to solve a two-domain problem, whereby the bulk flow (in the lumen) is governed by the multicomponent Navier-Stokes equations and the near-wall region by a porous-medium Brinkmann flow formulation. At the mesoscale, the glycocalyx is not modelled in a detailed form, but its effect on the flow is still properly addressed, using methods which are amenable to coupling other, more detailed, simulations with experiments. We develop here a *two-way coupled* model where the drop interface is forced by compression of the ESL, and the effect of perturbed or compressed glycocalyx is then communicated to the flow [40]. We assume here that the filaments are strongly anchored in the endothelium, where they are most resistant to deformation and that they deform preferably at their tip, i.e. towards the vessel lumen.

The mesoscale LB method is still used to solve the governing hydrodynamic equations, that involves multi-component fluid flow, off-lattice, or sub-grid, boundary surfaces and a porous-layer representative of the ESL. The governing hydrodynamic equations for flow in a porous media, with constant or variable porosity  $\epsilon$ , are an extension of eqn. (4) as in [41]:

$$\nabla \cdot \mathbf{u} = 0$$

$$\frac{\partial \mathbf{u}}{\partial t} + (\mathbf{u} \cdot \nabla) \frac{\mathbf{u}}{\epsilon} = -\frac{1}{\rho} \nabla(\epsilon P) + \nu \nabla^2 \mathbf{u} + \mathbf{F} \quad (9)$$

Here  $\mathbf{F}$  is the total body force due to the presence of both the porous material (drag) and other external forces:

$$\mathbf{F} = \frac{\epsilon \nu}{K} \mathbf{u} - \frac{\epsilon F_\epsilon}{\sqrt{K}} \mathbf{u} |\mathbf{u}| + \epsilon \mathbf{H} \quad (20)$$

where  $\mathbf{H}$  is the extra body force that will be used to incorporate further details of the ESL and particulate effects, such as the RBC interface force density (pressure step) defined below. To solve governing equations (9)–(10) we combine the LB methods of [41], with the model of [42], that allows for the introduction of two immiscible fluid components and the formation of interfaces embedding surface tension laws.

To complete the algorithm, we must mention that, for multiple fluid LB, the propagation step is augmented by a fluid segregation process that ensures the correct kinematics and dynamics and good integrity for an interface between completely immiscible fluid components, representing RBC and plasma, as discussed above [42]. The propagation step is expressed as:

$$R_p(\mathbf{x} + \mathbf{c}_p \Delta t, t + \Delta t) = \frac{R}{\rho} f_p^+ + w_p \beta \frac{RB}{\rho} \cdot \mathbf{c}_p \cdot \mathbf{n}$$

$$B_p(\mathbf{x} + \mathbf{c}_p \Delta t, t + \Delta t) = \frac{B}{\rho} f_p^+ - w_p \beta \frac{RB}{\rho} \cdot \mathbf{c}_p \cdot \mathbf{n} \quad (11)$$

where the density of each fluid component is given by  $R = \sum_p R_p(\mathbf{x}, t)$  and  $B = \sum_p B_p(\mathbf{x}, t)$ , the combined particle distribution function is  $f_p = R_p + B_p$  and  $f_p^+$  accounts for the propagated combined distribution. In eqn. (11)  $\beta$  represents an interfacial segregation parameter and  $\mathbf{n}$  the interfacial unit normal vector. We also note that, if only one fluid component exists, eqs. (11) reduce to the standard LB propagation step eqn. (2). Returning to the definition of the extra body force term,  $\mathbf{H}$  in eqn. (10), this incorporates both particulate and glycocalyx forces and is defined as

$$\mathbf{H} = \frac{\sigma}{2\rho} \pi \nabla \rho_N + \mathbf{E} \quad (32)$$

The left hand side term imposes an interfacial tension  $\sigma$  on multicomponent particles. Here  $\pi = \nabla \cdot \mathbf{n}$  is the local curvature and  $\rho_N = (R - B)/(R + B)$  is a phase field indicator. The right hand term  $\mathbf{E}$  is a glycocalyx force that acts upon the particles as described below.

In the proposed model of the ESL as a porous layer, the porosity is reduced by a compressive encounter with an erythrocyte. As a consequence, the ESL is squashed locally transporting the same mass into a smaller volume and consequently decreasing the porosity in that region. Even in the simplest situation, the ESL-lumen boundary should not be regarded as sharp and there is an *uncertainty region* between bulk, lumen and glycocalyx material [40]. Let us define a variable porosity  $\epsilon(x, y)$  that tends to 1 in the lumen region and gradually reduces, as it enters the glycocalyx region, where it approaches a minimum value,  $\epsilon_G$ .

This porosity transition is modelled through the increasing smooth function:

$$\epsilon(\mathbf{x}) = \epsilon_G + \frac{1 - \epsilon_G}{2} [1 - \tanh(\xi(s - l))] \quad (13)$$

where  $l$  is the mean ESL thickness and the parameter  $1/\xi$  determines the distribution of (i.e. the effective standard deviation of) protein chain lengths, while  $s(\mathbf{x})$  denotes distance measured normally to the endothelial surface. Note that  $\epsilon_G \leq \epsilon(\mathbf{x}) \leq 1$  and that for  $\epsilon \rightarrow 1$  we have  $\mathbf{F} \rightarrow \mathbf{H}$  (see eqn. (10)) and the equations (9)–(10) reduce to the multi-component Navier-Stokes equations for free multi-component fluid flows, and the described procedure reduces to the standard LB method for a two-component, incompressible fluid.

On the other hand, an additional, fictitious, repulsive body force density acts on the drop interface which enters the ESL region, impinging on the lumen. This force distribution is so designed that its accumulation produces an effective Hookean force acting at the centre of the local volume. Specifically, the erythrocyte is subjected to a surface force distribution, effective in the ESL only, which is directed everywhere in the drop-surface normal direction.

This force device effectively models the glycocalyx as a continuum of elastic springs, with modulus  $E$ , gradually decaying from a maximum value,  $E_G$  (in the ESL) to 0 (towards the bulk):

$$E(x) = \frac{E_G}{2} [1 - \tanh(\xi(s - l))] \quad (44)$$

where all notations are given in correspondence to eqn. (13). It is important to note that the above force acts solely on the drop and not upon the plasma. Hence, the relative density of the material which comprises the drop may be modelled by appropriate choice of the spring constant  $E_G$  in the above equation. A number of simulations have been carried out in the case of an axisymmetric channel having the same corrugation repeated along the length. Its size (of order of  $\mu\text{m}$ ) is slightly larger than a single RBC flowing through it, driven by a constant pressure gradient with periodic conditions. At such fine scale, for accuracy purposes, the off lattice non-slip endothelial surface uses continuous bounce back conditions [25]. The ESL structure has been modelled as a porous layer of constant thickness over the undulated wall. As one may expect, the average velocity of the drop is slower in the presence of the glycocalyx, which constitutes a hindrance for the lumen flow. Also, the mean deformation of the drop is more pronounced with the glycocalyx force (Fig. 7). Hence, when the drop is in the ESL influence region, it is subjected to the elastic force, which squeezes and lifts it, away from the boundary, whilst making its shape more elongated. Considering the action of the glycocalyx as a sensor of mechanical forces, it is worth computing the shear stress at the glycocalyx / lumen boundary (GSS). Fig. 8 shows the differences for WSS in the cases without and with glycocalyx: it evidences, in the latter case, a reduction of the shearing stress either at the wall (WSS, due to the plasma only) and at the ESL top (GSS, due to the particulate fluid).

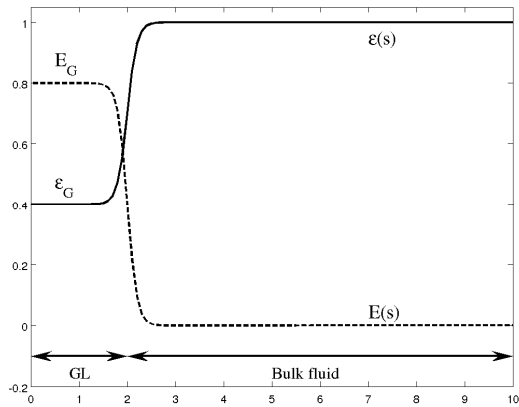


**Figure 6:** The porosity function  $\varepsilon$  (continuous line) as a function of the distance  $s$ : the latter increases from a minimum value  $\varepsilon_G$  (in the ESL or GL) to the bulk fluid ( $\varepsilon = 1$ ). Similarly the elasticity modulus  $E$  (dashed line) varies from a maximum value  $E_G$  in GL to 0 (no elastic force) out of it. Note the smooth transition region (due to the uncertainty ESL thickness) controlled by the parameter  $\xi$ .

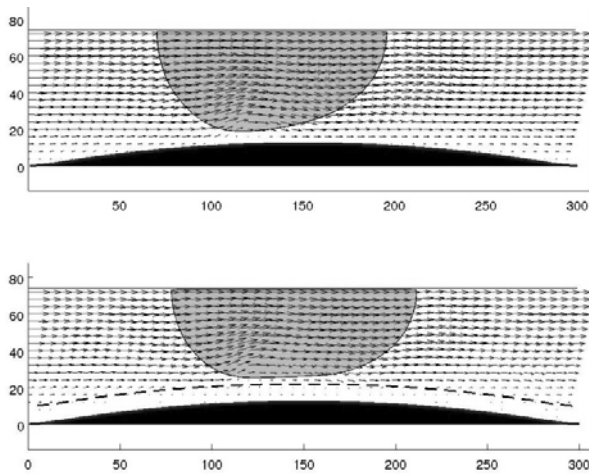


**Figure 7:** The velocity field for the particulate fluid in the region of the endothelium. The extent of the ESL is indicated by the broken line. An enhanced recirculation region is induced by the porous media (bottom), with respect to an experiment without glycocalyx (top). The single deformable drop has been acted on by encountering the glycocalyx body force field. The flow appears to be deflected up which would tend to protect the endothelial surface from increased WSS.

It is possible that cilia, which deform preferentially at their tip, would be more likely to protect the endothelial cell from WSS fluctuations associated with RBC's transits [8].

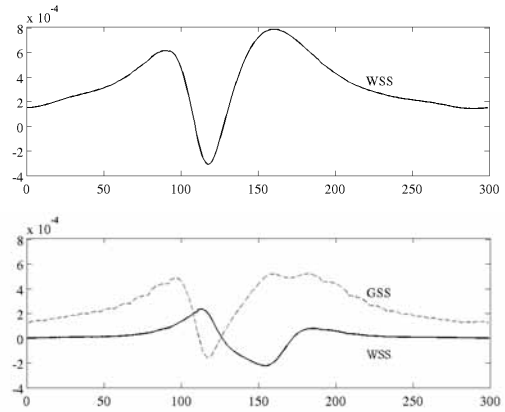


**Figure 8:** The WSS and GSS along the channel at the same time without (top) and with glycocalyx (bottom).

As a comprehensive computational tool to account the different aspects in blood flow simulation in a unified LB framework, we developed the software MUPHY that involves five basic steps: (1) Acquisition of MDCT data; (2) Data segmentation into a stack of slices; (3) Mesh generation from the segmented slices; (4) Flow simulation; (5) Data analysis and visualization. The MUPHY simulation package is designed to handle generic geometries, such as those provided by the MDCT acquisitions, and to run large scale simulations on commodity or high-performance hardware resources. The major advantage of MUPHY is the possibility of concurrently simulating fluid-dynamics together with suspended bodies at cellular and molecular scales. This multi-scale methodology arises from the combined use of LB and molecular dynamics techniques [19].

## 5 Conclusions

Studying the cardiovascular system and capturing the essence of blood circulation requires to cope with the complexity of such biological fluid, as much as the details of the vessel's anatomy. From the computational standpoint, taming such complexity is a hard work, as it requires to handle several concurrent actors. Choosing the right computational tool, therefore, is a delicate task that has been addressed in the present paper.

It was shown that the LB method is an extremely powerful framework to deal simultaneously with blood plasma, red blood cells and the glycocalyx in a unified and consistent form. The versatility of this framework is such to be a good candidate to study fluids of different types and at different scales without major differences.

When dealing specifically with blood and the development of cardiovascular disease, it is key to address the detailed structure and dynamics of blood in the surroundings of the endothelium, as recent work has revealed a correlation between the flow-induced mechano-transduction in the glycocalyx and the development of atherosclerosis. The presence of the glycocalyx is supposed necessary for the endothelial cells to react to fluid shear, and its role is characterized by studying its response to shear stress. A coarse-grained model and a preliminary numerical simulation of the blood flow over the exact, microscale, corrugated EC shape covered by a prototype ESL has been proposed. Another direction we are undertaking is to enhance our current, simplistic, interfacial tension model with additional stresses and bending properties associated with elastic structures. Our current effort is to modify and extend the behaviour our fluid-fluid interface so as to enrich and adapt its existing mechanical properties, in a manner which mimics the thin membrane of erythrocytes.

If, at one hand, the microscopic blood-wall interaction has a noticeable importance for pathological states, on the other hand, the simulation of large-scale circulatory systems relies on sophisticated imaging techniques and powerful computational tools. Owing to the basic assets of hydrokinetic modeling, the unifying LB methodology provides a reliable and robust approach to the understanding of cardiovascular disease in multiple-scale arterial systems, with great potential for impact on physiological and biomedical applications. The inclusion of red blood cells allows to reproduce realistic blood processes and represents a step forward for clinical purposes, as much as for the fundamental aspects in hemodynamics and hemorheology.

## References

- [1] Zhang J, Johnson P, and Popel A. Effects of erythrocyte deformability and aggregation on the cell free layer and apparent viscosity of microscopic blood flows. *Microvasc. Res.* 2009; 77(3):265-272
- [2] ChatzizisisYS, Jonas M, Coskun AU, Beigel R, Stone BV, Maynard C, Gerrity RG, Daley W, Rogers C, Edelman ER, Feldman CL, and Stone PH. Prediction of the localization of high-risk coronary atherosclerotic plaques on the basis of low endothelial shear stress: an intravascular ultrasound and histopathology natural history study. *Circ.* 2008; 117(8):993–1002
- [3] Shaaban AM and Duerinckx AJ. Wall shear stress and early atherosclerosis: a review. *AJR Am. J. Roentgenol.* 2000; 174(6):1657–1665
- [4] Caro C, Fitzgerald J, Schroter R. Arterial wall shear stress and distribution of early atheroma in man. *Nature.* 1969;223:1159–1161
- [5] Malek AM, Alper SL, Izumo S. Hemodynamic shear stress and its role in atherosclerosis. *J. Am. Med. Assoc.* 1999; 282(21):2035–2042
- [6] Vorp DA, Steinman DA, Ethier CR. Computational modeling of arterial biomechanics. *Comput. Sci. Eng.* 2001; P.51–64.
- [7] Pahakis M, Kosky J, Dull R, Tarbell J. The role of endothelial glycocalyx components in mechanotransduction of fluid shear stress. *Biochem. Biophys. Res. Comm.* 2007; 355(1):228–233
- [8] Pontrelli G, König C, Halliday I, Spencer T, Collins M, Long Q, Succi S. Modelling wall shear stress in small arteries using the Lattice Boltzmann method: influence of the endothelial wall profile. *Med. Eng. Phys.* 2011b; 33(7):832–839
- [9] Weinbaum S, Tarbell J, Damiano E. The structure and the function of the endothelial glycocalyx layer. *Ann. Rev. Biom. Eng.*, 2007; 9 (6.1)
- [10] Secomb T, Hsu R, Pries A. Blood flow and red blood cell deformation in nonuniform capillaries: effects of the endothelial surface layer. *Microcirculation.* 2002; 9:189–196
- [11] Arlsan, N. Mathematical solution of the flow field over glycocalyx inside vascular system. *Math. Comp. Appl.* 2007; 12:173–179
- [12] Vincent P, Sherwin S, Weinberg P. Viscous flow over outflow slits covered by an anisotropic Brinkman medium: a model of flow above interendothelial cell cleft. *Phys. Fluids.* 2008; 20(6):63-106
- [13] Succi S. *The Lattice Boltzmann Equation for Fluid Dynamics and Beyond.* Oxford University Press, USA; 2001.
- [14] Pontrelli G, Ubertini S, Succi S. The unstructured lattice Boltzmann method for Non-Newtonian flows. *J. Stat. Mech. Theory & Exp.* 2009; P.06005.
- [15] Rybicki FJ, Otero HJ, Steigner ML, Vorobiof G, Nallamshetty L, Mitsouras D, Ersoy H, Mather RT, Judy PF, Cai T, Coyner K, Schultz K, Whitmore AG, Di Carli MF. Initial evaluation of coronary images from 320-detector row computed tomography. *Intl. J. Cardiovasc. Imaging.* 2008; 24(5):535–546
- [16] Ouared R, Chopard B. Lattice Boltzmann simulations of blood flow: Non-Newtonian rheology and clotting processes. *J. Stat. Phys.* 2005; 121:209–221

- [17] Evans D, Lawford P, Gunn J, Walker D, Hose D, Smallwood R, Chopard B, Krafczyk M, Bernsdorf J, Hoekstra A. The application of multiscale modelling to the process of development and prevention of stenosis in a stented coronary artery. *Phil. Trans. R. Soc. A.* 2008; 366(1879):3343–3360
- [18] Melchionna S, Bernaschi M, Succi S, Kaxiras E, Rybicki FJ, Mitsouras D, Coskun AU, Feldman CL. Hydrokinetic approach to large-scale cardiovascular blood flow. *Comput. Phys. Comm.* 2010; 181:462–472
- [19] Bernaschi M, Melchionna S, Succi S, Fyta M, Kaxiras E, Sircar J. MUPHY: a parallel MUlti PHYsics/scale code for high performance bio-fluidic simulations. *Comp. Phys. Comm.* 2009; 180:1495–1502
- [20] Boyd J, Buick J, Green S. Analysis of the Casson and Carreau-Yasuda non-Newtonian models in steady and oscillatory flows using the lattice Boltzmann method. *Phys. Fluids.* 2007; 19:32-103
- [21] Janela J, Pontrelli G, Sequeira A, Succi S, Ubertini S. Unstructured lattice-Boltzmann methods for hemodynamics flows with shear-dependent viscosity. *Int. J. Modern Physics.* 2010; 21(6):1–17
- [22] Benzi R, Succi S, Vergassola M. Theory and application of the lattice Boltzmann equation. *Phys. Rep.*, 1992; 222(3):147
- [23] Boyd J, Buick JM. Three-dimensional modelling of the human carotid artery using the lattice boltzmann method: II. shear analysis. *Phys. Med. Biol.*, 2008; 53(20):5781–5795
- [24] Melchionna S, Kaxiras E, Bernaschi M, Succi S. Endothelial shear stress from large-scale blood flow simulations. *Phil. Trans. Royal Soc. A: Math., Phys. and Eng. Sci.* 2011; 369(1944):2354–2361
- [25] Bouzidi M, Firdaouss M, Lallemand P. Momentum transfer of a Boltzmann-lattice fluid with boundaries. *Phys. Fluids.* 2001; 13(11):3452–3459
- [26] Ladd AJC, Verberg R. Lattice-Boltzmann simulations of particle-fluid suspensions. *J. Stat. Phys.* 2001; 104(5):1191–1251
- [27] Guo Z, Zheng C, and Shi B. An extra-polation method for boundary conditions in lattice Boltzmann method. *Phys. Fluids.* 2002a; 14:2007
- [28] Sherman TF. On connecting large vessels to small. the meaning of Murray's law. *J. Gen. Physiol.* 1981; 78(4):431–453
- [29] Zou Q, He X. On pressure and velocity boundary conditions for the lattice Boltzmann BGK model. *Phys. Fluids.* 1997; 9(6):1591
- [30] Latt J, Chopard B, Malaspinas O, Deville M, Michler A. Straight velocity boundaries in the lattice Boltzmann method. *Phys. Rev. E.* 2008; 77(5):56-703
- [31] Melchionna S. A model for red blood cells in simulations of large-scale blood flows. *Macromol. Theory & Sim.* 2011b; 20:000
- [32] Brady JF, Bossis G. Stokesian dynamics. *Ann. Rev. Fluid Mech.* 1988; 20:111
- [33] Guo Z, Zheng C, Shi B. Discrete lattice effects on the forcing term in the lattice Boltzmann method. *Phys. Rev. E.* 2002b; 65(11):46-308
- [34] Melchionna S. Incorporation of smooth spherical bodies in the lattice boltzmann method. *J. Comput. Phys.* 2011a; 230(10):3966–3976
- [35] Gay JG, Berne BJ. Modification of the overlap potential to mimic a linear site–site potential. *J. Chem. Phys.* 1981; 74:3316
- [36] Melchionna S. Design of quasisymplectic propagators for langevin dynamics. *J. Chem. Phys.* 2007; 127:44-108
- [37] Dullweber A, Leimkuhler B, McLachlan R. A symplectic splitting method for rigid-body molecular dynamics. *J. Chem. Phys.* 1997; 107:5851
- [38] Reichlin T, Wild A, Dürrenberger M, Daniels A, Aebi U, Hunziker P, Stolz M. Investigating native coronary artery endothelium in situ and in cell culture by scanning force microscopy. *J. Structural Biol.* 2005; 152:52–63
- [39] Ubertini S, Succi S. Recent advances of lattice Boltzmann techniques on unstructured grids. *Prog. Comput. Fluid Dyn.* 2005; 5(1/2):84–96; PMID: 1870131.
- [40] Pontrelli G, Halliday I, Spencer T, Care C, König C, Collins M. Near wall hemodynamics: modelling the glycocalyx and the endothelium surface. *Proceedings Micro and Nano Flows Conference, MNF2011, CD rom;* 2011a.
- [41] Guo Z, Zhao T. Lattice Boltzmann model for incompressible flows through porous media. *Phys. Rev. E.* 2002; 66:36-304.
- [42] Halliday I, Hollis A, Care C. Lattice Boltzmann algorithm for continuum multicomponent flow. *Phys. Rev. E.* 2007; 76:26-708.

# Modelling Metabolic Pathways Involved in the Pathogenesis of Non-Alcoholic Fatty Liver Disease

Adviti Naik\*, Aleš Belič

Faculty of Electrical Engineering, University of Ljubljana, Tržaška Cesta 25, 1000 Ljubljana \*adviti.naik@fe.uni-lj.si

Simulation Notes Europe SNE 23(2), 2013, 71 - 76  
DOI: 10.11128/sne.23.tn.10183  
Received: Jan. 10, 2013 (Selected MATHMOD 2012 Postconf. Publ.); Revised Accepted: June 10, 2013;

**Abstract.** Abstract: Non-alcoholic fatty liver disease (NAFLD) is a poorly understood complex disorder that occurs at a high frequency in Western populations with unhealthy dietary and lifestyle habits. Systems biology tools may provide further insight into the multi-dimensional nature of NAFLD. A dynamic semiquantitative model of the metabolic and signaling pathways suggested to be important in the pathogenesis of NAFLD has been generated using an object-oriented library of components based on differential equations. Initial model validation procedures to draw a comparison between experimental data and model simulations has suggested a close correlation between experimental models and the *in silico* network. Furthermore, the stiffness of multi-substrate reactions indicates the presence of a balance between pathway fluxes within the network. The model aims to identify novel mechanisms of NAFLD pathogenesis and regulatory components, thus providing a basis for experimental hypotheses.

## Introduction

Non-Alcoholic fatty Liver Disease (NAFLD) is the most common chronic liver disease in Western countries affecting approximately 20-30% of the general population and 70-80% of obese populations. It encompasses a wide disease spectrum ranging from benign steatosis, non-alcoholic steatohepatitis (NASH) that is characterised by inflammation, hepatocellular carcinoma (HCC) and ultimately, cirrhosis ([2]). The accumulation of triglycerides in hepatocytes is a hallmark of hepatic steatosis. The major contributor of hepatic triglycerides is *de novo* lipogenesis and the plasma triglyceride pool derived from the adipose tissues ([3]).

Aberrant perturbations resulting in imbalances between lipid transport, oxidation, synthesis and storage contribute to the pathogenesis of NAFLD ([9]).

NAFLD is the hepatic manifestation of the metabolic syndrome as it encompasses several features of the metabolic syndrome such as dyslipidemia, obesity, insulin resistance, hyperglycaemia and hypertension. Although several molecular mediators and genetic polymorphisms have been implicated in the initiation and progression of NAFLD, this disease remains poorly understood due to inter-individual variations in disease pathogenesis, lack of representative animal models and non-invasive diagnostic methods ([1]). Polymorphisms in various genes, such as PNPLA3 that encodes adiponutrin ([14],[15]), have been identified in association with NAFLD, however a majority of these remain to be replicated in diverse and significantly powered populations and/or do not have a significant contributing effect. Western lifestyles, including insufficient physical activity and the consumption of high-fat and high-sugar diets have a major impact on disease pathogenesis. Hence, the complexity of NAFLD arising from the close interaction between genetic and environmental factors has proved to be difficult to dissect to fully understand its manifestations.

Biological systems can be considered as fundamentally nonlinear systems that operate at nominal equilibrium states, which on perturbation results in the activation of mechanisms to restore the equilibrium state or to reach a different state of equilibrium. Systems biology provides an integrated tool to study non-linear biological physiology using a mathematical modelling approach. It provides a rapid, cheap and repeatable analysis methodology in conjunction with experimentation in order to understand molecular biology. Systems biology has been increasingly utilized to study metabolic networks, especially in prokaryotes ([4]) due to their unicellular nature and the absence of complex metabolic and signalling pathways .

International collaborations are working towards ambitious projects such as the Physiome Project, which aims to provide a framework for modelling biochemistry, biophysics and anatomy aspects of the human body ([7]). However, the complexity of metabolic pathways in eukaryotes renders this task more challenging and as a result only a few reconstructions have been built for multicellular organisms, which are either static networks ([10]) or models focussing on a single cell type ([5]), hence not accounting for tissue-tissue interactions, which is an important deregulated mechanism in NAFLD. This article aims at describing the generation of a dynamic *in silico* model integrating the NAFLD metabolic and signalling pathways, whilst focussing at various hierarchical levels of metabolites and proteins regulated at the level of gene expression and post-translation.

## 1 Generation of the Metabolic Network

### 1.1 Modelling approach

An object-oriented modelling and simulation programme, Dymola 7.4, was utilised to curate a majority of the metabolic reactions implicated in the pathogenesis of NAFLD (Appendix Figure5). The metabolic network was generated utilising a systems biology library of components, wherein each component functions as a biological component on the basis of differential equations assigned to it.

### 1.2 Curation of reactions

The metabolic network includes enzyme-catalysed reactions, which are regulated by various transcriptional factors and molecular mediators at the transcriptional and post-translational levels. Evidence for the incorporation of these reactions within the metabolic network was derived from literature searches ( $n = 470$ ), the Kyoto encyclopaedia of genes and genomes (KEGG, <http://www.genome.jp/kegg/>) and the Reactome ([www.reactome.org](http://www.reactome.org)) databases. The reversibility and stoichiometry of the reactions were maintained only in the presence of evidence from the literature.

The major compartments modelled into the network include the liver, adipose tissue, peripheral tissue, pancreas and macrophages. Within each of these compartments, pathways involved in the metabolism of glucose and lipids, such as glycolysis, gluconeogenesis, citric acid cycle, pentose phosphate pathway, *de novo* lipo-

genesis,  $\beta$ -oxidation, lipolysis, amino acid metabolism and ketone body synthesis have been included (Appendix Figure6). Moreover, transport and excretory reactions between tissues via the blood have also been portrayed, thus ensuring a near-physiological distribution of metabolites. A total of 160 reactions involving 150 metabolites are depicted in the complete model.

### 1.3 Assigning flux distributions

At branch points in the network, approximate values of the metabolite flux distribution into each of the pathway branches were assigned based on a mass isotopomers study and flux analysis in a human hepatocellular carcinoma cell line, HepG2, using labelled  $^{13}\text{C}$  glucose ([6],[11])). Reactions with undetermined fluxes are assigned nominal flux values which allow stable simulations of the model.

## 2 Model Validation

The completed model was put through validation procedures, whereby model simulations of published experimental situations were compared to the experimental data to ensure correspondence. The value of all model variables at steady state has been defined as 1. A disagreement between model simulations and experimental data indicates errors or omitted components, which then need to be identified through a close evaluation of the network and further literature mining.

### 2.1 Simulation of fasting conditions

Fasting results in decreased glucose levels in the blood and hence, decreased insulin and increase in glucagon secretion. Changes in these blood parameters signals an upregulation of gluconeogenesis (synthesis of glucose), a decrease in glycogen stores due to conversion into glucose, decrease in *de novo* lipogenesis due to unavailability of glucose substrate, an increase in  $\beta$ -oxidation to serve as an energy source in the absence of sufficient glucose and an increase in the level of fatty acids in the blood ([8]).

In the *in silico* metabolic model if the component defining the source of mass flow of glucose in reduced by 10-fold, the levels of glucagon increases by 2-fold and insulin decreases by 4.5-fold (Figure1). The simulation of other variables using these parameters depicting fasting results in a close correlation between experimental data and model simulations. A 1.2-fold increase in glucose-6-phosphate levels, a crucial enzyme in gluconeogenesis, a 12.5-fold decrease in glycogen stores,

a 1.25-fold decrease in fatty acid synthase (FAS) levels, a rate-limiting enzyme in de novo lipogenesis, a 1.15-fold increase in carnitine acyl transferase 1 (CPT-1) levels, the first enzyme catalysing  $\beta$ -oxidation and a 1.2-fold increase in fatty acid levels in blood were observed (Figure2).

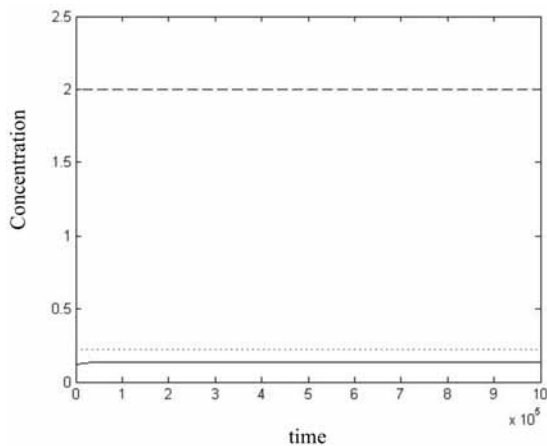


**Figure 1:** Modelling fasting conditions: Solid line- serum glucose levels, dotted line- serum insulin levels, dashed line- serum glucagon levels.

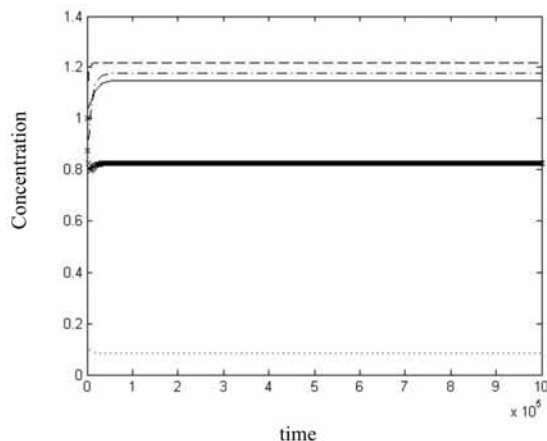


**Figure 2:** Simulation of fasting conditions: Solid line- Carnitine acyl-transferase (CPT-1), dotted line- hepatic glycogen stores, dashed line- glucose-6-phosphatase, dash-dotted line- serum fatty acid levels, thick line- Fatty acid synthase (FAS).

## 2.2 Simulation of the absence of Stearoyl CoA Desaturase-1 (SCD-1)

Stearoyl CoA desaturase (SCD-1) is a crucial lipogenic enzyme that converts saturated fatty acids into monounsaturated fatty acids, which is the major substrate for

triglyceride and cholesterol ester biosynthesis ([12]). Data from an experimental mouse model with null expression of the SCD-1 isoform due to targeted disruption of the gene on a high-fat diet, indicated a downregulation of lipogenic enzymes, decreased accumulation of hepatic triglycerides and plasma leptin and an upregulation of  $\beta$ -oxidation and plasma ketone bodies ([13]).

The equation describing enzyme levels in the metabolic model is as follows:

$$f = C.fi - k \cdot Q \quad (1)$$

where,  $f$  is the real value describing the utilization of the enzyme in the reaction,  $C.fi$  is the initial utilization of the enzyme at steady state,  $k$  is the real value describing the rate of enzyme degradation and  $Q$  is the concentration of the enzyme.

The disruption of SCD-1 in the in silico model was simulated by increasing the value of  $k$  from its initial value of 0.01 to 0.9999. The simulation other variables indicated a 3.3-fold decrease in hepatic triglycerides, 1-fold decrease in plasma leptin and 1.1-fold downregulation of FAS. Furthermore, a 1.47-fold decrease in sterol regulatory element-binding protein 1-c (SREBP1-c), which is a crucial transcription factor regulating de novo lipogenesis, was observed.  $\beta$ -oxidation and plasma ketone bodies were upregulated by 1.7-fold and 1.2-fold, respectively, as observed on simulating the CPT-1 enzyme and  $\beta$ -hydroxybutyrate and acetoacetate plasma concentrations (Figure3). Thus, the model simulations were in close correlation with experimental data. It is important to note that, as the physiological concentration of the metabolites and enzymes is not incorporated into the model, the model simulations provide only relative and not absolute values of variable changes.

## 2.3 Stiffness of fluxes through reactions with $\geq 2$ substrates

Model simulations testing varying values of fluxes through network branch points indicates that only a limited set of flux values can be defined for branch point reactions that involve  $\geq 2$  metabolite substrates. This limited tolerance can be explained for reactions whose substrates are generated via separate network branches as the reaction depends on reaching equilibrium between different pathway branch flux values.

The example of glycerol-3-phosphate acyltransferase has been described here to demonstrate this phenomenon. Glycerol-3-phosphate acyltransferase

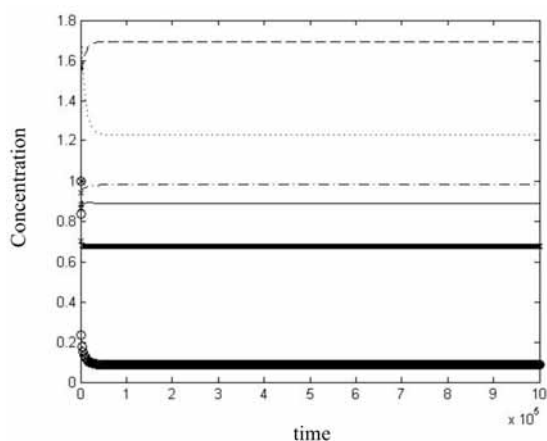


**Figure 3:** Simulation of Stearoyl CoA Desaturase-1 null conditions: Solid line- Fatty acid synthase (FAS), dotted line-serum ketone body levels, dashed line- Carnitine acyl-transferase (CPT-1), dash dotted line- serum leptin, thick line- SREBP1c, double thickness line- hepatic triglycerides.

catalyzes the biosynthesis of lysophosphatidic acid, the first intermediate in the formation of triglycerides. The generation of lysophosphatidic acid depends on the concentration of 2 substrates, glycerol-3-phosphate and fatty acyl CoAs (Figure 4). Hence, the fluxes from the glycolysis pathway as well as the fatty acid synthesis pathway govern the formation of lysophosphatidic acid. The flux through this reaction in the model has been assigned a percentage of 5% of the fatty acyl CoA pool.

On varying the reaction flux percentage to any value  $>10\%$ , the model reached instability, thus suggesting an intolerant focal point within the network. This observation is true for the majority of reactions involving  $\geq 2$  substrates. Interestingly, these reactions are catalyzed by highly-regulated enzymes, thus providing an explanation for the evolutionary development of stringent regulatory mechanisms to ensure the maintenance of the flux within narrow limits, thus preventing disruptions of rate-limiting metabolic reactions. Hence, enzymes catalysing these reactions may signify novel molecular mediators that may play a crucial role in the pathogenesis of NAFLD.

### 3 Discussion

The multi-dimensional nature and complexity of NAFLD has resulted in the poor understanding of the disease pathogenesis. As the progression of NAFLD

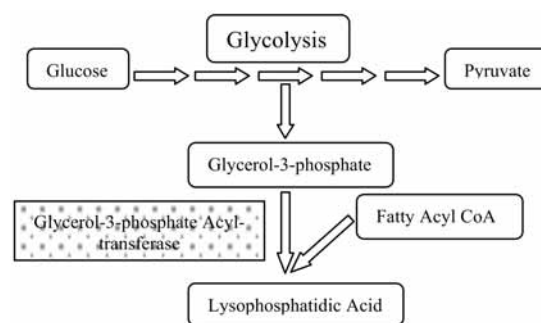


**Figure 4:** Diagrammatic scheme of the reaction catalysed by glycerol-3-phosphate acyl-transferase.

appears to be a result of multiple perturbations or pre-disposition factors, the application of systems biology may provide an additional dimension to the dissection of the disease. The generation of the metabolic network, focussing on tissue-tissue interaction as well as intra-tissue signalling, aims to provide a framework to test various hypotheses of NAFLD initiation and progression by *in silico* simulations and thus prove as a basis for further experimental analysis. The object-oriented differential equation-based model provides an easy to manipulate, dynamic and visual network, which may be made available to the wider scientific community for utilization as a systems biology tool. Due to the interconnected nature of the metabolic and signalling pathways that have been identified in relation to NAFLD, the model size and complexity depicts the intricacy of the disease network.

The future aim of this project is to substantially simplify the network to its core components for further transparency, whilst still maintaining the precision and full functionality of the model. An initial step in model simplification is to reduce linear pathways into single components and clump similarly regulated reactions or reactions for which regulatory mechanism have not yet been identified. In spite of the drawback that the model generation is based solely on evidence from the literature, model simulations that do not correspond to experimental data indicate the presence of unidentified components in the system. Hence, permutations and combinations of various regulatory components for specific reactions may provide a basis for experimental hypotheses to identify novel regulatory mechanisms. This method will also allow further model validation in order to generate a robust model of NAFLD pathogenesis.

In order to enable the generation of more physiological and quantitative simulations, flux data is required

## Appendix

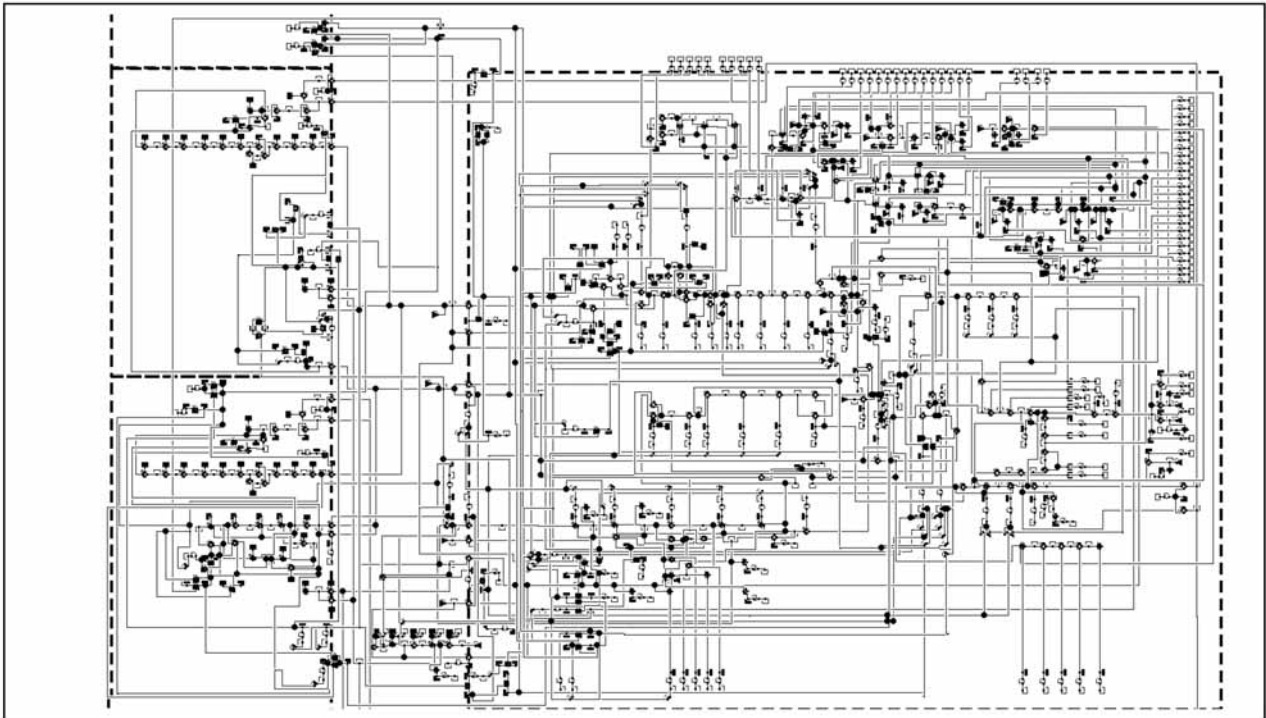


**Figure 5:** Dymola model of NAFLD metabolism. Dashed lines- tissue compartments, straight lines- regulatory signalling pathways and metabolic reactions, black and white shapes- systems biology components (metabolites, proteins, regulatory blocks etc.).

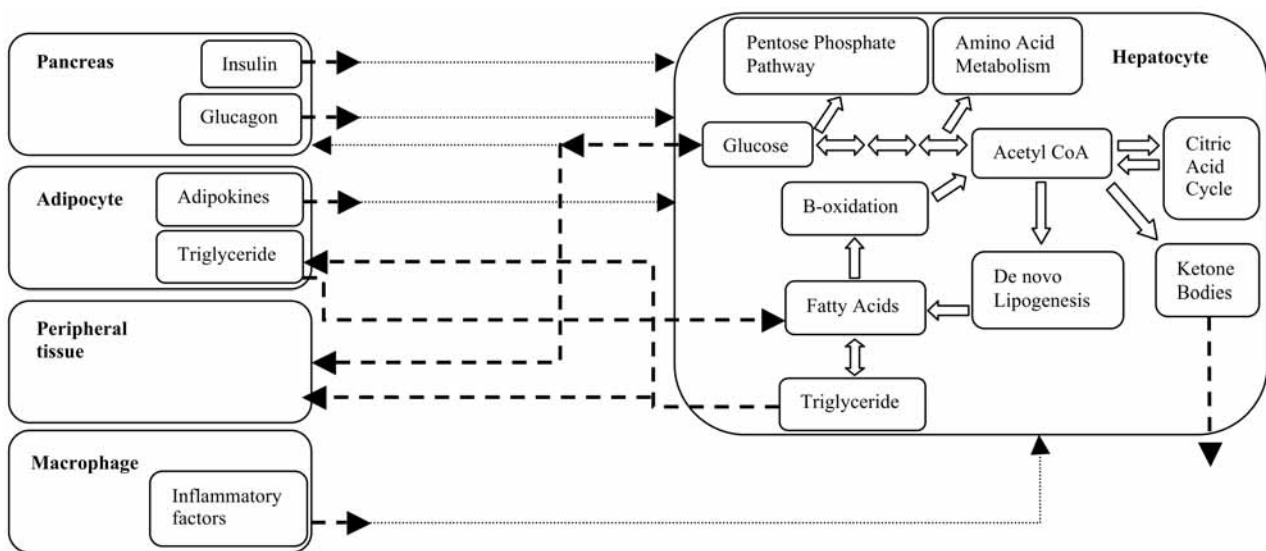


**Figure 6:** Schematic diagram of NAFLD metabolic model. Dashed lines- transport pathways, dotted lines- regulatory signalling pathways.

to be incorporated within the model. The observation of the stiffness of reactions involving  $\geq 2$  substrates indicates the significance of determining the fluxes in metabolic pathways. Moreover, it also suggests that the balance between fluxes in various interconnected pathways within the network is stably maintained. Hence, it may be hypothesised that this balance is disrupted in NAFLD due to various dietary perturbations or genetic predispositions, thus resulting in the accumulation of lipid intermediates. The simulation of probable molecular disruptions or dietary effects within the model may suggest novel mechanisms of lipid accumulation and inflammatory responses, which are characteristic of NAFLD. Furthermore, metabolic flux analysis comparing normal and steatotic experimental models will aid in the identification of pathways with disturbed fluxes in NAFLD pathogenesis.

The diversity in the manifestation of the NAFLD disease spectrum has proved as a major hindrance in effective treatment strategies. Liver biopsy, an invasive and expensive procedure, is the golden standard for diagnosing the progression of NAFLD in patients. The in silico NAFLD model also aims at identifying non-invasive serum markers that correspond to intrinsic perturbations and hence, can predict the transition of NAFLD from relatively benign to more detrimental forms.

## References

- [1] Cohen JC, Horton JD, Hobbs, HH. Human Fatty Liver Disease: Old Questions and New Insights. *Science*. 2011; 332: 1519-1523.
- [2] De Alwis NM, Day CP. Non-alcoholic fatty liver disease: the mist gradually clears. *Journal of Hepatology*. 2008; 48(1): 104-112.
- [3] Donnelly KL, Smith CI, Schwarzenberg SJ, Jessurun J, Boldt MD, Parks EJ. Sources of fatty acids stored in liver and secreted via lipoproteins in patients with nonalcoholic fatty liver disease. *Journal of Clinical Investigation*. 2005; 115: 1343-1351.
- [4] Feist AM, Palsson BO. The growing scope of applications of genome-scale metabolic reconstructions using *Escherichia coli*. *Nature Biotechnology*. 2008; 26: 659-667.
- [5] Gille C, Bolling C, Hoppe A, Bulik S, Hoffmann S, Hubner K, Karlstadt A, Ganeshan R, Konig M, Rother K, Weidlich M, Behre J, Holzhutter HG. HepatoNet1: a comprehensive metabolic reconstruction of the human hepatocyte for the analysis of liver physiology. *Molecular Systems Biology*. 2010; 6: 411.
- [6] Hofmann U, Maier K, Niebel A, Vacun G, Reuss M, Mauch K. Identification of metabolic fluxes in hepatic cells from transient <sup>13</sup>C-labeling experiments: Part I Experimental observations. *Biotechnology and Bioengineering*. 2008; 100: 344-354.
- [7] Hunter P, Robbins P, Noble D. The IUPS human physiome project. *Pflügers Archiv-European Journal of Physiology*. 2002; 445: 1-9.
- [8] Kersten S, Seydoux J, Peters JM, Gonzalez FJ, Desvergne B, Wahli W. Peroxisome proliferator-activated receptor alpha mediates the adaptive response to fasting. *Journal of Clinical Investigation*. 1999; 103: 1489-1498.
- [9] Kohjima, M, Enjoji M, Higuchi N, Kato M, Kotoh K, Yoshimoto T, Fujino T, Yada M, Yada R, Harada N, Takayanagi R, Nakamuta M. Re-evaluation of fatty acid metabolism-related gene expression in nonalcoholic fatty liver disease. *International Journal of Molecular Medicine*. 2007; 20: 351-358.
- [10] Ma H, Sorokin A, Mazein A, Selkov A, Selkov E, Demin O, Goryanin I. The Edinburgh human metabolic network reconstruction and its functional analysis. *Molecular Systems Biology*. 2007; 3: 135.
- [11] Maier K, Hofmann U, Reuss M, Mauch K. Identification of metabolic fluxes in hepatic cells from transient <sup>13</sup>C-labeling experiments: Part II Flux estimation. *Biotechnology and Bioengineering*. 2008; 100: 355-370.
- [12] Miyazaki M, Kim YC, Gray-Keller MP, Attie AD, Ntambi JM. The biosynthesis of hepatic cholesterol esters and triglycerides is impaired in mice with a disruption of the gene for stearoyl-CoA desaturase 1. *Journal of Biological Chemistry*. 2000; 275: 30132-30138.
- [13] Ntambi JM, Miyazaki M, Stoehr JP, Lan H, Kendziorski CM, Yandell BS, Song Y, Cohen P, Friedman JM, Attie AD. Loss of stearoyl-CoA desaturase-1 function protects mice against adiposity. *JProceedings of National Academy of Science USA*. 2002; 99: 11482-11486.
- [14] Romeo S, Kozlitina J, Xing C, Pertsemlidis A, Cox D, Pennacchio LA, Boerwinkle E, Cohen JC, Hobbs HH. Genetic variation in PNPLA3 confers susceptibility to nonalcoholic fatty liver disease. *Nature Genetics*. 2008; 40: 1461-1465.
- [15] Speliotes EK, Yerges-Armstrong LM, Wu J, Hernaez R, Kim LJ, Palmer CD, Gudnason V *et al*. Genome-Wide Association Analysis Identifies Variants Associated with Nonalcoholic Fatty Liver Disease That Have Distinct Effects on Metabolic Traits. *PLoS Genet* 2011; 7(3): e1001324. doi:10.1371/journal.pgen.1001324

# Identification of the Long-Term Effects of Mild to Moderate Neonatal Cerebral Hypoxia Based on EEG Signals Analysis

Aleš Belič<sup>1\*</sup>, Milena Čukić<sup>2</sup>, David Neubauer<sup>3</sup>, Tina Bregant<sup>3</sup>

<sup>1</sup>Faculty of Electrical Engineering, University of Ljubljana, Tržaška c. 25, 1000 Ljubljana, Slovenia;  
\*ales.belic@fe.uni-lj.si

<sup>2</sup>Institute for Neurology, Clinical Center Serbia, Belgrade, Serbia

<sup>3</sup>Pediatric Clinic, University Clinical Center Ljubljana, Slovenia

Simulation Notes Europe SNE 23(2), 2013, 77 - 84  
DOI: 10.11128/sne.23.tn.10185  
Received: Jan. 20, 2013 (Selected MATHMOD 2012 Postconf. Publ.); Revised Accepted: June 15, 2013;

**Abstract.** AbstractHypoxic-ischemic encephalopathy (HIE) during perinatal period is the most common cause of neonatal seizures and is associated with an increased risk of epilepsy in later life. Among newborns affected by perinatal brain injury 20-50% die during the newborn period, and 25-60% of the survivors suffer from permanent neurodevelopmental handicap, including cerebral palsy, seizures, mental retardation, and learning disabilities. In the present study EEG data from 11 patients were analysed with power spectra analysis of the principal components of the EEG signals, fractal dimension estimation and sample entropy estimation. The preliminary results show that the power density properties in the alpha frequency range correlate with learning difficulties of the subjects.

## Introduction

Hypoxic-ischemic encephalopathy (HIE) during perinatal period is the most common cause of neonatal seizures and is associated with an increased risk of epilepsy in the later life. Long-term neurological sequelae in children after HIE can be attributed to both disturbed brain development and functioning as well as tissue loss after hypoxic-ischemic insult. Although delivery can be a critical point, since it presents a shock to a child's organism that can be accompanied with several

complications, hypoxia can occur also prior the delivery due to many causes such as: prolapsed or compressed cord, ruptured uterus, incidents during delivery, etc. Despite the improved pre- and perinatal health care, neonatal encephalopathy still occurs with the incidence of 1-6/1000 [11]. Hypoxia is a situation where oxygen supply to the body is severely reduced and can cause several problems of which the most serious are related to the brain development [10]; [2]; [6]; [7]; [5]. One of the causes for hypoxia is ischemia which is reduced blood flow through the organs. However, as this is still an early stage of life, the affected tissues can recover and the quality of life is not seriously affected. As brain is a very complex organ there are no models to predict the long term effects of perinatal hypoxia on the basis of the hypoxia duration and severity. In our study we analysed data from the long-term observations of children with mild to moderate HIE.

The subjects were examined at the age of 21 and the following tests were performed: Magnetic resonance imaging (MRI), electroencephalography (EEG), and psychological evaluation. The analysis of the test results showed that there is a wide spectrum of possible outcomes that included significantly reduced brain structures, epileptic lability, cerebral paralysis, reduced mental capacity, etc. In most of the subjects EEG analysis showed normal EEG or some epileptic outbreaks. Therefore, the question was raised, how does the EEG correlate with the observed reduced volumes of brain structures, psychological evaluation and HIE grade. HIE grade was performed by Sarnat and Sarnat criterium [9]. The criterium was developed in 1976 and combines clinical and EEG findings of the newborn babies, when only clinical findings are used, it is called modified Sarnat criterium.

The criterium score has three stages: I - mild, II - moderate and III - severe. The following characteristics define the stages:

- I - mild stage:
  - hyper-alert,
  - eyes wide open,
  - does not sleep,
  - irritable,
  - no seizures, and
  - the effect usually last less than 24.
- II - moderate stage:
  - lethargy (difficult to rouse),
  - reduced tone of the extremities and/or trunk,
  - diminished brainstem reflexes (pupil/gag/suck), and
  - possible clinical seizures.
- III - severe stage:
  - coma (cannot be roused),
  - weak or absent respiratory drive,
  - no response to stimuli (may have spinal reflex to painful stimuli),
  - flaccid tone of the extremities and trunk (floppy),
  - diminished or absent brainstem reflexes (pupil/gag/suck),
  - diminished tendon reflexes, and
  - EEG severely abnormal.

In order to analyse the EEG spectral properties as well as complexity of the EEG patterns, principal component analysis, fractal dimension estimation, and sample entropy were used, while the results were compared with HIE score, learning difficulties, and reduced volumes of the brain structures.

## 1 Origins and Measurements of the EEG Signals

EEG signals are measurements of electrical activity of brain obtained by using electrodes on the scalp surface. The magnitude of the measured EEG signal varies with the position of the electrodes and their distance from the electrical source [8]. The measured activity represents the sum of the repetitive and periodic electrical

activity, and most likely originates from the sum of the excitatory and/or inhibitory postsynaptic potentials in large populations of pyramidal cells in the neocortex [8]. Local postsynaptic potentials along the pyramidal cell membranes cause an electrical gradient, and the sum of all the gradients results in an electrical current, which is reflected in an electrical potential that can be measured on the surface of a human scalp [8]. Brain is a large interconnected system of neurons that fire when sufficient level of the signal is sent to their inputs. In order to sense the neuronal activity on the scalp, we need a large group of synchronised neurons that fire simultaneously.

As brain activity is always divided among groups of neurons, the EEG is a sum of all the neuronal groups' activities in the neocortex and some underlying structures. The depth from which EEG can receive signals is limited by the conductive properties of the brain, liquor, bones and scalp. The values of the potentials are in the range of microvolts and need to be attenuated to obtain measurable values. Usually, the measurements are performed in electrically shielded room that filters electromagnetic noise (Faraday cage); however, it is practically impossible to filter out the frequencies of the power lines (50 Hz in EU and most of the world); therefore, notch filters are used to reduce the disturbance.

In parallel to brain signals, muscle artefacts can also be found in the EEG measurements. Most often these artefacts are eye-blinking, swallowing, head motions, and in some cases even breathing and heart rate. All potential must be measured as voltages, meaning that we measure a difference between two potentials. Therefore, a reference electrode must be mounted in the scalp as well and all the potentials are then measured against the reference electrode. Reference electrodes are usually placed on ear lobes, center of the forehead or centrally between the mid forehead and central electrode of the EEG cap. Later on, the values of the electrodes are recalculated on the average value of the electrodes to reject the disturbances that are picked up by all the electrodes. Electrodes are mounted on the cap to ensure secure spatial positioning of the electrodes on the scalp.

There are several standardised systems of electrode mountings, such as international 10-20 system that defines the positions of 32 electrodes as well as its modifications with intermediate electrodes that use 64 or 128 electrodes. Equal stress as for the measuring equipment must be put on the measurement protocol. Measurement protocol must ensure that subject activity is

focused on the processes that are under investigation. As brain parallelly processes large amounts of the information, it is essential that investigated processes are stimulated and the rest of the processes are attenuated by the measurement protocol. Only carefully performed measurements of EEG are useful for more detailed numerical analysis.

In the presented case the measurements were performed on Nicolet One, version 5.7.1., standard EEG apparatus (CareFusion Corporation, San Diego, California, USA). Standard 19 EEG electrode sites and ear lobes were recorded at 256Hz sampling rate, using a bipolar longitudinal montage. We used a set of recording conditions after whole night sleep deprivation using: eye movements and alpha blocking followed by eyes closed resting; eyes open resting; hyperventilation; and photic stimulation. Data were exported and further analysed. An average reference was used for the signals, and the signals were filtered with the 50Hz notch filter and band-pass filter between 0.1Hz and 70Hz. Numerical analysis was performed in Matlab 2009b (The Mathworks inc., Natick, Massachusetts, USA) Eleven subjects were enrolled in the study with mild or moderate HIE.

## 2 Principal Components and EEG

Principal component analysis [3] is frequently used when high-dimensional data is analysed. By high-dimensional data a matrix of signal values that describe the state of the system is meant. There are two important aspects that can be analysed by PCA: dimensionality of the signals, linear dependency of the signals. When the result are reviewed in the context of the observed system, the dimensionality and linear dependence can be interpreted in the frame of system's properties. The dimensionality of the EEG signals is directly linked with the number of most active synchronous groups of neurons which are considered as signal sources. The source identification in the brain is however a lengthy procedure that involves solving inverse problem of electric field computation from dipole sources.

However, the inverse problem does not have a unique solution so some prior assumptions must be made considering the number of sources and their approximate locations before it can be calculated. PCA provides the number of active sources while the activity

indicates the approximate location of dipoles that represent the synchronised groups of neurons. There is, however, one thing that must be mentioned at this stage. Computational activity of the brain usually desynchronises the active regions; therefore, what is expected is that PCA would in fact identify idle regions rather than active ones. However, linear coupling of the inactive regions reduces the effect and PCA is quite effective in finding the number and also some general location of the active regions. If the measurement protocol is well prepared, then PCA can produce significant results. In our case we had several sections of the measured activity as described above. We performed PCA within the sections and on the whole signal. Regardless of the signal or the subject selection there were three most significant components (PC) while the rest can be considered as measurement or background noise.

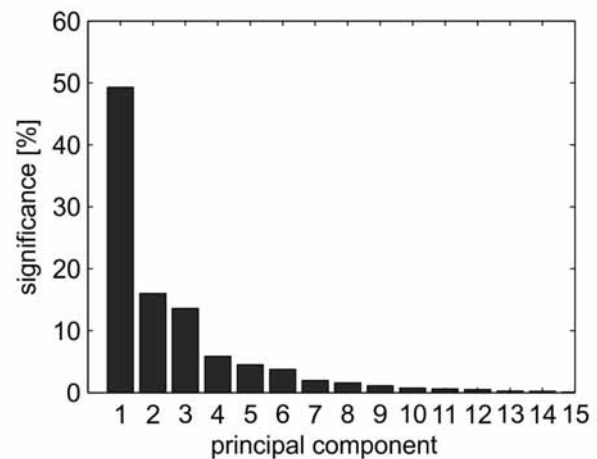


**Figure 1:** A typical significance composition of principal components of the measured EEG signals.

The significance composition of the components is presented in Figure 1. In Figure 1 it can be seen that there is one very significant principal component and two almost equally significant ones. To see, how the three most significant components are composed of the electrode signals, an interpolated plot of the eigenvectors was performed. Each eigenvector component is associated with the contribution of the corresponding signal to the component.

The typical principal component compositions are shown in Figure 2. From the compositions of the PC one can see that first principal component is oriented from frontal to occipital electrodes, suggesting that it originates in the occipital region that receives visual signals from eyes.

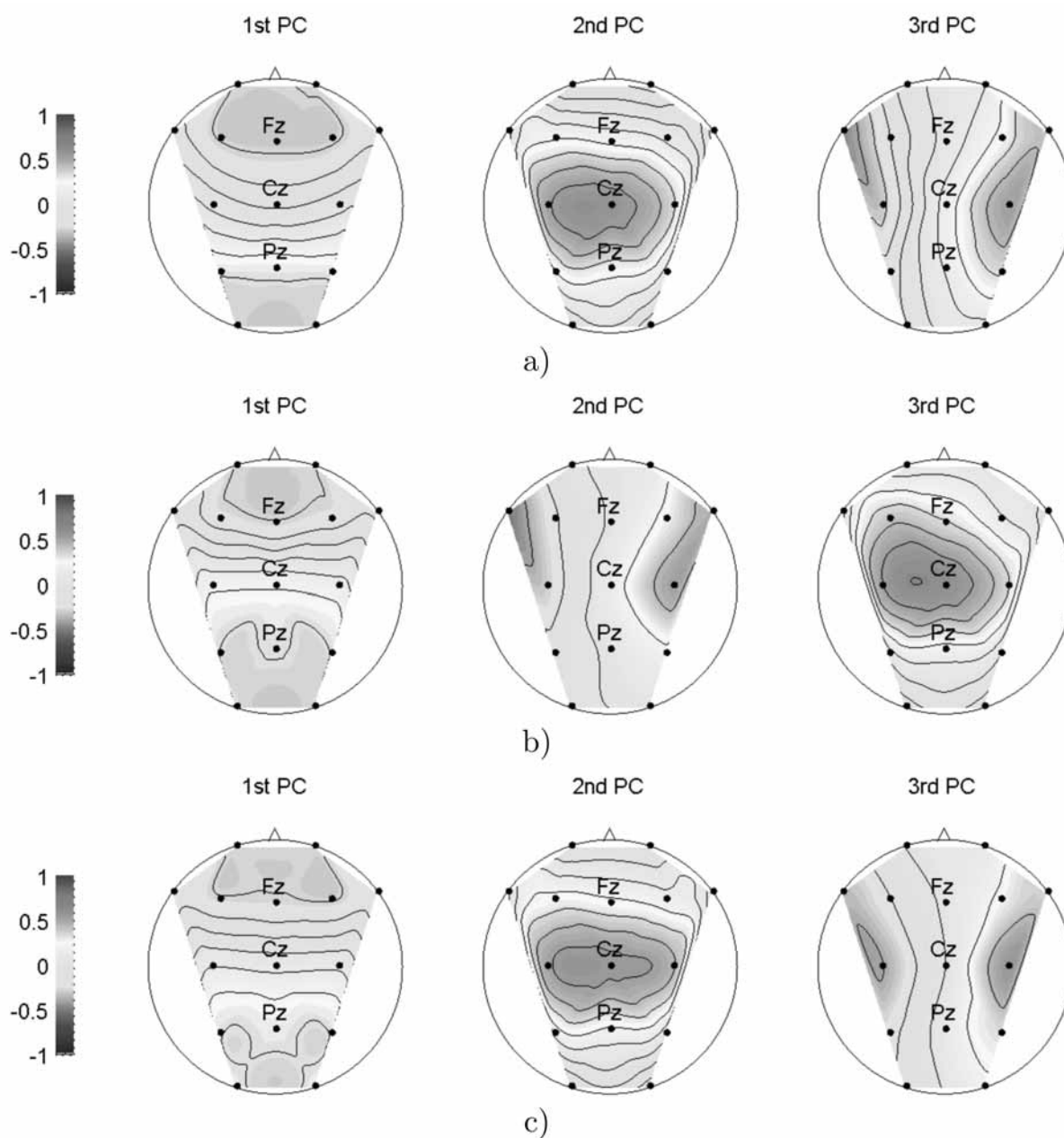


**Figure 2:** A typical compositions of the three most important principal components of the measured EEG signals: a) resting, hyperventilation, b) photic stimulation, c) whole signal.

The assumption is further backed up by the fact that the significance of the first PC rises up to 80% during photic stimulation while it becomes even more polar (see Figure 2 b). The second principal component is oriented upwards with its more or less symmetrical origin in the central region which suggests diaphragm activation during breathing. The interpretation of the third

principal component is not clear and would be discarded, however, its significance is almost the same as for the second component and in some subjects it even positioned as the second component. The compositions of the rest of the components is quite unstable (data not shown).

### 3 Spectral Analysis of the EEG Signals

Spectral analysis of the raw EEG signals showed no significant pattern. The spectral power density showed the usual high power-density values for low frequency signals and approximately exponential decay towards higher frequencies for all subjects. However, spectral analysis of the principal components was more informative. Spectral analysis of the first subject's EEG PC's is shown in Figure 3. In Figure 3 one can see a significant rebound in the alpha rhythm frequency range (8 - 10 Hz). Considering the fact that during measurements the eyes were closed, the rebound was expected in the component that represents the activity of the visual region of the brain. Alpha rhythms are associated with resting and become more dominant when we close the eyes and are known to spread from occipital areas to the front.

### 4 PC Spectral Analysis Relation to Clinical Data

Comparison of spectral analysis of principal components and clinical data showed some interesting relations. Closer inspection of power spectrums of first principal component of the subjects showed, that they can be grouped into two groups regarding the rebound of the spectrum in the alpha frequency range. In one group there were subjects that had an obvious local maximum of the power spectrum located in the alpha range. The next group had no apparent visible local maximum in the alpha range. A power spectra of twins that were included in the study and belonged to different groups are shown in Figure 4. Interestingly, when inspectin clinical data, we could observe that the two groups correlate with learning difficulties of the subjects. All the subjects that had no learning difficulties also had obvious rebounds in the alpha range. Subjects with learing problems had typically no rebound in alpha range, except for one sujet; however the subject had additional psy- chological problems that might have affected the learning abilities.

### 5 EEG Pattern Complexitiy Estimation

To further characteris the properties of the EEG signals, we calculated fractal dimension of the signals from O1 and O2 electrodes, as this seemed to be above the source of the main alpha activity. Higuchi dimension was calculated [1]. However, no correlation with clinical data could be found. In all cases very high values of Higuchi dimension around 2 were obtained, which suggest highly random character od the signals. Next, we calculated sample entropy [4]. Again signals from O1 and O2 were selected for the analysis, however, the results again showed no correlation with clinical findings. The values of the sample entropy were similar for the two electrode signals and ranged from 0.6 to 1.5. More systematic analysis is planned in this field in the future.

### 6 Discussion

The interesting correlation between power spectrum of the first principal components of the EEG signals and learning difficulties of the subjects was an important finding. Although alpha spectrum brain waves are associated with resting, their function, although sometimes controversial, is not irrelevant for the higher functions of the brain. It is known that our memories consolidate during resting, since severe disruption of resting cycle, such as prolonged sleep deprivation, can cause memory problems. Alpha waves are also associated with the long range synchronisations of brain areas that requires good connectivity between several brain regions. Considering hypoxic-ischemic encephalopathy it would be reasonable to expect that HIE can cause connectivity problems in brain that can have different effects on the brain functioning. The size of the brain structures seems to have no direct effect on the connectivity, however, systemic analysis of the brain rhythms can show reduced connectivity through reduced power densities at the frequencies of the major brain rhythms. Surprisingly, the connectivity does not seem to correlate with any of the complexity measures used in this study.

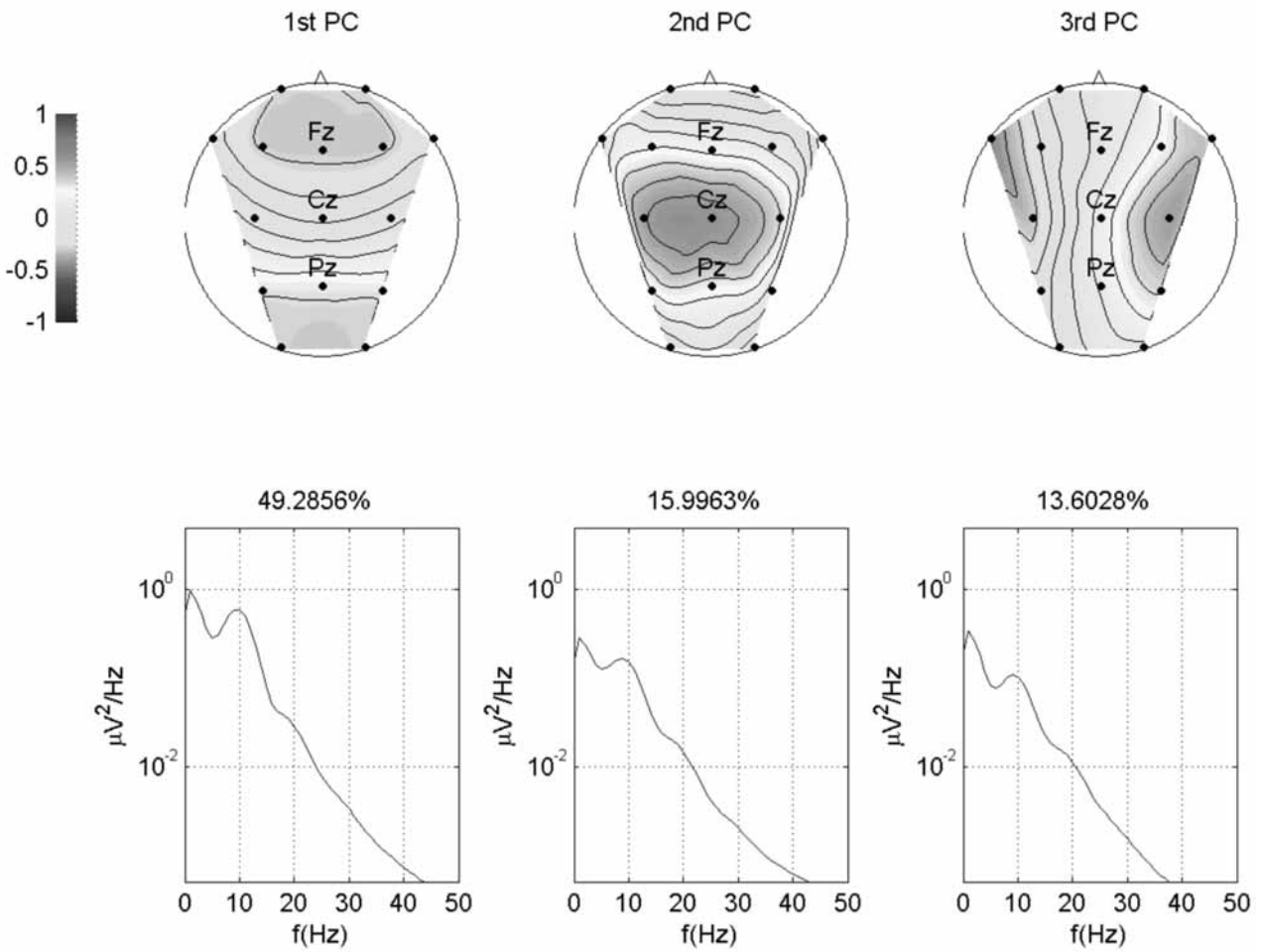


**Figure 3:** A spectra of the principal components of the measured EEG signals of the first subject.

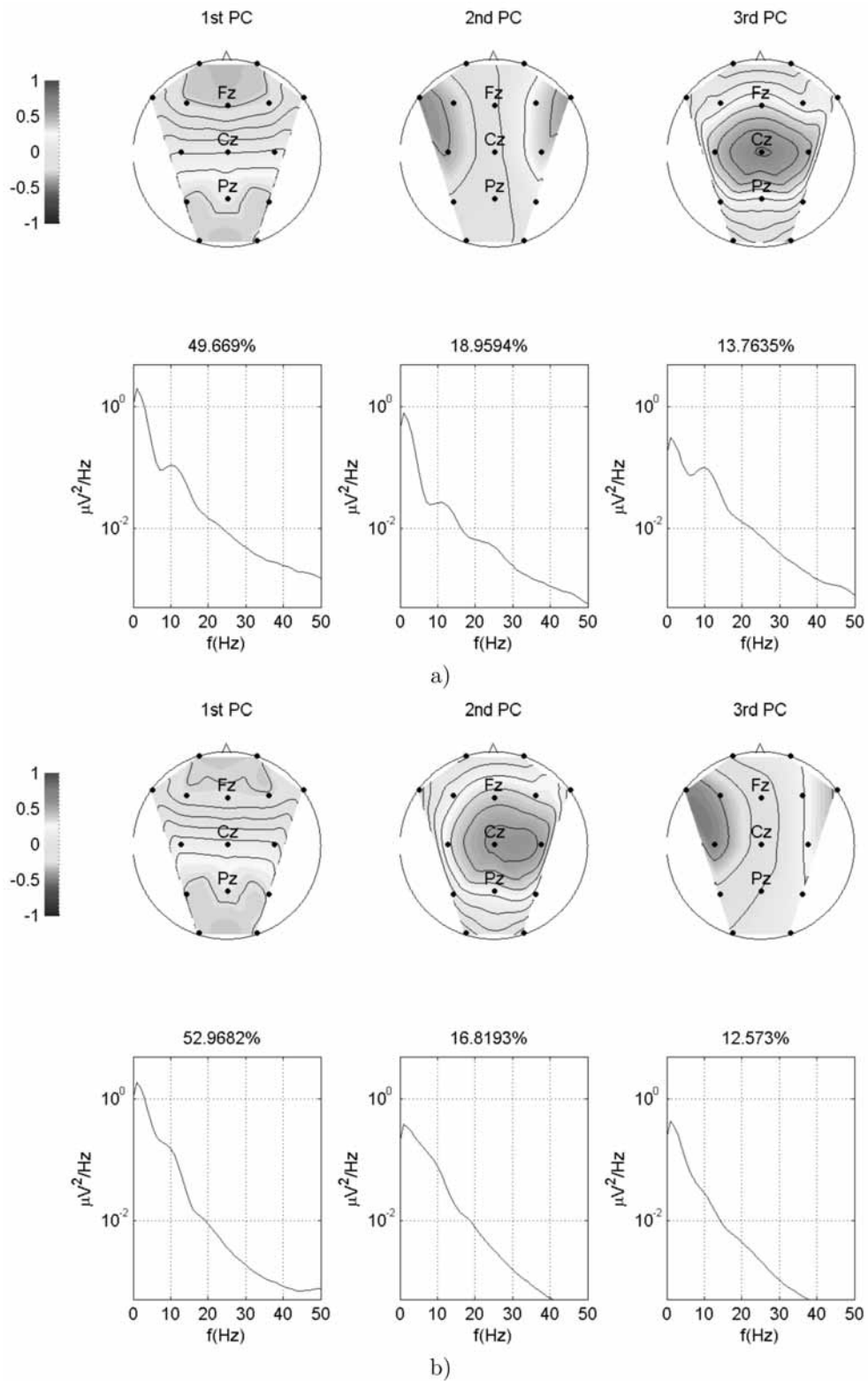


**Figure 4:** A power spectra of twins from different groups according to the alpha range rebound in the spectrum: a) the twin without learning difficulties, b) the twin with learning difficulties.

## References

- [1] Higuchi T. Approach to an irregular time series on the basis of fractal theory. *Physica D: Nonlinear Phenomena*. 1998; 31(2): 277-283. doi:10.1016/0167-2789(88)90081-4.
- [2] Inder TE, Volpe JJ. Mechanisms of perinatal brain injury. *Seminar in Neonatology*. 2000; 5(1): 3-16. doi:10.1053/siny.1999.0112.
- [3] Jackson JE. *A User Guide to Principal Components*. 4th Edition. New York: John Wiley & Sons, inc; 1991. 575p.
- [4] Lake DE, Richman JS, Griffin MP, Moorman JR. Sample entropy analysis of neonatal heart rate variability. *Am J Physiol*. 2002; 283(3): 789-797. doi:10.1152/ajpregu.00069.2002.
- [5] Marlow N, Rose AS, Rands CE, Draper ES. Neuropsychological and educational problems at school age associated with neonatal encephalopathy. Marlow N, Rose AS, Rands CE, Draper ES. Neuropsychological and educational problems at school age associated with neonatal encephalopathy. *Archives of Disease in Childhood-Fetal and Neonatal*. 2005; 90(5): F380-F387. doi:10.1136/adc.2004.067520.
- [6] Mercuri, E, Anker S, Guzzetta A, Barnett A, Haataja L, Rutherford M. Early prognostic indicators in infants with neonatal cerebral infarction: a clinical, eeg and mri study. *Pediatrics*. 1999; 103(1): 39-46. PMID:9917437.
- [7] Mercuri, E, Guzzetta A, Haataja L, Cowan F, Rutherford M, Counsell S, Papadimitriou M, Cioni C, Dubowitz L. Neonatal neurological examination in infants with hypoxic ischaemic encephalopathy: Correlation with mri findings. *Neuropediatrics*. 1999; 30(2): 83-89. PMID:10401690.
- [8] Nuñez PL, Srinivasan R. *TElectric Fields of the Brain: The Neurophysics of EEG*. 2nd Edition. Oxford: Oxford University Press; 2006. 611p.
- [9] Sarnat HB, Sarnat MS. Neonatal encephalopathy following fetal distress - clinical and electroencephalographic study. *Archives of Neurology*. 1976; 33(10): 696-705. doi:10.1001/archneur.1976.00500100030012.
- [10] Vannucci RC. Hypoxic-ischemic encephalopathy. *American Journal of Perinatology*. 2000; 17: 113-120.
- [11] Volpe JJ. *Neurology of the newborn*. 4th Edition. Philadelphia: W.B. Saunders Company; 2001. 912p.

# Burdens of Obesity: Multi-Model Description

Maja Atanasijević-Kunc<sup>1\*</sup>, Jože Drinovec<sup>2</sup>, Tina Sentočnik<sup>3</sup>

<sup>1</sup>University of Ljubljana, Faculty of Electrical Engineering, Tržaška 25, 1000 Ljubljana, Slovenia;

\**maja.atanasijevic@fe.uni-lj.si*

<sup>2</sup>University of Maribor, Faculty for Medicine, Slomškov trg 15, 2000 Maribor, Slovenia

<sup>3</sup>Medico dr. Sentočnik, d.o.o., Levčeva 11, 1000 Ljubljana, Slovenia

Simulation Notes Europe SNE 23(2), 2013, 85 - 92  
 DOI: 10.11128/sne.23.tn.10187  
 Received: Jan. 25, 2013 (Selected MATHMOD 2012 Postconf. Publ.); Revised Accepted: June 15, 2013;

**Abstract.** Obesity was in 1997 by World Health Organization recognized as a disease. It has reached epidemic extensions and as such it has become an important social and economic burden, not only because of itself but also because it is an important risk factor for developing diabetes type 2, hyperdislipidemia and hypertension. These four chronic diseases are known as deadly quartet because they are essentially increasing the development of cardiovascular diseases which have already become the main reason for mortality. In the paper the modeling structure is proposed with which it is possible to evaluate the diseases' burdens important for certain country or population. In this case a number of active and inactive people, overweight and obese, and a number of people with healthy nutrition habits were estimated for Austria and Slovenia. Their influence to development of pre-diabetes and diabetes type 2 is also presented. In addition the costs for health care and also some expectations regarding population ageing are illustrated.

## Introduction

Unhealthy life style very frequent consists of inactivity, stress, improper and/or too rich or abundant food resulting in a number of problems among which the first one is usually overweight. A simple index of weight-for-height (known as body mass index - BMI) is commonly used in classifying overweight and obesity in adult populations. It is defined as the weight in kilograms divided by the square of the height in meters (kg/m<sup>2</sup>).

It provides rough but very useful population-level measure of overweight and obesity as it is the same for both sexes and for all ages of adults [22]. It is important to mention that nowadays physicians pay attention also to waist circumference but this parameter was not taken into account during this study because of the lack of statistical data.

Regarding WHO [22] overweight is defined as a BMI equal to or more than 25, and obesity as a BMI equal to or more than 30. Children were defined as overweight or obese using the 85<sup>th</sup> and 95<sup>th</sup> percentiles of the reference curves. WHO's latest estimations indicate that globally in 2008 approximately 1.5 billion adults (age 20+) were overweight [22].

It is important to point out that overweight and obesity are not the problem only by itself (more difficult movement, not very high self-opinion, social elimination), but they lead also to serious health consequences. Risk increases progressively as BMI increases. Raised body mass index is a major risk factor for chronic diseases such as diabetes type 2, hyperdislipidemia and hypertension, but can evolve also to serious cardiovascular disease (mainly heart disease and stroke), musculoskeletal disorders, and also some cancers [22].

These conditions have also a significant social consequences and economic impact on the health care systems. Medical treatment can be separated into non-pharmacological measures, pharmacological treatment and surgical treatment.

On the other hand costs are frequently regarded as direct and indirect [11], [1]. Direct medical costs include diagnostics and treatment services, while indirect costs are very often caused by health problems because of decreased immune system due to obesity. These patients have to visit their physician more frequently as the people with healthy body mass.

Their rehabilitation time after surgical operations or other health problems is longer, and therefore also the absence from work. Sometimes they need to be requalified, retired and also mortality is among these people earlier. It was estimated that indirect costs are in the same range (sometimes even higher) as direct expenses [2], [3], [4].

In this paper a four – level modeling structure is suggested. The goal is to enable the estimation of social and economic burdens. At the same time also the advantage of the coexistence of different dynamical processes can be taken into account.

The paper is organized in the following manner. In the next section the proposed modeling structure is presented. Some of simulation results are illustrated in the third section where also burden estimations are given. Further also some predictions regarding the problems of population aging are presented. The paper ends with conclusion remarks where also some of the topics for future study are indicated.

### 1 Modeling Process

Proposed modeling structure is illustrated in Figure 1. It consists of four main levels which indicate problem observation from the population perspective. In addition also some other important dynamical processes or modeling results of complementary models can be combined with the results of the main structure.

At the first level therefore the whole observed population is taken into account. The input signal to the second level is a unity step indicating the observation start time that is at birth. At the second level the processes which are defining life style are taken into account. Among them is, as an exception, also obesity as one of the earliest chronic diseases. In the third level the most frequent chronic diseases are indicated, starting with the pre-diabetes which can sometimes be regarded as a curable disease. At the fourth level serious health complication are taken into account.

This representation can be understood as an extension of decision tree formalism [5], [6] which is frequently used in pharmacoeconomical studies [1], [20]. In contrast to classical decision tree it comprises also a time component, namely the age of observed people (or patients). This time component is of crucial importance because the prevalence of great number of diseases is in correlation with patients' age. Another advantage of this

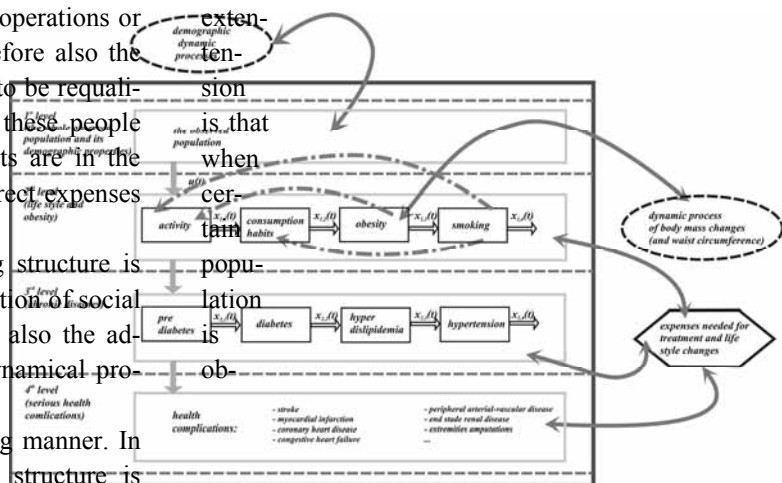


Figure 1 Proposed modelling structure.

served proposed structure responses (prevalence) can be combined with demographic data to evaluate the number of observed people or patients as will be presented in the next section. In addition it is important to point out that this information can further be combined with treatment expenses and so also economic burden can be estimated.

Such representation is very useful when the whole population is taken into account, and when mainly sequential influences are observed. But in some cases such interpretation can be extended to include also dynamical processes at individual level of certain patient or at a group of patients. This can be important also from treatment and prevention activity which can have feedback consequences as indicated in Figure 1.

In this paper one part of the whole structure in Figure 1 is used to present some important aspects of obesity:

- the connections to the main reasons which lead to development of obesity; here activity and nutrition habits are taken into account;
- the influence of obesity to development of other health problems; here different approaches are indicated: the simplest way is to present the average statistical expectations; more demanding approach uses further structural model development;
- estimation of social and economic burdens on the basis of diseases' development; regarding this step it is important to evaluate patients' number and direct and indirect costs in observed population.

Modeling has started taking into account the following important facts. Inactivity is an important risk factor regarding health threatening [13], [10] and it can't be

neglected when body weight is observed. It is not very important during slimming programs, but is very helpful for body mass maintenance. Those people who are active 30 minutes or more at least five days a week are classified as active [8]. Usually activity in men and women slightly differ (men and boys are slightly more active), but average data, which were used for modeling purposes, are summarized in Table 1 [8]. Here also statistical information regarding physical activity of children is included. It is recommended that children are active 60 minutes or more on all seven days per week.

age [years]	0	1	2	3	4	5
average [%]	70	69	68.5	69	70	62
age [years]	6	7	8	9	10	11
average [%]	62.5	69	68.5	64.5	64.5	64
age [years]	12	13	14	15	16-	25-
average [%]	64.5	64.5	58.5	56.5	43	44
age [years]	35-	45-	55-	65-	75+	
average [%]	40.5	36	31	18.5	6.5	

Table 1: Prevalence of activity.

The prevalence of obesity differs from country to country and is also different regarding men and women. An average situation is presented in Table 2 [9]. The ratio between overweight and obese population is slightly changing through the life time, but as these changes are not very distinctive the assumption that it is equal to 1.33 (average value from Table 2) can be taken into account.

age [years]	2-15	16-34	35-54	55-74	75+
average prevalence: 25=<BMI<30 [%]	13.5	27	39	41.5	37.5
Average prevalence: BMI=>30 [%]	16	19	33.5	31.5	22.5
Average prevalence: BMI>=25 [%]	29.5	46	72.5	73	60

Table 2: Prevalence of overweight and obesity.

It is also very well known that people who are overweight or obese are inclined to inactivity, but there is practically no quantitative data available regarding the statistical correlation on the population level among these two variables. The interesting exception represents the paper of Brock [10], where the association between physical inactivity and the prevalence of obesity is described for the USA in the form of linear regression model. Testing this description in comparison to information from Table 2 and developed model response showed that it is expected that the prevalence of obesity is slightly lower in EU countries. Further also nonlinearity can be presumed because of complex involved processes.

Both, inactivity and obesity are very important regarding the development of diabetes type 2 (D2) [21]. It was discovered that most adults (85.4 - 86% in average) with diagnosed diabetes were overweight or obese [15], 52% were obese, and 8.1% had morbid obesity [12].

Before this chronic disease is fully developed patients have a pre-diabetes which in general significantly differ from D2 regarding the fact that when strict life change is adopted taking into account corresponding diet and activity, sometimes complemented by corresponding drug treatment, patients can return to normal condition. Sometimes this transition is (for example due to a long lasting pre-diabetes) not possible, but in such situations D2 development is in most cases significantly postponed. Prediabetes is not a true disease but can be interpreted as a serious risk factor for developing D2 and cardiovascular diseases. Over 30% of people with pre-diabetes develop D2 within five years [21]. The average conversion rate was estimated at 5.8% per year with wide variations which depend on differences in age, BMI, ethnicity, etc..

It is very important to accent that several well-designed randomized controlled trials [21] have been reported that categorically confirm the benefits of interventions in the prediabetes. Standardized diet with reduced food intake, increased physical activity and sometimes also additional drug treatment can reduce the incidence of D2 for almost 60% (in mentioned studies from 25% to 58%). But, it is important to point out that the intensive lifestyle modification was nearly twice as effective in preventing D2. It is therefore evident that an active management of pre-diabetes can be very effective in preventing the progression of diabetes.

For modeling purposes the information given in Tables 3 [16], [14], [17], [21] and 4 [7] was taken into account. Again the average data between men and women are presented.

age [years]	5-11	12-19	20+	40-75	65+
average prevalence [%]	3.7	16.1	35	40	50

**Table 3:** Prevalence of pre-diabetes.

age [years]	25-34	35-44	45-54	55-64	65+
average prevalence [%]	3.5	4.2	8.9	15.5	19

**Table 1:** Prevalence of diabetes type 2.

## 2 Simulation Results

From data given in Tables 1 to 4 it is clear that activity or inactivity, as well as overweight and obesity can together with other diseases be interpreted as dynamical processes where age of people is chosen as an independent variable. In Figure 2 the first modeling result is presented – the prevalence of activity through practically the whole life time.

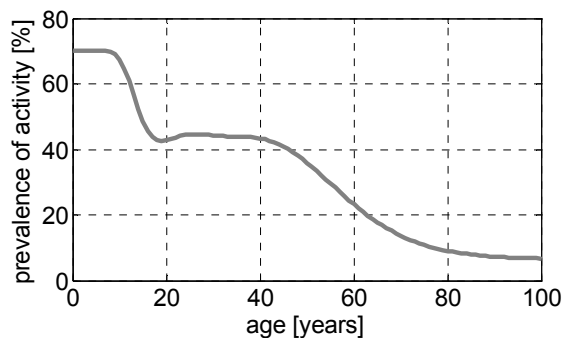


**Figure 2:** Prevalence of activity.

This model response shows that activity is decreasing through the whole life time and is becoming especially intensive after the age of 40. When activity is defined also the prevalence of inactive population is known. The dynamical structure which gives this result was identified so that good matching was achieved with data in Table 1 (dynamical nonlinear model of 11<sup>th</sup> order).

Taking into account all previously mentioned data in the next modeling step also the model (11<sup>th</sup> order with time delays) of overweight and obese population was identified. Responses are presented in Figure 3. It is also possible to differ among overweight and obese taking into account mentioned ratio.

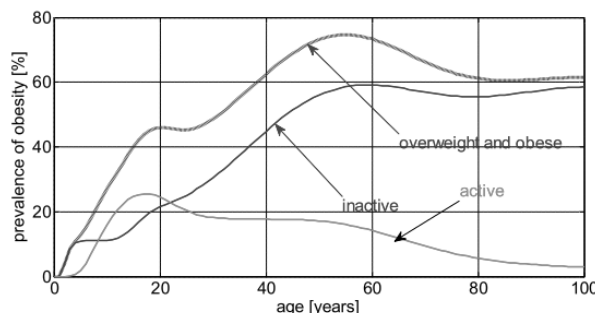


**Figure 3:** Prevalence of overweight and obesity.

Only 15% of all people in observed population have healthy nutrition habits, but they are not from the group of overweight or obese. We have made an assumption that among active population there is two times more such people than from inactive. The results are illustrated in Figure 4.

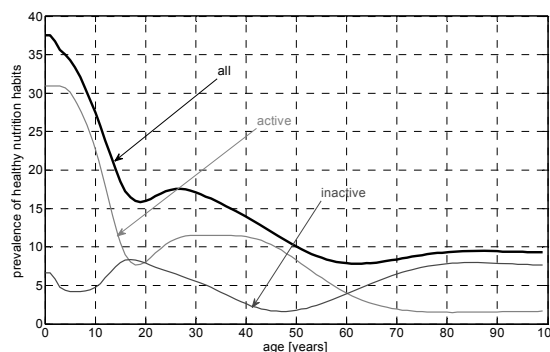


**Figure 4:** Prevalence of healthy nutrition habits.

In Figure 5 model responses are given regarding pre-diabetes (16<sup>th</sup> order model with time delays) and D2 (5<sup>th</sup> order with time delays).

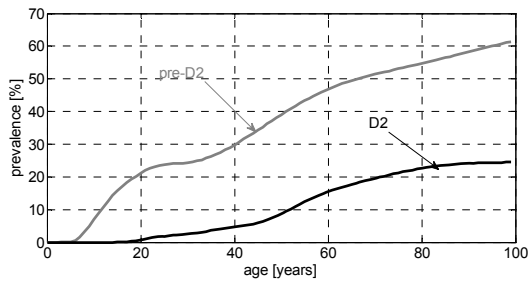


Figure 5: Prevalence of overweight and obesity.

When prevalence of observed processes is calculated, these results can be combined with demographic data for chosen population. We have decided to study and to compare the situation in Slovenia and Austria. In both countries populations are growing older. To estimate contemporary and also possible future burdens, for both countries, population models were developed, taking into account average values of mortality and migrations in the past five years and average fertility among the population from 18 to 45 years [19], [18]. These results are for both countries illustrated in Figs. 6 and 7. For Austria the results are presented only in intervals of ten years.

Now it is possible to combine the presented results and calculate the number of observed groups of people or patients in both countries. In Figure 8 number of active people is illustrated regarding their age. From this it becomes clear that in Austria live 3.2 million people who are active, while in Slovenia this number is over 780 000. For both countries this represents approximately 38% of the whole population.

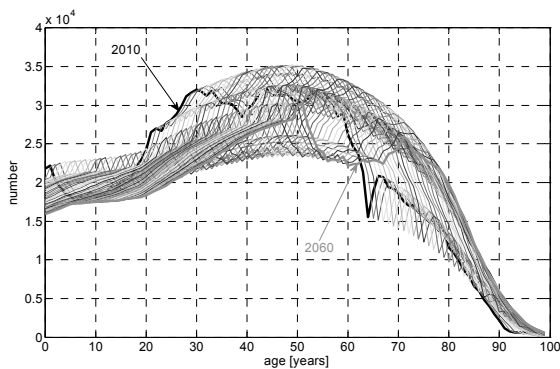


Figure 6: Number of people in Slovenia from 2010 (real number) to 2060 (model prediction).

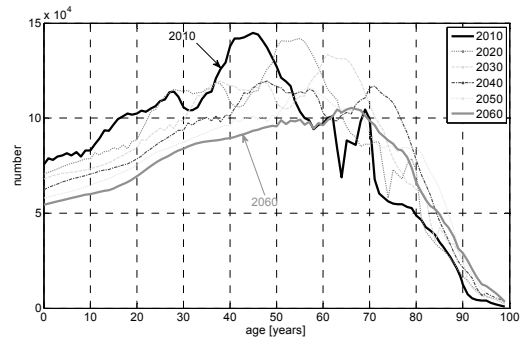


Figure 7: Number of people in Austria from 2010 (real number) to 2060 (model prediction).

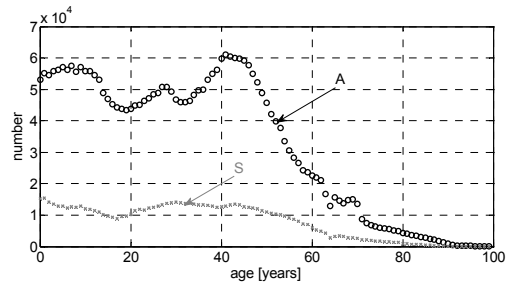
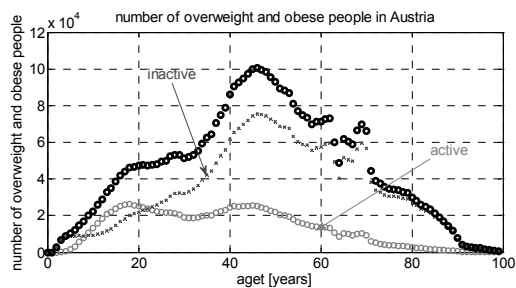


Figure 8: Number of active people in Austria and in Slovenia in 2010.

Regarding the number and distribution of overweight and obese population the situation is illustrated in Figure 9 for Austria, while in Figure 10 normalized distributions regarding patients' number in both countries are compared. In both countries around 55% of population is overweight or obese and the model enables to distinguish among those who are active and those, who are not.

As patients' number and distribution is known also the expenses can be evaluated. Practically all who have unhealthy body mass would like to lose their weight. 40% from the age window of 18 to 60 are experimenting with the drugs which are available without the medical prescription. 30% of people from the same age window are using drugs, prescribed by physician (20%- sibutramin; 80%- orlistat). 80% of patients with BMI>40 need also anti-depressive treatment (fluoxetin). In addition the expenses are needed for these patients due to examination and laboratory. Slovenia and Austria have practically the same costs for drugs, while the prices of medical services are two to three times higher in Austria.

The exceptions are only bariatric operations which are in Austria ten times more expensive than in Slovenia. In Table 5 the expenses are presented needed only for the treatment of overweight and obesity. Cosmetic surgical treatments were not taken into account because these data are not available.



**Figure 9:** Number of overweight and obese people in Austria (4.4 million people or 55% have BMI >= 25).

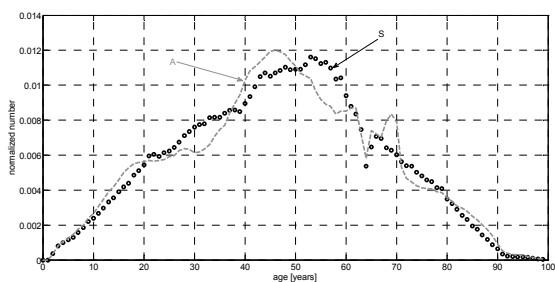


**Figure 10:** Normalized number (regarding the population number) of overweight and obese people in Slovenia and in Austria (55% have BMI >= 25).

The huge expenses are needed for the treatment of consequences of obesity, among which is also diabetes type 2 (D2), to mention only one. In Slovenia there are over 645 000 patients with pre-diabetes (31%) and 159000 (7.8%) with D2. Percentage of these patients is the same in Austria. Normalized distribution of D2-patients is presented in Figure 11 for both countries. For these patients additional 56 million € is needed in Slovenia and 231 million € in Austria.

	Slovenia	Austria
Alli	73 311 606€	288 161 848€
orlistat	167 220 900€	657 284 400€
sibutramin	14 631 750€	57 512 385€
fluoxetine	14 368 050€	56 475 630€
prescriptions+lab.	48 772 710€	383 415 900€
bariatric operations	1 000 000€	8 000 000€
specialists' treatment + medical service	5 838 750€	63 585 000€
	<b>325 143 766€ per year</b>	<b>1 514 435 163€ per year</b>
	159 (318)€/each per year	181 (362)€/each per year
	288 (576)€/each with BMI >= 25 per year	329 (658)€/each with BMI >= 25 per year

**Table 5:** Expenses for patients with BMI >= 25.

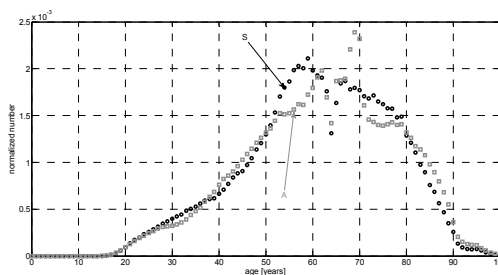


**Figure 11:** Normalized number (regarding the population number) of D2-patients in Slovenia and Austria.

We have to include also indirect expenses, which are of the same range. Each inhabitant of Slovenia has to pay more than 370€ and in Austria more than 410€ per year because of increased body mass in their population. That what is even more concerning is the population distribution in 2010 and expectations for 2060. If D2 prevalence remains unchanged this will influence the distribution of patients, as is for Slovenia illustrated in Figure 12. Number of D2 patients will increase, but only for 16% in Slovenia and 11% in Austria. But as the number of young people is decreasing the ratio between D2 patients and active population will increase for almost 50% in both countries.

A great number of mathematical models is available to compute energy - balance strategies for healthy body mass reduction [6]. But, two main obstacles can be identified regarding this important social and economic aspect: relative low budget for prevention purposes and insufficient integrative treatment activities which would increase efficacy of slimming process.

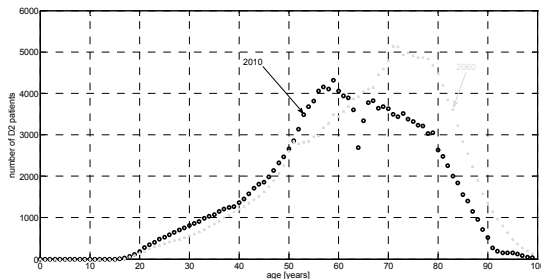


Figure 12: Number of D2-patients in Slovenia in 2010 and 2060.

### 3 Conclusions

In the paper modeling structure is introduced, which can be used for estimation of economic and social burdens of different diseases. It also enables the combination of modeling results, what was used for estimation of overweight and obesity burdens in Slovenia and Austria. In the future the strategy with which this burden could be decreased, will be investigated.

### References

- [1] Arnold RJG, Editor. *Pharmacoeconomics, From Theory to Practice*. Boca Raton: CRC Press, Taylor & Franics Group, Drug Discovery Series/13; 2010.
- [2] Atanasijević-Kunc M, Drinovec J, Ručigaj S, Mrhar A. Modelling of risk factors and chronic diseases that influence the development of serious health complications. *Slovenian Medical Journal*. 2008a; 487-98.
- [3] Atanasijević-Kunc M, Drinovec J, Ručigaj S, Mrhar A. Modeling the influence of risk factors and chronic diseases on the development of strokes and peripheral arterial-vascular disease. *Simulation Modelling Practice and Theory*. 2008b; vol. 16 (8), 998-1013.
- [4] Atanasijević-Kunc M, Drinovec J, Ručigaj S, Mrhar A. Simulation analysis of coronary heart disease, congestive heart failure and end-stage renal disease economic burden. *Mathematics and Computers in Simulation*. 2011. <http://dx.doi.org/10.1016/j.matcom.2010.10.024>
- [5] Atanasijević-Kunc M, Drinovec J. Burden of diabetes type 2 through modelling and simulation. *Topics in the prevention, treatment and complications of type 2 diabetes*. Zimering, M. B. (Ed.). Rijeka: InTech, cop.; 2011a; 3-28.
- [6] Atanasijević-Kunc M, Drinovec J. Social and economical burden of obesity - multi-model analysis. *Proceedings of the ITI 33 rd International Conference on Information Technology Interfaces*. 2011b; ITI, 509-514.
- [7] Behl GFE, Copeland JA, Wiggins J. The District of Columbia Diabetes Surveillance Report. Washington, DC: DC Department of Health; 2004. [#search=%22columbia%20diabetes%20prevalence%22](http://dchealth.dc.gov/doh/lib/doh/services/special_programs/diabetes/pdf/final_data_and_stat_diabetes.pdf)
- [8] British Heart Foundation Statistics Website – BHFSW. *Age differences and physical activity*. 2008. <http://www.heartstats.org/atozpage.asp?id=4955>.
- [9] British Heart Foundation Statistics Website – BHFSW. *Trends in the prevalence of overweight and obesity*. 2010. <http://www.heartstats.org/datapage.asp?id=1011>.
- [10] Brock DW, Thomas O, Cowan CD, Allison DB, Gaesser GA, Hunter GR. (2009). Association Between Insufficiently Physically Active and the Prevalence of Obesity in the United States. *Journal of physical activity & health*. 2009; 6(1): 1-5.
- [11] CDC - Centers for Disease Control and Prevention. *Overweight and Obesity*. 2011. <http://www.cdc.gov/obesity/defining.html>.
- [12] Daousi C, Casson IF, Gill GV, MacFarlane IA, Wilding JPH, Pinkney JH. Prevalence of obesity in type 2 diabetes in secondary care: association with cardiovascular risk factors. *Postgraduate Medical Journal*, 2006; 82: 280-284. doi:10.1136/pmj.2005.039032.
- [13] Defay R, Delcourt C, Ranvier M, Lacroux A, Papoz L. Relationships between physical activity, obesity and diabetes mellitus in a French elderly population: the POLA study. *International Journal of Obesity*. 2001; 25(4): 512-518.
- [14] Li C, Ford ES, Zhao G, Mokdad AH. Prevalence of Pre-Diabetes and Its Association With Clustering of Cardiometabolic Risk Factors and Hyperinsulinemia Among U.S. Adolescents. *Diabetes Care*. 2009; 32(2): 342-347.

- [15] MMWR. Centers for Disease Control and Prevention (CDC). Prevalence of Overweight and Obesity Among Adults with Diagnosed Diabetes - United States, 1988-1994 and 1999-2002. *Morbidity and Mortality Weekly Report (MMWR)*. 2004; 53(45): 1066-1068. <http://www.cdc.gov/mmwr/preview/mmwrhtml/mm5345a2.htm>.
- [16] Narayanappa D, Rajani HS, Mahendrapa KB, Prabhakar AK. Prevalence of Prediabetes in School-Going Children. *Indian Pediatrics*. 2011; 48:295-299.
- [17] NDS. U.S. Department of Health and Human Services, National Institutes of Health. National Diabetes Statistics. *NIH Publication*. 2011; 11:3892. [http://diabetes.niddk.nih.gov/DM/PUBS/statistics/DM\\_statistics.pdf](http://diabetes.niddk.nih.gov/DM/PUBS/statistics/DM_statistics.pdf).
- [18] Statistik Austria, <http://www.statistik.at>. 2011.
- [19] Statistical Office of the Republic of Slovenia, <http://www.stat.si/eng/index.asp>. 2011.
- [20] Stahl JE. Modelling Methods for Pharmacoeconomics and Health Technology Assessment, An Overview and Guide. *Pharmacoeconomics*. 2008; 26(2), 131-148, ISSN 1170-7690.
- [21] Valensi P, Schwarz P, Hall M, Felton AM, Maldonato A, Mathieu C. (2005). Pre-diabetes essential action: a European perspective. *Diabetes & Metabolism*. 2005; 31(6), 606-620.
- [22] WHO - World health organization. Obesity and overweight. *Fact sheet No. 311*. 2011. <http://www.who.int/mediacentre/factsheets/fs311/en/>.

# Modeling Elastic Walls in Lattice Boltzmann Simulations of Arterial Blood Flow

Xenia Descovich<sup>1,4\*</sup>, Giuseppe Pontrelli<sup>2</sup>, Sauro Succi<sup>2</sup>,  
Simone Melchionna<sup>3</sup>, Manfred Bammer<sup>4</sup>

<sup>1</sup>Vienna University of Technology, Institute of Analysis and Scientific Computing, Vienna, Austria;  
\**xenia.descovich@tuwien.ac.at*

<sup>2</sup>Consiglio Nazionale delle Ricerche, Istituto per le Applicazioni del Calcolo, Rome, Italy

<sup>2</sup>Consiglio Nazionale delle Ricerche, Istituto Processi Chimico-Fisici, Rome, Italy

<sup>4</sup>AIT Austrian Institute of Technology GmbH, Vienna, Austria

Simulation Notes Europe SNE 23(2), 2013, 93 - 100  
DOI: 10.11128/sne.23.tn.10189  
Received: Jan. 10, 2013 (Selected MATHMOD 2012 Postconf. Publ.); Revised Accepted: June 15, 2013;

**Abstract.** An essential part in the simulation of blood flow in arteries is the incorporation of the arterial elasticity by modeling the vessel wall and its interaction with the fluid inside the vessel. We suggest a simple approach for modeling elastic walls in lattice Boltzmann simulations of arterial blood flow that produces physically correct results. We have developed a simulation software that implements this approach combined with the lattice Boltzmann method and conducted numerical experiments on a generic vessel model. Preliminary results presented in this work are promising and encourage using this method for further simulations with real physiological parameters in medical applications.

## Introduction

Cardiovascular diseases are the most common cause of death in industrialized countries [1]. Since experimental methods in the cardiovascular system are difficult and limited, mathematical models and numerical methods to simulate the hemodynamic processes have gained importance in the past years. Research in that domain includes studies incorporating the whole arterial tree [2] as well as studies of only parts of it, e.g. a segment of an artery [3].

Since arteries are elastic and change in diameter depending on the blood pressure inside (which oscillates due to the periodic pumping of the heart), it is of particular importance to incorporate this elasticity in models of physiological flows in blood vessels.

Common numerical methods for blood flow simulations with elastic walls are complex. We present a simple method for modeling the blood flow in an artery and the elastic walls of the vessel. The flow field inside the vessel is computed by using the lattice Boltzmann method, which is a numerical approach for solving problems of computational fluid dynamics. In the lattice Boltzmann simulation, we include the developed model for the elastic walls. The model fulfills the essential properties of an elastic wall and respects the basic conservation laws.

This paper shows a short overview of the lattice Boltzmann method and its use in hemodynamics in Section 1. In Section 2, we present the method to model the elastic vessel wall. Numerical experiments presented in Section 3 show that the developed approach provides correct physical behavior. Section 4 gives an outlook on the possible application of the method in the simulation of blood flow in stented arteries.

## 1 Lattice Boltzmann Method

The lattice Boltzmann (LB) method is a mesoscopic approach based on the Boltzmann equation and can be used to solve various problems of computational fluid dynamics. It describes the dynamics of fictitious particles on nodes of a regular lattice.

The dynamics of the flow field are modeled by the

evolution of density distribution functions (also called 'populations')  $f_i(\mathbf{x}, t) = f_i(\mathbf{x}, \mathbf{c}_i, t)$ ,  $i = 1, \dots, q$ , which describe the probability of finding at time  $t$  a particle located at site  $\mathbf{x}$  and traveling along the lattice in direction  $i$  with the speed  $\mathbf{c}_i$ . For a more detailed introduction to the LB method the reader is referred to [4] and [5].

### 1.1 LBGK model for blood flow simulation

The lattice Boltzmann method has been successfully applied to hemodynamics by many authors [6, 7, 3, 8], which has proven its value as an alternative to numerical methods based on the discretization of the Navier-Stokes equations of continuum mechanics.

For our simulations of the blood flow, we consider a so-called D2Q9 model (2 spatial dimensions, 9 directions  $i$ ) and calculations are based on the lattice Boltzmann equation with single-time relaxation (LBGK approximation)

$$f_i(\mathbf{x} + \mathbf{c}_i \Delta t, t + \Delta t) - f_i(\mathbf{x}, t) = \omega \Delta t (f_i - f_i^{eq})(\mathbf{x}, t) \quad (1)$$

with  $\Delta t$  being the temporal resolution and  $\omega$  being the relaxation frequency. The right-hand side of (1) represents molecular collisions through a relaxation towards local equilibrium  $f_i^{eq}$  which is given by a second-order expansion of the Maxwell-Boltzmann equation. The fluid density  $\rho$  and the momentum  $\rho \mathbf{u}$  are defined based on the distribution functions  $f_i$ :

$$\rho = \sum_{i=0}^8 f_i \quad (2)$$

$$\rho \mathbf{u} = \sum_{i=0}^8 f_i \mathbf{c}_i \quad (3)$$

Since we focus on large arteries, the flow in the vessel can be assumed to be Newtonian. Investigation of non-Newtonian flows in hemodynamics can be found elsewhere [9].

### 1.2 Elastic walls

In simulations of blood flow, it is important to consider the compliance of the vessel. Therefore, a model for the vessel wall has to be developed that describes its spatial displacement as it interacts with the flow dynamics. Fang *et al.* [6], for example, uses a parametrization of the vessel wall with special treatment for curved boundaries.

The method has been successfully applied to unsteady flow in elastic tubes in two dimensions (see [10]). However, the method is very complex in three dimensions where the vessel wall is described by means of surfaces.

For our approach, we have developed a simple method to model the elastic vessel which does not need a parametrization of the wall. It is based on the method of Leitner [3] and acts strictly locally like the LB method itself. By this, the complexity of the algorithm is not increased and the method can be used for simulations in two and three dimensions.

In the method of Leitner [3], lattice nodes can have two different states: fluid, representing the blood inside the vessel, and solid, describing the vessel wall. The compliance of the wall is modeled by changing the type of a node – from solid to fluid in the case of expansion and vice versa in the case of contraction of the vessel. This change of node type, which models the displacement of the wall, is dependent on the local pressure of the surrounding fluid nodes. To avoid a rupture of the vessel wall, Leitner [3] uses a cellular automaton (CA) with rules to update the wall in every simulation time step.

In the following section, we present an improved method to model the elastic wall that does not require the use of cellular automata.

## 2 Improved Method to Model Elastic Vessel Wall

Our approach for the elastic wall is based on the work of Leitner [3] which uses node type changes in a lattice as mentioned above to model the displacement of the wall. In order to ensure mass conservation in the model, we developed methods that redistribute the populations when a node changes its type. Node type changes are based on the local fluid properties and are performed by means of pressure thresholds, which will be explained below.

## 2.1 Wall modeling

We consider a computational domain of dimensions  $N_x \times N_y$ , where  $N_x$  and  $N_y$  are the number of lattice nodes (equally spaced) in direction  $x$  and  $y$ , respectively. Each node  $(x, y)$  can have two different states: fluid or solid. Solid nodes represent the tissue of the vessel, fluid nodes represent the blood inside the vessel. The initial configuration of solid and fluid nodes is gained by reading the data from a PGM binary image. Contrary to the modeling described by Leitner [3], the wall of the vessel is not situated on the solid nodes but is imagined to be located between the last fluid and first solid node in a given direction. All nodes that are not fluid are by default solid. Thus, the problem of rupture of the vessel wall does not occur and the approach does not require the use of CA.

In the following, the terms *destruction* and *creation* of nodes are used to signify the state change of a node. One must be aware that in this type of modeling, nodes are neither destroyed nor created – the geometrical domain being fixed of dimensions  $N_x \times N_y$  – but that nodes change only their type. The state change 'fluid to solid' will be termed as *destruction* and 'solid to fluid' as *creation*.

Created fluid nodes need to be initialized with values of the density  $\rho$  and the velocity  $\mathbf{u}$  (corresponding to the momentum  $\rho\mathbf{u}$ ). This is done by averaging the populations from the fluid nodes surrounding the new fluid node (one average for each direction  $i$ ) and assigning these values to the new node. The values of  $\rho$  and  $\mathbf{u}$  can be computed based on the assigned values of the distribution functions  $f_i$  by using (2) and (3). Compared to the method of Leitner [3], who initializes new fluid nodes with an equilibrium distribution function, this approach includes also the non-equilibrium part of the populations, which is not negligible for nodes in proximity of the wall.

A mass conservation problem arises when nodes are created or destroyed in a way that the total number of fluid nodes changes. Mass is a priori not conserved as mass is added when initializing a new fluid node or subtracted when a fluid node is destroyed. Leitner [3] does not refer to this problem, and it is not clearly evident how it is circumvented. In order to ensure mass conservation in our approach, we have developed methods that rescale the populations in a part of the domain when a node type change occurs.

## 2.2 Population rescaling methods

Mass conservation is imposed each time fluid nodes change their type (from solid to fluid in the case of expansion and vice versa in the case of contraction of the vessel). Below, we present two methods to rescale the populations.

**Local Rescaling.** The local rescaling takes into account only the nearest neighbors of the node changing its state. At expansion, mass (density) is redistributed in the following way: Let  $(x, y)$  be a node changing its state from solid to fluid and  $\sum \rho_{nb}$  the sum of the densities at fluid nodes neighboring node  $(x, y)$ . After initializing the new

fluid node  $(x, y)$ , its populations and those from the neighboring fluid nodes are rescaled by the factor  $\frac{\sum \rho_{nb}}{\sum \rho_{nb} + \rho(x, y)}$ . Density and velocity are computed based on these new populations. In this way, mass is conserved. The scaling factor is equal to the fraction  $\frac{\text{old local mass}}{\text{new local mass}}$  and is smaller than 1. This approach models the transfer of mass to a new fluid node from the neighboring nodes.

In a similar way, mass is redistributed locally when a fluid node is destroyed, i.e., when a node changes its state from fluid to solid (contraction). The scaling factor is again  $\frac{\text{old local mass}}{\text{new local mass}}$  and is in this case greater than 1. All fluid nodes surrounding the disappearing fluid node are rescaled by this scaling factor. By this procedure, mass is transferred from the destroyed node to the neighboring fluid nodes.

The local rescaling influences the flow field in the vessel only locally. Depending on the fluid viscosity and the vessel geometry, it takes a certain time until this perturbation of the flow field is damped in the simulation.

**Rescaling 'by columns'.** This method of rescaling takes into account the whole column of nodes - the vessel can be considered as a sequence of 'rings' adjacent to each other – in which a node type change occurs. When a node next to the wall changes its state (from solid to fluid or vice versa), the populations of every node in the same column are rescaled to ensure mass conservation (a rescaling factor similar to the one above is used.)

### 2.3 Pressure thresholds

Node type changes occur depending on the local pressure surrounding a given node. In our model, pressure thresholds are assigned to each node, increasing with the radius of the vessel segment. Nodes that are further away from the center of the vessel have a higher threshold that has to be exceeded for an outwards displacement of the wall, i.e., for changing the type of the neighboring solid node to fluid.

A linear relationship between the pressure  $p$  and the radius  $R$  is assumed, similar to the one of the pulmonary blood vessels (see [11]):

$$p = p_0 + \alpha(R - R_0) \quad (4)$$

Here,  $\alpha$  is a compliance constant.  $R_0$  is the radius when the transmural pressure is zero and  $p_0$  the pressure at a node located at distance  $R_0$  from the center of the vessel. The linear pressure-radius relationship is a good approximation for large arteries [10].

Pressure thresholds are computed based on this linear relationship and assigned to each node. Since the vessel is embedded in a lattice of fixed dimensions, there are nodes that can never become fluid considering that there is a maximum expansion of the vessel. To all those nodes, a pressure threshold exceeding the allowed pressure range is assigned. This prevents that, in the simulation, the vessel expands more than is physiologically possible.

Our model uses the precomputed thresholds to simulate wall displacement by appropriate node type changes. The following shall exemplarily explain our procedure of node type changes based on the pressure thresholds. Let  $(x, y)$  be a solid node neighboring a fluid node  $(x, y - 1)$  at the upper wall of the vessel. The wall is imagined to be located between those two nodes. Let  $p_t(x, y)$  be the pressure threshold of node  $(x, y)$ . If the pressure at node  $(x, y - 1)$  exceeds  $p_t(x, y)$ , i.e.  $p(x, y - 1) > p_t(x, y)$ , the node  $(x, y)$  becomes fluid, i.e., the vessel expands. Conversely, let us suppose that the nodes  $(x, y)$  and  $(x, y - 1)$  are both fluid. If  $p(x, y) < p_t(x, y - 1)$ , node  $(x, y)$  changes its state from fluid to solid, i.e., the vessel contracts.

## 3 Simulation and Preliminary Results

We implemented a simulation software for the lattice Boltzmann algorithm combined with our elastic wall model using the programming language C. The program includes the rescaling methods and the pressure threshold algorithm described above. Using our software program, we conducted numerical experiments to show the feasibility of our approach.

### 3.1 Numerical experiments

The main objective of the numerical experiments presented here is to prove that the model provides correct physical behavior. Simulation with real physiological conditions will be performed in a later work.

For our experiments, we consider a straight channel with flat walls modeling the vessel. We impose periodic boundary conditions in direction of the channel to model an infinite long tube. This condition will be replaced by inlet/outlet boundary conditions in a later work. At the wall, we impose bounce-back boundary conditions which represent a no-slip condition (i.e., the fluid velocity at the wall is zero.) Furthermore, the pressure is increased 'manually' at a certain time, just enough to provoke an increase of the channel radius of one unit (expansion), and at a later time decreased again, just enough to induce a decrease of the radius of one unit (contraction). Thus, we investigate the behavior of the flow field for only one cycle of expansion and subsequent contraction (of the whole channel). The uniform pressure increase/decrease is used only to test the method. In a later stage, it will be replaced by an oscillating pressure gradient at the inlet simulating the periodic pumping of the heart.

For the simulation, the following physical parameters are used: viscosity  $\nu = \frac{1}{3}$ , maximum velocity  $U_{max} = 0.01$ , and initial density  $\rho_0 = 1.0$ . All parameters and variables are normalized and thus dimensionless. The computational domain is fixed with  $200 \times 100$  nodes.

As mentioned above, a straight channel is considered having the macroscopic variables  $\rho$  (and thus  $p$ ) and  $\mathbf{u}$  at nodes with the same  $y$ -coordinate equal, respectively. Furthermore, all nodes with the same  $y$ -coordinate have the same pressure threshold. By this, the flat wall of the straight channel is displaced at all nodes with the same  $y$ -coordinate (i.e., one layer of nodes) within a single time step.

To induce an expansion in our model, the pressure is increased manually by adding an amount  $\Delta p$  to the pressure of all fluid nodes at a certain time  $t_{add}$  and then decreased again at time  $t_{sub} > t_{add}$ . We chose  $\Delta p$  so that the wall is moved by only one layer at the lower and upper boundary. Due to the forced increase (decrease) of pressure at  $t_{add}$  ( $t_{sub}$ ), mass increases (decreases) by a value proportional to  $\Delta p$  at  $t_{add}$  ( $t_{sub}$ ).

In order to check whether the implemented method provides correct physical behavior, the following steps are executed:

1. Wait for fully developed flow (until time  $t_0$ ).
2. At time  $t_0$  ( $= t_{add}$ ), when flow is fully developed, add mass by adding a small value  $\Delta f_i$  to the populations  $f_i$  at each node. This corresponds to an increase of pressure by  $\Delta p = c_s^2 \Delta \rho$  in each node, with  $\sum_{i=0}^8 f_i$  and  $c_s = 1/\sqrt{3}$  being the speed of sound. Then wait for the flow to be fully developed (until time  $t_1$ ).
3. At time  $t_1$ , expansion occurs because the pressure thresholds at the wall are exceeded due to the increase of pressure at time  $t_0$ . The channel is expanded by one layer at the upper and lower wall, respectively. The populations  $f_i$  are rescaled so as to ensure mass conservation. Then wait for fully developed flow (until time  $t_2$ ).
4. At time  $t_2$  ( $= t_{sub}$ ), reduce mass by subtracting  $\Delta f_i$  from the populations  $f_i$  at each node. This corresponds a decrease of pressure. Wait again until flow is fully developed (until time  $t_3$ ).
5. At time  $t_3$ , contraction occurs because the pressure has fallen below the pressure threshold due to the decrease of pressure at time  $t_2$ . The radius of the channel is reduced by one unit, so one layer of nodes is destroyed at the lower and upper wall, respectively. The populations  $f_i$  are rescaled so as to ensure mass conservation.

In this procedure, we ensure that mass is conserved any time except when mass is added (step 2) or subtracted (step 4) by proper rescaling. The results of this approach are presented hereafter.

### 3.2 Simulation results

**Comparison between analytical solution and simulation result.** The analytical solution of a 2-dimensional fully developed steady flow in a channel of width  $H$ , driven by a constant pressure gradient  $F$  and with constant viscosity  $\nu$  (Newtonian flow assumed) is given by the following formula (Poiseuille flow):

$$u_{\text{analytical}}(y) = \frac{-F(y - y_{\text{lower}})(y - y_{\text{upper}})}{2\nu} \quad (5)$$

Herein,  $y_{\text{upper}}$  and  $y_{\text{lower}}$  denote the  $y$ -coordinates of the upper and lower boundary, respectively. Thus,  $H = (y_{\text{upper}} - y_{\text{lower}})$ . The pressure gradient  $F$  is given by

$$F = \frac{8\nu U_{\text{max}}}{H^2} \quad (6)$$

We compared our simulation output to the analytical solution using the same parameters. Figure 1 displays the velocity profile of the exact solution and the result of the numerical simulation of a symmetric straight channel. It can be observed that the computed velocity profile (blue crosses) and the analytical solution by Poiseuille (green dashed line) coincide.

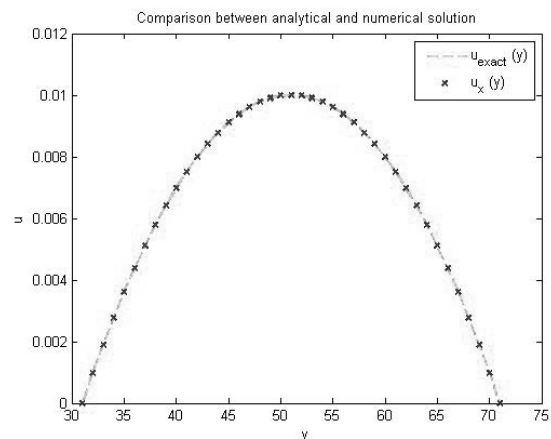
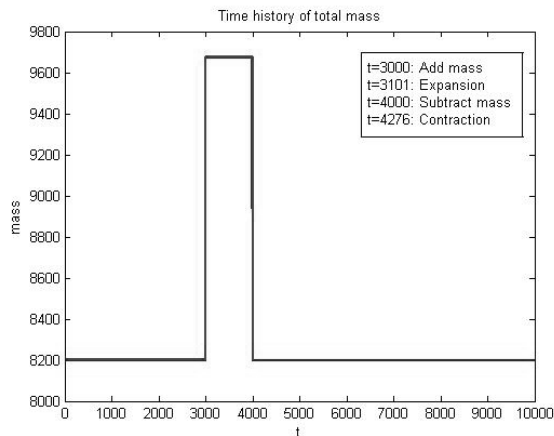


Figure 1: Velocity: Comparison between analytical solution and numerical result.

**Approach for testing the modeling of elasticity using local rescaling.** We conducted a simulation in the straight channel using the local rescaling method to show that it follows expected physical behavior. The procedure described below is only an artificial setup to enforce expansion and contraction through pressure increase/decrease for conducting this simulation experiment.

For this simulation, the problem of expansion and contraction has been separated in the parts explained in Section 3.1 and local rescaling has been used. Figure 2 shows the total mass (equal to the sum of the density  $\rho$  at each fluid node of the lattice) over time. It can be seen that mass is conserved at expansion (occurring at time  $t = 3101$ ) and contraction (occurring at time  $t = 4276$ ). After the wall has reached its initial position again, i.e., after having performed the steps 1 to 5 cited above, the value of the total mass is the same as the initial value. However, to reach the same value of the total mass as at the beginning,  $\Delta f_i$  in step 4 has to be multiplied by  $\frac{H}{H+2}$ ,  $H$  being the width of the initial channel. This is due to the fact that the diameter (width) of the channel increases by 2 after expansion, i.e., there are two layers of fluid nodes more than before expansion. Thus,  $\Delta f_i$ , being subtracted at every node, has to be reduced by this proportionality factor to take into account the increase of nodes.



**Figure 2:** Total mass as a function of time.

Figure 3 depicts the density at a fluid node next to the wall resulting from this simulated experimental setup. It can be observed that the density oscillates after expansion or contraction due to the propagation of the local perturbation throughout the channel (oscillation period) created by the local rescaling.

The duration of the oscillations is influenced by the fluid parameters (viscosity). The value of  $\rho$  returns to the initial value after one cycle (expansion and subsequent contraction). Due to the local rescaling of the populations at the changed nodes and their neighbors, the value of  $\rho$  decreases at expansion and increases at contraction.

The resulting velocity component  $u_x$  at a fluid node next to the wall is displayed in Figure 4. Small oscillations occur at expansion and contraction due to the local perturbation of the flow field. After one cycle, the value of  $u_x$  returns to the initial value (when flow is fully developed).

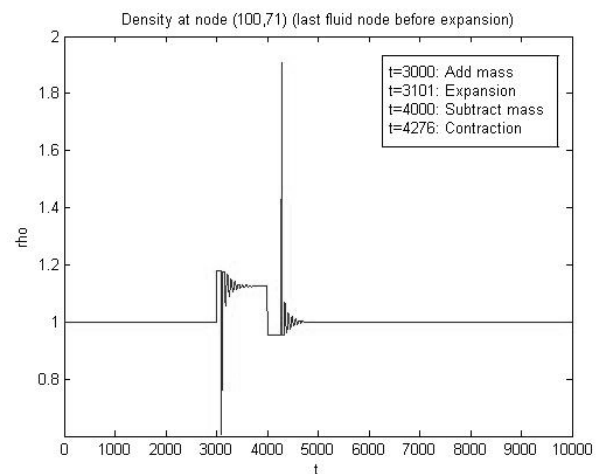


**Figure 3:** Density at fluid node next to the upper wall as a function of time (local rescaling used).

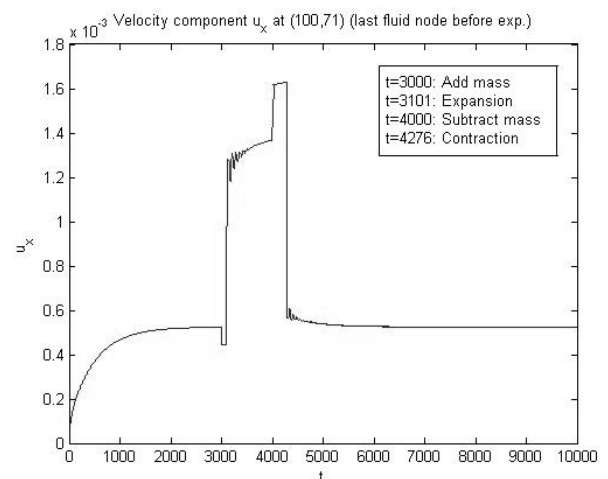


**Figure 4:** Velocity component  $u_x$  at fluid node next to the upper wall as a function of time (local rescaling used).

The simulation results presented above show expected physical behavior. Mass is conserved and initial values of the density and the velocity are recovered after one cycle of expansion and subsequent contraction. The oscillatory transient lasts a few hundred time steps, which is an expected duration for the chosen viscosity. As described, the method works strictly locally as does the lattice Boltzmann method itself. This allows straight-forward implementation of the method in lattice Boltzmann simulations and makes it suitable for parallel computation.

**Approach for testing the modeling of elasticity using rescaling 'by Columns'.** For this simulation, the same steps 1–5 cited in Section 3.1 have been performed and rescaling 'by columns' has been used. The time history of the total mass shows the same behavior as the one for the local rescaling method. Contrary to the local rescaling method, where contraction (as well as expansion) occurs at both the upper and lower wall at the same time step in the simulation, the contraction of the channel when using rescaling 'by columns' is split into two steps. First, contraction at the lower boundary occurs followed by a contraction at the upper boundary a few hundred time steps later. This is related to the order in which the lattice nodes are processed in the implementation (here, from lower boundary to upper boundary). Since rescaling 'by columns' does not affect only the nearest neighbors of a node becoming fluid (as in the local rescaling method), but the populations of all nodes in the same column, a node type change at the lower wall affects the flow field at the upper wall in the same time step. As a consequence, the condition for expansion or contraction at the upper wall is not necessarily fulfilled anymore as soon as a node type change (and thus rescaling of the whole column) has occurred at the lower wall.

Figure 5 displays the density at a fluid node next to the wall. It can be observed that the density oscillates much less after expansion (contraction) compared to the oscillations occurring with the local rescaling method as local perturbations are limited. Furthermore, oscillations are completely absent at contraction. The value of  $\rho$  returns to the initial one after one cycle (expansion and subsequent contraction) as expected.

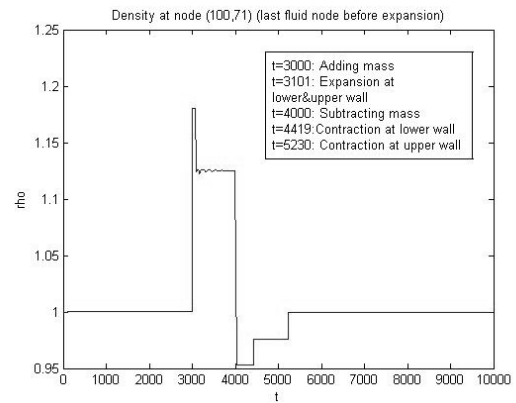


Figure 5: Density at fluid node next to the upper wall as a function of time (rescaling 'by columns' used).

The time history of the velocity component  $u_x$  at a fluid node next to the wall, depicted in Figure 6, exhibits a similar shape as the time history of  $u_x$  when using local rescaling, but without oscillations at expansion and contraction. After one cycle, the initial value of  $u_x$  is recovered.

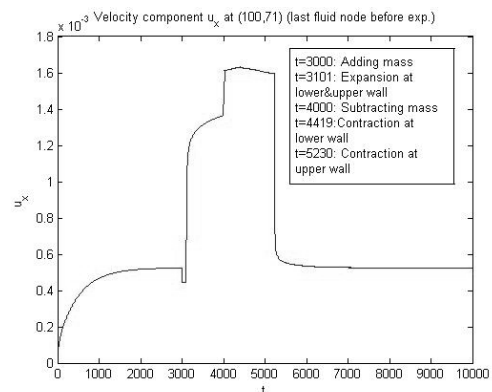


Figure 6: Velocity component  $u_x$  at fluid node next to the upper wall as a function of time (rescaling 'by columns' used).

Although the rescaling 'by columns' provides expected physical behavior (mass conservation, recovery of the initial values after one cycle) and minimizes local perturbation, it exhibits the drawback that node type changes at one wall boundary affect the flow field within the whole channel without propagation latency. Since this specific effect does not correspond to real fluid dynamics, the method can only be used in special cases where this side effect is negligible. Therefore, the rescaling 'by columns' method minimizes perturbations in the simulation but lacks the generality of the local rescaling method.

## 4 Outlook

The aim of the future work is the simulation of blood flow in stented arteries. A stent is a wire metal mesh inserted into a blood vessel to prevent its occlusion. Due to the geometry and the different elasticity of the stent, the behavior of the blood flow changes and thus, turbulences can occur. It is assumed that those turbulences can cause a renewed narrowing of the vessel, so-called *in-stent restenosis*, which is a pathobiologic process prevalently occurring after stent implantation [12].

The modeling of elastic walls presented in this work has the advantage that it can also be applied to stented arteries. For the modeling, we consider three different types of nodes: `fluid`, representing the blood inside the vessel, `tissue`, describing the tissue of the vessel, and `stent`, representing the stent. Since the stented part is stiffer than the rest of the vessel, nodes of type `stent` will have higher pressure thresholds. This enhanced model will be implemented in our simulation software and further elaboration of our approach will be reported in a later work.

## 5 Conclusion

We presented a simple approach for modeling elastic walls in lattice Boltzmann simulations of blood flow in arterial segments. The described method provides correct physical behavior of vessel walls interacting with the simulated blood flow. The preliminary results are promising and encourage extending our approach to allow simulations of stents placed in arteries to investigate their influence on the flow field.

## Acknowledgement

This research was accomplished within the context of the project 'BioCompatible Materials and Applications – BCMA' initiated by the AIT Austrian Institute of Technology GmbH. It was partly funded by AIT and the federal state of Lower Austria and co-financed by the EC (EFRE).

## References

- [1] Eurostat. *Health statistics – Atlas on mortality in the European Union*. Office for Official Publications of the European Communities, Luxembourg; 2009.
- [2] Kropf J. *Multiscale Blood Flow Modelling and Simulation*. Ph.D. thesis, Vienna University of Technology; 2007.
- [3] Leitner D. *Simulation of Arterial Blood Flow with the Lattice Boltzmann Method*. Ph.D. thesis, Vienna University of Technology; 2007.
- [4] Succi S. *The Lattice Boltzmann Equation*. Oxford University Press, Oxford; 2001.
- [5] Wolf-Gladrow D. *Lattice-Gas Cellular Automata and Lattice Boltzmann Models: An Introduction*. Springer, 2000.
- [6] Fang H, Wang Z, Lin Z, Liu M. Lattice Boltzmann method for simulating the viscous flow in large distensible blood vessels. *Physical Review E*. 2002; 65(5):51925
- [7] Artoli A. *Mesoscopic computational haemodynamics*. Ph.D. thesis, University of Amsterdam; 2008.
- [8] Melchionna S, Bernaschi M, Succi S, Kaxiras E, Rybicki F, Mitsouras D, Coskun A, Feldman C. Hydrokinetic approach to large-scale cardiovascular blood flow. *Computer Physics Communications*. 2010; 181(3):462–472
- [9] Pontrelli G, Ubertini S, Succi S. The unstructured lattice Boltzmann method for non-Newtonian flows. *Journal of Statistical Mechanics: Theory and Experiment*. 2009; 6:06005
- [10] Hoekstra A, van't Hoff J, Artoli A, Sloot P. Unsteady flow in a 2D elastic tube with the LBGK method. *Future Generation Computer Systems*. 2004; 20(6):917–924
- [11] Fung Y. *Biomechanics: Circulation*. Springer Verlag; 1997.
- [12] Lowe H, Oesterle S, Khachigian L. Coronary in-stent restenosis: current status and future strategies. *Journal of the American College of Cardiology*. 2002; 39(2):183–193

# Simulating Aortic Blood Flow and Pressure by an Optimal Control Model

Stephanie Parragh<sup>1,2\*</sup>, Bernhard Hametner<sup>2</sup>, Siegried Wassertheurer<sup>2</sup>

<sup>1</sup> AIT Austrian Institute of Technology GmbH, Health & Environment Department, Biomedical Systems, Donau-City-Str. 1, 1220 Vienna, Austria; \* *Stephanie.Parragh.fl@ait.ac.at*

<sup>2</sup> Institute of Analysis and Scientific Computing, Vienna University of Technology, Wiedner Hauptstraße 8-10, 1040 Vienna, Austria;

Simulation Notes Europe SNE 23(2), 2013, 101 - 106  
DOI: 10.11128/sne.23.tn.10191  
Received: February 10, 2013; Revised: June 15, 2013;  
Accepted: June 30, 2013;

**Abstract.** Parameters derived from aortic pressure and flow waves are considered to be important indicators of cardiovascular risk. To reduce the measurement effort, validated methods already exist to transfer non-invasively assessed peripheral blood pressure curves to central ones. In this work, an optimal control model is introduced, which could potentially be used to simulate the corresponding ejection from the heart. It is based on the well-established three-element Windkessel model of the arterial system, coupled with an optimality criterion. The resulting optimal control problem was solved in part symbolically, in part numerically and simulation experiments were performed to investigate the capability of the model to generate pathophysiological flow and pressure patterns with meaningful parameter values. Moreover, the sensitivity of the model to variations in the parameters, that were considered relevant for the use as a blood flow model, was analysed. The results show that it is indeed possible to simulate realistic flow and pressure waves for parameters within the pathophysiological range of humans. Moreover, the sensitivity analysis indicates that parameter identification based on a pressure measurement might be possible. Overall, the model shows a big potential for the simulation of blood flow based on pressure alone.

## Introduction

The hemodynamics in the human body is determined by the characteristics of the heart and the vascular system as well as by their interplay. The corresponding state variables, blood pressure and flow, are therefore sup-

posed to hold important information about the status of the cardiovascular system of a specific person. Parameters derived from one or both of these two quantities are used for the stratification of cardiovascular risk and have been shown to have predictive power for the occurrence of adverse events [1].

However, measuring aortic pressure and flow requires elaborate equipment and trained operators and represents, in the case of invasive measurements, an additional risk for the patient. To overcome this limitation, methods have been developed to estimate the aortic pressure waveform from non-invasive peripheral readings [2,3]. Part of these methods has been validated for various cardiac conditions and is now commercially available for the use in everyday (clinical) life [4-7]. Central pressure parameters derived from these synthesized curves have proven their value in a multitude of studies [1].

Regarding the flow waves, different attempts have been made to provide an approximation using solely information from the corresponding pressure signal [8-10]. In the 1970ies, an approach based on the assumption of minimal cardiac cycle work was proposed [11,12]. The main idea is to combine a so called Windkessel (WK) model of the arterial system with an optimality criterion. For a given parameterisation of the WK model and a suitable choice of constraints, the resulting optimization problem then simultaneously yields optimal patterns of flow and pressure [13]. By comparing the latter to a measured pressure curve, a fitting procedure can be used to identify the parameters in the WK model and thus, finally, a flow curve is obtained. This approach has been investigated extensively in the 1970ies and 80is [14-17] using different optimality criteria and WK models. A blood flow model of this type is also used nowadays in a commercially available device [18].

The aim of this work is to examine an optimal control model based on an optimality criterion proposed by Hämäläinen *et al.* [19] using a slightly different WK model as well as different boundary conditions. Simulation experiments were performed and the ability of the model to imitate physiological as well as pathological flow and pressure patterns was investigated. Furthermore, the sensitivity of the model to variations in the parameters, that are considered relevant for the use as a blood flow model, was analysed.

## 1 Methods

The optimization model presented in this work is based on the well-established 3-element Windkessel (WK) model that describes the dynamic relation between pressure and flow when the system is in steady state, and the idea that the heart works in an optimal manner. Combination of the WK model and the optimality criterion results in an optimal control problem which has to be solved appropriately. Therefore, suitable boundary conditions have to be formulated and adequate methods have to be chosen to subsequently solve the problem numerically.

### 1.1 Modelling

Aortic pressure  $p$  and flow  $q$  are assumed to be related according to the so called 3-element Windkessel model

$$p(t) = Z_c \cdot q(t) + p_{wk}(t) + P_\infty \quad (1)$$

$$\dot{p}_{wk}(t) = -\frac{1}{RC} p_{wk}(t) + \frac{1}{C} q(t) \quad (2)$$

whereby the dot represents the time derivative. The peripheral resistance  $R$  describes the resistance opposed to the flow by the vascular system, which is mostly caused by the small arteries and arterioles. The arterial compliance  $C$  specifies the distensibility of the large elastic arteries, in particular the aorta, and the characteristic impedance  $Z_c$  takes into account the compliance and inertance of the very proximal aorta [20].  $P_\infty$  is an asymptotic pressure level that represents the pressure that is not caused by the ejection of the heart but is maintained by the vascular system. It is often set to zero for simplicity [20].  $p_{wk}$  is an auxiliary quantity called the Windkessel pressure.

An optimization problem proposed by Hämäläinen *et al.* [19] was chosen for this work ( $t_s$  denotes the ejection duration): Find  $(p, q)$  such that

$$J = \int_0^{t_s} \alpha p(t)q(t) + \dot{q}(t)^2 dt \rightarrow \min \quad (3)$$

under the constraint that a given stroke volume

$$SV = \int_0^{t_s} q(t) dt \quad (4)$$

has to be reached.

The first term of the integral (3) represents the hydraulic work done by the heart per beat, times a nonnegative weighting factor  $\alpha$ . Thus, one tries to find those patterns of pressure and flow that minimize the energy used by the heart to generate a given stroke volume. The second term in (3) is a structural penalty term that penalizes peaks in the acceleration of blood, which are considered to lower the efficiency of the cardiac contraction [19].

In order to formulate an optimal control problem, equation (1) is used to eliminate  $p$  from equation (3) and the acceleration  $\dot{q}$  is set to be the control, which is denoted by  $u$ . Furthermore, an additional equation for the left ventricular volume  $V$  is included in order to enable the specification of the stroke volume  $SV$  as a boundary condition. In systole, the volume of blood contained in the left ventricle changes solely due to the ejection of blood into the arterial system and hence, the derivative of  $V$  is given by  $-q(t)$ . The optimal control problem then reads:

Minimize

$$J(u) = \int_0^{t_s} \alpha(Z_c q + p_{wk} + P_\infty)q + u^2 dt \quad (5)$$

under

$$\begin{pmatrix} \dot{V}(t) \\ \dot{q}(t) \\ \dot{p}_{wk}(t) \end{pmatrix} = \begin{pmatrix} -q(t) \\ u(t) \\ -\frac{1}{RC} p_{wk}(t) + \frac{1}{C} q(t) \end{pmatrix} \quad (6)$$

$$\begin{aligned} V(0) &= V_0 & V(t_s) &= V_0 - SV \\ q(0) &= 0 & q(t_s) &= 0 \\ p_{wk}(0) &= P_0 - P_\infty & p_{wk}(t_s) &= (P_0 - P_\infty)e^{-\frac{t_s}{RC}} \end{aligned} \quad (7)$$

$V_0$  denotes the left ventricular end-diastolic volume, which can be chosen arbitrarily since the absolute values of  $V$  do not affect  $p_{wk}$  or  $q$ . At the end of systole, this initial volume has been reduced by  $SV$ , i.e.  $V(t_s) = V_0 - SV$ . During diastole, the aortic valve is closed and therefore flow from the heart is assumed to be zero during this phase, which yields the boundary conditions for  $q$ . Those for  $p_{wk}$  result from the assumption of the system being in a steady state, i.e.  $p_{wk}$  has to be a periodic function.

More precisely,  $q(0) = 0$  yields  $p_{wk}(0) = P_0 - P_\infty$  according to equation (1). From equation (2) it follows that  $p_{wk}$  describes an exponential decay in diastole, when  $q \equiv 0$ . Together with the assumption of periodicity, i.e.  $p_{wk}(0) = p_{wk}(T)$ , for  $T$  denoting the duration of the heartbeat, the diastolic WK pressure is thus given by

$$p_{wk}(t) = (P_0 - P_\infty)e^{\frac{T-t}{RC}}, \quad t_s \leq t \leq T \quad (8)$$

which finally yields the boundary condition stated in (7).

The optimal control problem (5)-(7) can be solved with Pontryagin's maximum principle [21] which results in a system of 6 linear ordinary differential equations (ODE) for the optimal solution: 3 for the state variables  $V, q, p_{wk}$  and 3 for the costate variables  $\lambda_1, \lambda_2$  and  $\lambda_3$ .

$$\begin{aligned} \dot{V}(t) &= -q(t) \\ \dot{q}(t) &= \frac{1}{2}\lambda_2(t) \\ \dot{p}_{wk}(t) &= -\frac{1}{RC}p_{wk}(t) + \frac{1}{C}q(t) \\ \dot{\lambda}_1(t) &= 0 \\ \dot{\lambda}_2(t) &= \alpha(2Z_c q(t) + p_{wk}(t) + P_\infty) + \lambda_1(t) \\ &\quad - \frac{1}{C}\lambda_3(t) \\ \dot{\lambda}_3(t) &= \alpha q(t) + \frac{1}{RC}\lambda_3(t) \end{aligned} \quad (9)$$

This system has 6 degrees of freedom. Thus, together with the boundary conditions specified in (7), the solution of the optimal control problem is, if it exists, uniquely described.

### 1.2 Implementation

A numerical solution of the system given in (9) satisfying the boundary conditions (7) cannot be found straight forward with common ODE solvers, since these require initial values for all variables. An iterative procedure like the shooting method would be needed that adjusts the unknown initial values of the costates until (7) is satisfied. However, this again requires an adequate initial guess of  $\lambda_i(0)$  for  $i = \{1,2,3\}$ , which is difficult since the costates do not represent physiological quantities and thus their magnitude is hard to estimate.

Therefore, another approach was used in this work. The system of ODEs (9) with the initial values  $V(0), q(0)$  and  $p_{wk}(0)$ , i.e. the left hand side in (7), was symbolically solved using Maple 15 (Maplesoft, a division of Waterloo Maple Inc., Waterloo, Ontario).

The solutions obtained for  $V, q$  and  $p_{wk}$  thus depend on the time  $t$ , the ejection duration  $t_s$  and the length of the heartbeat  $T$ , the parameters  $V_0, P_0, P_\infty, R, C, Z_c$  and  $\alpha$  as well as three unknown constants  $c := (C_1, C_2, C_3)$ , which represent the remaining degrees of freedom.

In a next step, a system of linear equations  $Ac = b$  for the unknowns was built up using the right hand side of (7), whereby the matrix  $A$  as well as the vector  $b$  depend on  $t_s, T, P_0, P_\infty, R, C, Z_c$  and  $\alpha$ . Finally, the expressions for  $q(t), p_{wk}(t), A$  and  $b$  were simplified and automatically translated to Matlab code using the "CodeGeneration" package in Maple.

All further computations and simulation experiments were performed by using Matlab R2011b (The MathWorks, Inc., Natick, Massachusetts, United States). To generate pressure and flow for a given parameter set, first, the system of linear equations is solved to obtain  $C_1, C_2$  and  $C_3$ . From these,  $q(t)$  and  $p_{wk}(t)$  are evaluated during systole and finally  $p(t)$  is obtained from equation (1). During diastole,  $p_{wk}(t)$  is computed according to (8) and since it holds that  $p(t) = p_{wk}(t) + P_\infty$  during this phase,  $p(t)$  can be determined for the whole cardiac cycle.

### 1.3 Simulation experiments

In order to examine the capability of the model to represent different physiological as well as pathological conditions, simulation experiments were performed. In a first step, the possible shape variations were investigated for parameterisations within the pathophysiological range of humans found in literature [17,22].

Then, the sensitivity of the model to changes in the model parameters was assessed. Since the final goal of this approach is to provide an estimate of the flow curve for a given pressure signal, the initial pressure  $P_0$ , the duration of the heartbeat  $T$  as well as the mean pressure  $mBP$  were supposed to be given. Furthermore, the time constant  $RC$  of the modelled exponential pressure decay (8) as well as  $P_\infty$  and the ejection duration can be estimated from the pressure wave [23,24] and were thus also assumed to be known. Therefore, only  $R, C, Z_c$  and  $\alpha$  were varied and the corresponding  $SV$  was computed from the following equation which can be easily derived from the Windkessel model (1), (2) and the definition of the total peripheral resistance:  $TPR := mBP \cdot T/SV$ .

$$SV = \frac{(mBP - P_\infty) \cdot T}{R + Z_c} \quad (10)$$

## 2 Results

Figure 1 shows 2 pairs of pressure and flow curves obtained with the parameterisation given in table 1. For both, pressure and flow, substantial differences in the shapes can be seen. The parameters chosen for case 1 are in a physiological range for a healthy individual, whereas those for case 2 imitate a pathological arterial stiffness. The corresponding pressure and flow waves reflect these characteristics.

For the sensitivity analysis, the parameterisation of case 1 was taken as default and  $R, C, Z_c$  and  $\alpha$  were varied, see figure 2. The diastolic part of the pressure signals is the same for all parameters because the time constant of the decay remained unchanged. Moreover, since mean pressure is fixed, the variations generally have a stronger effect on the flow than on the pressure curves.

Figure 2A shows the effect of changes in  $R$  and  $C$  while keeping their product  $RC$  fixed and adapting the stroke volume according to (10). In the pressure signal, small changes in the upstroke, the height of the maximum as well as its position can be observed. The flow curves are mainly affected by the decrease in stroke volume resulting from the increase in resistance. However, for very elastic arteries, i.e.  $C$  high, and little resistance, also the wave shape is altered.

Simulation runs for different values of the characteristic impedance  $Z_c$  are depicted in figure 2B. When  $Z_c$  increases, the maximum pressure is shifted to the right and the decline of the flow curve changes from convex to concave.

Finally, simulation results for variations in  $\alpha$  are presented in figure 2C. The higher  $\alpha$  becomes, the earlier maximum flow is reached. Also, the decline of the flow wave is affected in a similar way as before for varying  $Z_c$ . The pressure wave exhibits a flatter shape for higher values of  $\alpha$ .

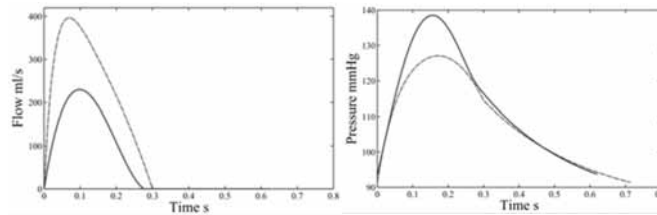


Figure 1. Comparison of qualitatively and quantitatively different, simulated flow and pressure patterns corresponding to the parameterisation of case 1 (dashed line) and case 2 (solid line) given in table 1.

Parameter	Case 1	Case 2	Unit	
<b>R</b>	0.204	0.410	mmHg*s/ml	
<b>C</b>	1.50	0.67	ml/mmHg	
<b>Z<sub>c</sub></b>	0.04	0.09	mmHg*s/ml	
<b>α</b>	25000	500	-	
<b>P<sub>∞</sub></b>	83.4	83.4	mmHg	
<b>P<sub>0</sub></b>	91.4	93.5	mmHg	
<b>mBP</b>	108.8	113.6	mmHg	
<b>t<sub>s</sub></b>	300	276	ms	
<b>T</b>		714	625	ms
<b>SV</b>		73.5	37.8	ml
<b>TPR</b>		1.0571	1.879	mmHg*s/ml

Table 1. Parameterisation simulating a healthy (case 1) and a pathological (case 2) case.

## 3 Discussion

The aim of this work was to investigate the capability of the introduced optimal control model to generate pathophysiological flow and pressure patterns with meaningful parameter values. Furthermore, we wanted to examine its potential to be used to simulate blood flow for a given pressure signal.

The parameters  $C, TPR$  and  $Z_c$  chosen for case 1 are within the range reported in literature for healthy individuals [22] and also the pressure and flow waves resemble typical contours as given for example in [1].

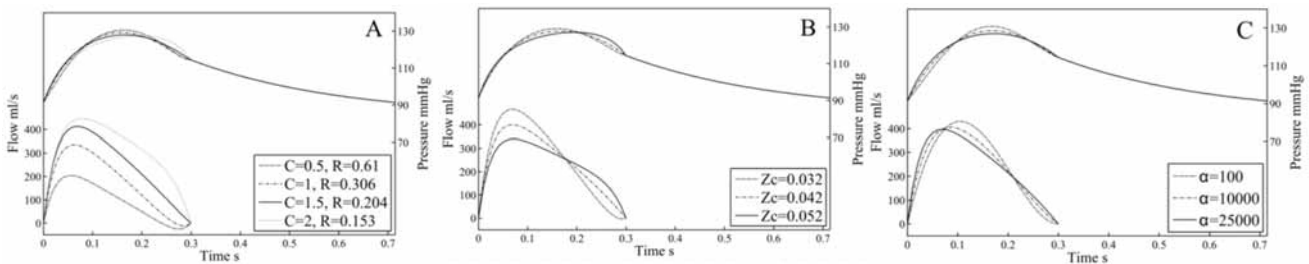


Figure 2. Sensitivity of the model to variations in  $R$  and  $C$  for fixed  $RC$  (A), in  $Z_c$  (B) and in  $\alpha$  (C).

In case 2, the lower value of arterial compliance, a direct index of arterial stiffness, and the higher value of characteristic impedance, an indirect index of arterial stiffness, imitate stiffer arteries compared to case 1 [25]. The furthermore elevated resistance is typical for subjects with hypertension [1]. As would be expected based on these parameters, the pressure indeed rises higher than for case 2 even though the stroke volume is lower. These examples indicate that (1) it is possible to generate realistic flow and pressure patterns with the optimal control model and (2) the different model parameters affect the simulated patterns in accordance with their physiological meaning.

In order to use this model to simulate blood flow for a given pressure curve, the model parameters have to be identified by comparing the modelled pressure to a measurement (e.g. minimizing the squared error between them). For this purpose, it is desirable to reduce the number of unknown parameters, since the complexity of the model identification increases with the number of parameters. As it is assumed that the pressure pattern is known anyways, it seems logical to derive as much information as possible beforehand. Therefore, we assumed the initial pressure level  $P_0$ , mean pressure  $mBP$  as well as the timing information  $T$  and  $t_s$  to be given. The first three can be extracted directly from the recorded signal, the latter can be estimated from it [24]. Furthermore, the diastolic part of the pressure curve can be used to determine  $P_\infty$  and  $RC$  [23]. Thus, altogether,  $P_0$ ,  $mBP$ ,  $P_\infty$ ,  $RC$ ,  $T$  and  $t_s$  can be assumed to be known and only the remaining parameters  $R$ ,  $C$ ,  $Z_c$ ,  $SV$  and  $\alpha$  have to be found. Because  $RC$  is fixed and  $SV$  can be calculated according to (10), this set of parameters is further reduced to  $R$  (or  $C$ ),  $Z_c$  and  $\alpha$ . Therefore, we studied the sensitivity of the model only with regards to these parameters.

The results of the sensitivity analysis show that changing these parameters does affect important characteristics of the shape of the simulated pressure wave, like its upstroke or the position of its maximum. Thus, although the quantitative changes were overall rather subtle, parameter identification from a pressure recording might be feasible. However, since the effect of lowering  $Z_c$  resembles that of increasing  $R$ , providing good first estimates for the fitting procedure might be a crucial point.

The weighting factor  $\alpha$  strongly affected the position of maximum flow. For healthy individuals, it seems

convincing from an evolutionary point of view to assume that the heart works in such a manner that the energy expenditure is minimized [26]. Applied to the optimality criterion given in (3), this corresponds to high values of  $\alpha$ . In this case, the simulated flow patterns show an early maximum resembling those reported for healthy hearts [1]. Lower values of  $\alpha$  indicate that less emphasis is led on the minimization of stroke work in (3), which could imply that the heart cannot work optimally any more. The obtained ejection patterns reach their maximum later in systole and also the shape of the decline is changed, which is indeed characteristic for failing hearts [1].

The optimal control model used in this investigation is based on an optimality criterion by Hämäläinen *et al.* [19]. However, in contrast to [19], we included an asymptotic pressure level  $P_\infty$  in the WK model. Moreover, we used different boundary conditions (BC) for the WK pressure  $p_{wk}$ . Hämäläinen *et al.* tried 6 different options for fixed  $t_s$ , namely specifying both or only one value of  $p_{wk}(0)$  and  $p_{wk}(t_s)$ , their difference, their sum as well as using purely periodic BC. Their model reacted very sensitively to changes in the BC, which the authors stated as major drawback. It has to be kept in mind though, that the BC have to meet the assumptions of the WK model and thus, not all choices of BC are valid. For example, for fixing both values  $p_{wk}(0)$  and  $p_{wk}(t_s)$ , the periodicity, i.e. the assumption of steady state, is not fulfilled. The same holds for specifying the difference or the sum of  $p_{wk}(0)$  and  $p_{wk}(t_s)$ . Therefore, it seems logical that the choice of BC strongly affects the model itself. In our approach, the value of  $p_{wk}(t_s)$  depends on  $P_0$  as well as on  $R$  and  $C$  and thus, the periodicity is fulfilled for any value of  $R$  and  $C$ .

Hämäläinen *et al.* also reported a hypersensitivity of their models to variations in single parameters. However, satisfying an optimality criterion is a very strong requirement and both, the parameter values and the BC form the optimal solution. In other words, BC and model parameters are not independent from each other. It therefore seems logical that changing one parameter independently possibly destroys this balance.

Our results furthermore show that by using all information available from a pressure signal and by considering the dependency between  $R$ ,  $Z_c$  and  $SV$  (10) induced by the WK model, a wide range of parameter values produces realistic results.

## 4 Conclusion

The results show that it is indeed possible to generate flow curves with this approach that resemble physiological ones. Furthermore, the identification of the model parameters from a given pressure curve seems feasible. However, further research is needed to verify these considerations.

## References

- [1] Nichols W, O'Rourke M, Vlachopoulos C. McDonald's Blood Flow in Arteries: Theoretical, Experimental and Clinical Principles. 6. ed., Hodder Arnold, London, 2011.
- [2] Karamanoglu M, O'Rourke M, Avolio A, Kelly R. An analysis of the relationship between central aortic and peripheral upper limb pressure waves in man. *Eur. Heart J.* 1993; 14(2):160-167
- [3] Wassertheurer S, Mayer C, Breitenecker F. Modeling arterial and left ventricular coupling for non-invasive measurements. *Simul. Model. Pract. Th.* 2008; 16(8):988-997
- [4] Weber T, Wassertheurer S, Rammer M, Maurer E, Hametner B, Mayer C, Kropf J, Eber B. Validation of a Brachial Cuff-Based Method for Estimating Central Systolic Blood Pressure. *Hypertension.* 2001; 58:825-832
- [5] Wassertheurer S, Kropf J, Weber T, van der Giet M, Baulmann J, Ammer M, Hametner B, Mayer C, Eber B, Magometschnigg D. A new oscillometric method for pulse wave analysis: comparison with a common tonometric method. *J. Hum. Hypertens.* 2010; 24:498-504
- [6] Sharman JE, Lim R, Qasem AM, Coombes JS, Burgess MI, Franco J, Garrahy P, Wilkinson IB, Marwick TH. Validation of a Generalized Transfer Function to Noninvasively Derive Central Blood Pressure During Exercise. *Hypertension.* 2006; 47(6):1203-1208
- [7] Nunan D, Wassertheurer S, Lasserson D, Hametner B, Fleming S, Ward A, Heneghan C. Assessment of central haemodynamics from a brachial cuff in a community setting. *BMC Cardiovasc. Disord.* 2012; 12:48
- [8] Wesseling K, Jansen J, Settels J, Schreuder J. "Computation of aortic flow from pressure in humans using a non-linear, three-element model. *J. Appl. Physiol. Respir. Environ. Exerc. Physiol.* 1993; 74(5):2566-2573
- [9] Westerhof BE, Guelen I, Westerhof N, Karemaker JM, Avolio A. Quantification of Wave Reflection in the Human Aorta From Pressure Alone A Proof of Principle. *Hypertension.* 2006; 48(4):595-601
- [10] Hametner B, Wassertheurer S, Hughes A, Parker K, Weber T, Eber B. Reservoir and excess pressures predict cardiovascular events in high-risk patients. *Int. J. Cardiol.* 2014; 171:31-36
- [11] Yamashiro S, Daubenspeck J, Bennett F. Optimal regulation of left ventricular ejection pattern. *Appl. Math. Comput.* 1979; 5(1):41-54
- [12] Noldus E. Optimal control aspects of left ventricular ejection dynamics. *J. Theor. Biol.* 1976; 63(2):275-309
- [13] Hametner B, Parragh S, Mayer C, Kropf J, Wassertheurer S. Optimizing ventricular work: a matter of constraints In: *Proceedings of the 24th European Modeling & Simulation Symposium, EMSS*; 2012; P.322-327
- [14] Pfeiffer K, Kenner T: Minimization of the external work of the left ventricle and optimization of flow and pressure pulses. In: *The arterial system*, edited by Bauer R and Busse R. Springer. 1978; P.216-223
- [15] Kenner T. On the role of optimization in the cardiovascular system. *Basic Res. Cardiol.* 1986; 81:73-78
- [16] Estelberger W. Eine neue nichtinvasive Pulskontur-Schlagvolumenbestimmungsmethode aufgrund eines Optimierungsmodells der Herzarbeit. *Biomed. Tech.* 1977; 22(9):211-217
- [17] Hämäläinen J, Hämäläinen R. Energy cost minimization in left ventricular ejection: an optimal control model. *J. Appl. Physiol.* 1986; 61(5):1972-1979
- [18] Hametner B, Wassertheurer S, Kropf J, Mayer C, Holzinger A, Eber B, Weber T. Wave reflection quantification based on pressure waveforms alone-Methods, comparison, and clinical covariates. *Comput. Meth. Prog. Bio.* 2013; 109(3):250-259
- [19] Hämäläinen R, Hämäläinen J, Miekka U. Optimal control modelling of ventricular ejection - do the endpoint conditions dominate the performance criteria? *Modelling and Data Analysis in Biotechnology and Medical Engineering.* 1083; P.151-162
- [20] Westerhof N, Lankhaar J, Westerhof B. The arterial Windkessel. *Med. Biol. Eng. Comput.* 2009; 47(2):131-141
- [21] Pontrjagin L, Boltjanskij V, Gamkrelidze R, Misčenko E. *Mathematische Theorie optimaler Prozesse.* R. Oldenburg, München, 1964.
- [22] Segers P, Rietzschel E, De Buyzere M, Stergiopoulos N, Westerhof N, Van Bortel L, Gillebert T, Verdonck P. Three- and four-element Windkessel models: assessment of their fitting performance in a large cohort of healthy middle-aged individuals. *Proc. Inst. Mech. Eng. H J. Eng. Med.* 2008; 222(4):417-428
- [23] Wang JJ, O'Brien AB, Shrive NG, Parker KH and Tyberg JV. Time-domain representation of ventricular-arterial coupling as a windkessel and wave system. *Am. J. Physiol. Heart Circ. Physiol.* 2003; 284(4):H1358-H1368
- [24] Hoeks S, Jansen J, Blom J, Schreuder J. Detection of Dicrotic Notch in Arterial Pressure Signals. *J. Clin. Monitor.* 1997; 13(5):309-316
- [25] O'Rourke MF, Mancia G. Arterial stiffness. *J. Hypertens.* 1999; 17(1):1-4
- [26] Swan G. *Applications of Optimal Control Theory in Biomedicine.* Dekker, 1984.

# A Comparative Analysis of CA Model and ODE Model for SIR-type Epidemics

## A MATLAB – based Solution to ARGESIM Bench-mark C17 ‘Spatial Dynamics of SIR-Type Epidemic’

Anita Gerstenmayer<sup>1\*</sup>, Florian Miksch<sup>2</sup>

<sup>1</sup>inst. of Analysis and Scientific Computing, Vienna University of Technology,  
Wiedner Hauptstrasse 8-10, 1040 Vienna, Austria; \*Anita.Gerstenmayer@tuwien.ac.at

<sup>2</sup>dwh Simulation Services, Neustiftgasse 57-59, 1070 Vienna, Austria

Simulation Notes Europe SNE 23(2), 2013, 107 - 110  
DOI: 10.11128/sne.23.bn17.10193  
Received: February 20, 2013; Revised: May 25, 2013;  
Accepted: June 30, 2013;

**Abstract.** This paper presents an extended and modified approach and solution to ARGESIM benchmark C17 ‘Spatial Dynamics of SIR-type Epidemic, which is comparing modelling and simulation approach with ODEs (McKendrick’s SIR model) and with cellular automata (LGCA - Lattice Gas Cellular Automaton). Model implementations (ODE and CA) are directly programmed in MATLAB, using the MATLAB ODE solvers, and programming the CA update by means of vector and matrix manipulations. The contribution analyses and documents the differences between ODE solutions and aggregated CA solutions, mainly investigating dependencies on initial values. And on the other hand, the contributions presents ‘similarities’ between ODE solutions and CA solutions by balancing spatial inhomogenities in the CA dynamics using equally distributed populations.

## 1 Modeling

### 1.1 ODE model

The differential equations model is based on Kermack and McKendrick’s SIR model and consists of three equations for the numbers of susceptible ( $S$ ), infected ( $I$ ) and recovered ( $R$ ) individuals as functions of the time  $t$ :

$$\begin{aligned} S'(t) &= -\gamma S(t)I(t) \\ I'(t) &= \gamma S(t)I(t) - \delta R(t) \\ R'(t) &= \delta R(t) \end{aligned}$$

The infection rate  $\gamma$  can be expressed by  $\gamma = \alpha \frac{c}{N-1}$  as stated in Benchmark C17. The recovery rate  $\delta$  can simply be expressed by the provided parameter  $\beta$ . This model was simulated using Matlab’s numerical ODE-solver `ode45`, which is based on an explicit Runge-Kutta (4,5) method.

### 1.2 LGCA model

The LGCA was implemented in Matlab using a three dimensional  $n \times n \times 6$  array for the cellular automaton ( $n^2$  cells with 6 sub cells each). Each array entry takes one of the four following values representing its state: 0 (empty), 1 (susceptible), 2 (infected) or 3 (recovered).

For the initialization the given initial numbers of individuals are distributed randomly across the LGCA. In each time step, the three phases of the update rules are carried out. For the infections, recoveries and collisions a loop among all cells is made. First, the number of infected individuals in the cells is calculated, as it is necessary for computing the infection probability. Then the recoveries and infections are executed using the probabilities  $\alpha_c$ , for infection of a susceptible particle from an infected particle and  $\beta_c$  for recovery of an infected particle. Next it is checked whether the cell is in one of the possible configurations for collisions and the reflections of the particles take place.

The movement phase was implemented according to the FHP-I rules, particles on the boundary reenter the LGCA on the opposite side. For each time step, the number of individuals in the three states is calculated as a result. The model parameters  $\alpha_c$ ,  $\beta_c$  and  $n$  are identified with provided system parameters according to the specifications of Benchmark C17.

## 2 Differences in ODE and CA Solutions

The aim of this first investigation is to compare the simulations obtained by the two modeling approaches varying the parameters  $I_0$  (and correspondingly  $S_0$ ),  $\alpha$  and  $\beta$  to find settings for similar and different results and analytical explanations for these findings. The other three parameters, the population  $N = 100\,000$  as well as the initially recovered persons  $R_0 = 0$  and the number of contacts  $C$ , are kept constant.

The results for both models in the first parameter setting, in which the initial number of infected people is rather high and  $\alpha$  and  $\beta$  quite low, are nearly indistinguishable, as can be seen in Figure 1.

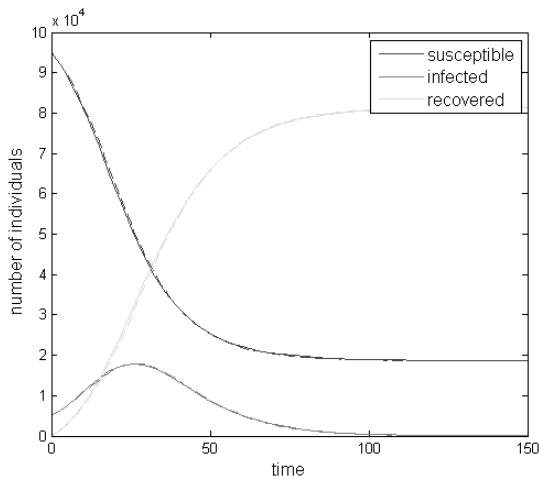


**Figure 1:**  $S(t)$ ,  $I(t)$  and  $R(t)$  simulated with differential equations (solid line) and LGCA (dashed line) for  $I_0 = 5000$ ,  $\alpha = 0.1$  and  $\beta = 0.1$ .

In the second setting (Figure 2), where only  $I_0$  is diminished by a factor 100, the outbreak of the epidemic is delayed by approximately 50 time steps in comparison to the first setting. Qualitatively the behavior of both models is still the same, but the LGCA epidemic occurs slightly later with a lower maximum of infected individuals.

The increase of  $\alpha$  and  $\beta$  in the third setting (Figure 3) leads to a faster outbreak and shorter duration of the epidemic. There are considerable differences between the results for both models. The maximal value of  $I$  is about four times as high for the differential equations model than for the LGCA and the duration of the epidemic is about twice as long for the LGCA.

Also, with the LGCA model a lot more individuals stay susceptible for all time.

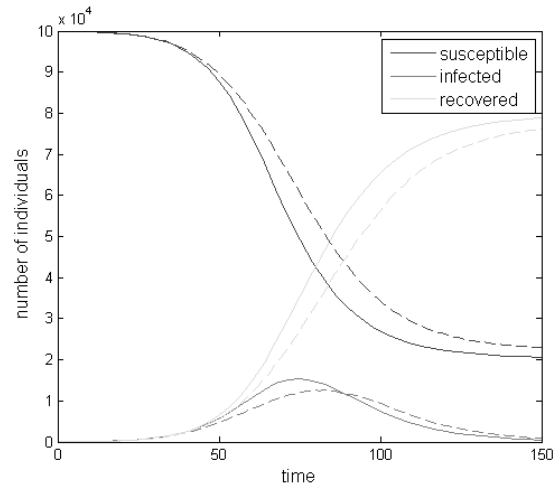


**Figure 2:**  $S(t)$ ,  $I(t)$  and  $R(t)$  simulated with differential equations (solid line) and LGCA (dashed line) for  $I_0 = 50$ ,  $\alpha = 0.1$  and  $\beta = 0.1$ .

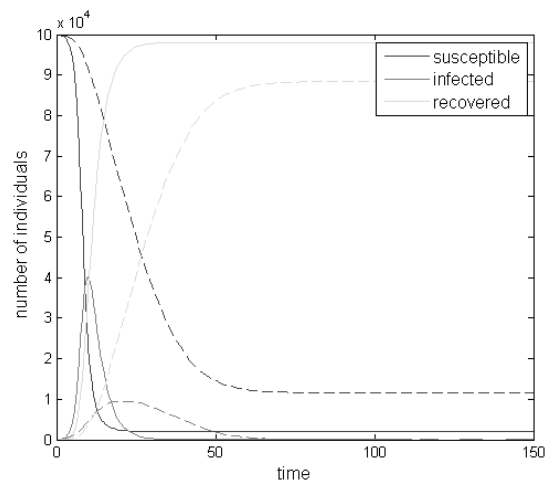


**Figure 3:**  $S(t)$ ,  $I(t)$  and  $R(t)$  simulated with differential equations (solid line) and LGCA (dashed line) for  $I_0 = 50$ ,  $\alpha = 0.6$  and  $\beta = 0.3$ .

In the last setting (Figure 4)  $I_0$  is set to the very low number of only five individuals. For the differential equations model this just results in a small time delay compared to the third simulation. The LGCA model on the other hand responds quite differently, the curve of infected individuals is so flat that an outbreak of the epidemic is hardly visible and  $R$  and  $S$  increase and decrease very slowly.

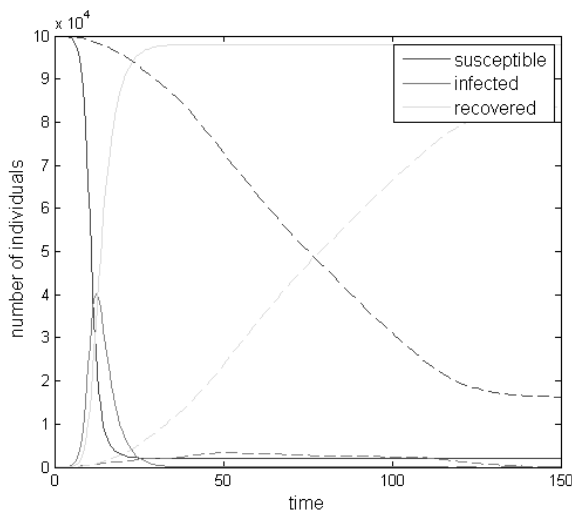


**Figure 4:**  $S(t)$ ,  $I(t)$  and  $R(t)$  simulated with differential equations (solid line) and LGCA (dashed line) for  $I_0 = 5$ ,  $\alpha = 0.6$  and  $\beta = 0.3$ .

One conclusion that can be drawn from these results is that the LGCA reacts much more sensitively to changes of the initial values  $I_0$  and  $S_0$  than the continuous model. For the differential equations model the changed initial values merely seem to shift the outbreak of the epidemic to the left or right, the shape of the curves hardly changes. This does not hold for the LGCA. The smaller the initial number of infected individuals, the flatter the graph for  $I$  becomes due to the spatial distribution of the individuals. If just a small number of infected individuals is placed in the LGCA, the propagation of the disease takes very long because only the few individuals in the neighborhood of the infected ones can get infected, but as the speed of recovery is not affected,  $I$  is kept down and reaches a lower maximum.

So the results for high values of  $I_0$  are similar in both models, but for low initial values of infections the LGCA epidemic curve is a lot flatter. This shows that in some cases the LGCA does not provide a sufficiently homogeneous mixing of infected and susceptible particles, and hence the simulation results differ from the ODE.

Also the infection parameter  $\alpha$  can cause different behavior for the two models. For low values of  $\alpha$  both models behave alike. This can be explained analytically by calculating the expected number of new infections per time unit in the LGCA.

The probability of an infection is given by  $\sum_{i=0}^5 q_i (1 - (1 - \alpha)^i)$ , where  $q_i$  is the probability of  $i$  places in the cell being occupied by infected individuals (given by a hypergeometric distribution), and the probability of an infection of a susceptible individual in this cell is  $(1 - (1 - \alpha)^i)$ . For values of  $\alpha$  close to zero it is reasonable to approximate this term with the Taylor expansion of first order. This yields

$$\sum_{i=0}^5 q_i (1 - (1 - \alpha)^i) \approx \alpha \sum_{i=0}^5 q_i i = \alpha I \frac{C}{N-1} \quad (1)$$

Multiplied with the number of susceptible individuals we have that the expected number of infections equals  $\alpha SI \frac{C}{N-1}$ , which is consistent with the differential equations. For higher values of  $\alpha$  the Taylor approximation is not sufficiently accurate, it overestimates the infection probability  $(1 - (1 - \alpha)^i)$  and thus the actual number of infections per time step in the LGCA is much lower than for the simulation with differential equations.

The recovery parameter  $\beta$  has the same influence on both models, as the expected number of infected individuals in the LGCA who recover per time step equals  $\beta I$  which corresponds to the differential equations. Also the recoveries are not dependent in any way on the spatial distribution. Higher values of  $\beta$  lead to smaller epidemic outbreaks in both models.

### 3 Balancing Spatial Inhomogeneities in CA Model

In this investigation a modified version of the LGCA model, in which all individuals are distributed randomly across the LGCA after each time step, was implemented and compared to the previous results.

For the implementation, the movement and collision parts of the LGCA code were simply replaced by a random permutation of all array entries. This was achieved by reshaping the three-dimensional array into a vector, using Matlab's random permutation function `randperm` to permute its entries, and then converting the vector back into an  $n \times n \times 6$  array.

All three models were simulated with the parameter values  $S_0 = 99\,900$ ,  $I_0 = 100$ ,  $R_0 = 0$  and  $\beta = 0.5$ .

This time  $\alpha$  and  $C$  were varied, for the first simulation  $\alpha = 0.075$  and  $C = 4$  were used, for the second  $\alpha = 0.3$  and  $C = 1$ . The results are shown in figure 5.

It can be observed that the differential equations model yields the exact same result for both simulations. This is due to the fact that only the product of  $C$  and  $\alpha$  is relevant for this model in form of the infection rate

$$\gamma = \alpha \frac{C}{N-1}$$

As this product equals 0.3 in both settings, there cannot be any difference in the simulation results of this deterministic model.

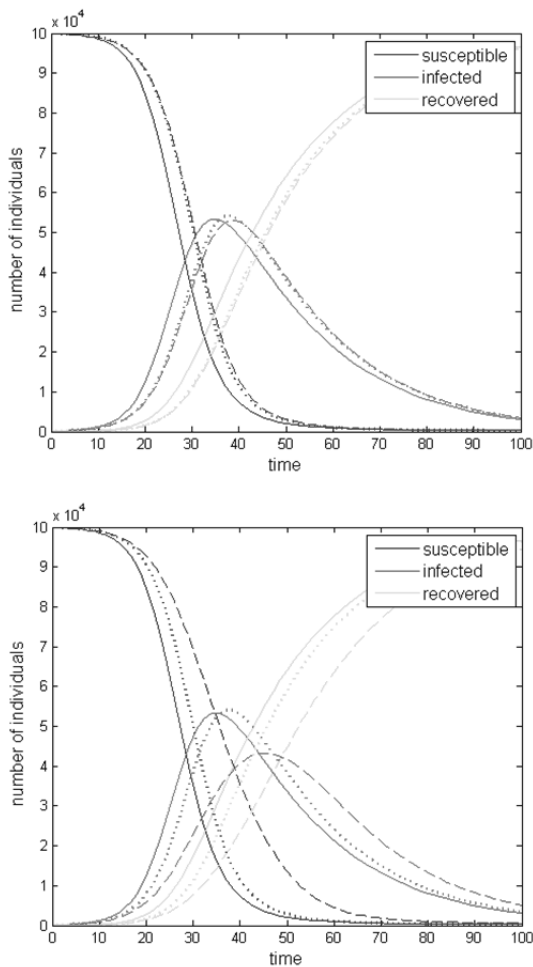


**Figure 5:**  $S(t)$ ,  $I(t)$  and  $R(t)$  simulated with differential equations (solid line), LGCA (dashed line) and LGCA with random distribution (dotted line) for  $C=4$  and  $\alpha=0.075$  (upper panel) and for  $C=1$  and  $\alpha=0.3$  (lower panel).

In the first setting, both LGCA versions lead to very similar results, and also match the differential equation simulation rather closely, with approximately the same maximal number of infected individuals. A small delay in the outbreak of the epidemic is probably caused by the relatively small number of initially infected individuals  $I_0 = 100$  in a population of  $N = 100\,000$ .

The second simulation gives more interesting results. As already observed in the previous task, the higher value for  $\alpha$  leads to a quite different behavior of the LGCA. Here the epidemic occurs later and with a lower maximum of infected individuals than obtained with the differential equations model. The results for the modified LGCA however have not changed with the parameter  $\alpha$ . The random placement of all individuals after each time step riddens the model of the spacial inhomogeneities that would otherwise form and delay the outbreak of the epidemic.

## 4 Conclusions

It can be concluded from the previous tasks and simulations that for some situations, especially those with a low infection rate and a high number of infected individuals at time zero, both models behave very much alike. In some cases however, the locality of the LGCA leads to spatial groupings of the infected individuals and thus slows down the speed of the epidemic in comparison to the differential equations model. This occurs for high values of  $\alpha$  and low values of  $I_0$ . By distributing all individuals randomly across the LGCA after each time step the influence of this locality can be prevented, but still a difference remains between the discrete calculations and the continuous model.

### Model sources

ODE models are implemented with MATLAB ODE solvers, and the CA propagation is directly programmed in MATLAB using vector and matrix feature. All MATLAB m-files and a short file documentation can be downloaded (zip format) by EUROSIM societies' members from SNE website, or are available from the author.

### References

- [1] Hötendorfer H, Popper N, Breitenacker F. Temporal and Spatial Evolution of SIR-type Dynamics – ARGES-IM Comparison C17 – Definition. *SNE Simulation News Europe*. 2004; 14(2): 42-44.

# SNE Simulation News

## EUROSIM Data and Quick Info



## EUROSIM 2013

### 8<sup>th</sup> EUROSIM Congress on Modelling and Simulation

The City Hall, Cardiff, Wales, United Kingdom 10-13 September 2013

[www.eurosim2013.info](http://www.eurosim2013.info)

#### Contents

Info EUROSIM .....	2
Info EUROSIM Societies .....	3 - 7
Info ASIM, CROSSIM .....	3
Info CSSS, HSS, DBSS, FRANCOSIM .....	4
Info ISCS, PSCS, SIMS, SLOSIM .....	5
Info UKSIM, LSS, CAE-SMSG, ROMSIM .....	6
Info RNSS, LIOPHANT Info SNE .....	7
News EUROSIM, ASIM, SLOSIM .....	9
Introduction & News RNSS – Russian Sim. Society .....	10

Simulation Notes Europe SNE is the official membership journal of EUROSIM and distributed / available to members of the EUROSIM Societies as part of the membership benefits. SNE is published in a printed version (Print ISSN 2305-9974) and in an online version (Online ISSN 2306-0271). With Online SNE the publisher ARGESIM follows the Open Access strategy for basic SNE contributions. Since 2011 Online SNE contributions are identified by DOI 10.11128/sne.xx.nnnn. for better web availability and indexing.

Print SNE, high-resolution Online SNE, and additional SNE contributions are available for subscription via membership in a EUROSIM society.

This *EUROSIM Data & Quick Info* compiles data from EUROSIM societies and groups: addresses, weblinks, officers of societies with function and email, to be published regularly in SNE issues.

#### SNE Reports Editorial Board

EUROSIM Khalid Al-Begain, [kbegin@glam.ac.uk](mailto:kbegin@glam.ac.uk)  
Borut Zupančič, [borut.zupancic@fe.uni-lj.si](mailto:borut.zupancic@fe.uni-lj.si)  
Felix Breitenecker, [Felix.Breitenecker@tuwien.ac.at](mailto:Felix.Breitenecker@tuwien.ac.at)  
ASIM Thorsten Pawletta, [pawel@mb.hs-wismar.de](mailto:pawel@mb.hs-wismar.de)  
CROSSIM Vesna Dušak, [vdusak@foi.hr](mailto:vdusak@foi.hr)  
CSSS Mikuláš Alexík, [alexik@frtk.utc.sk](mailto:alexik@frtk.utc.sk)  
DBSS A. Heemink, [a.w.heemink@its.tudelft.nl](mailto:a.w.heemink@its.tudelft.nl)  
FRANCOSIM Karim Djouani, [djouani@u-pec.fr](mailto:djouani@u-pec.fr)  
HSS András Jávör, [javor@eik.bme.hu](mailto:javor@eik.bme.hu)  
ISCS M. Savastano, [mario.savastano@unina.it](mailto:mario.savastano@unina.it)  
PSCS Zenon Sosnowski, [zenon@ii.pb.bialystok.pl](mailto:zenon@ii.pb.bialystok.pl)  
SIMS Esko Juuso, [esko.juuso@oulu.fi](mailto:esko.juuso@oulu.fi)  
SLOSIM Rihard Karba, [rihard.karba@fe.uni-lj.si](mailto:rihard.karba@fe.uni-lj.si)  
UKSIM Richard Zobel, [r.zobel@ntlworld.com](mailto:r.zobel@ntlworld.com)  
CAE-SMSG Emilio Jiminez, [emilio.jiminez@unirioja.es](mailto:emilio.jiminez@unirioja.es)  
LSS Yuri Merkuryev, [merkur@itl.rtu.lv](mailto:merkur@itl.rtu.lv)  
ROMSIM Florin Stanculescu, [sflorin@ici.ro](mailto:sflorin@ici.ro)  
RNSS Y. Senichenkov, [sneyb@dcn.infos.ru](mailto:sneyb@dcn.infos.ru)  
LIOPHANT F. Longo, [f.longo@unical.it](mailto:f.longo@unical.it)

#### SNE Editorial Office /ARGESIM

→ [www.sne-journal.org](http://www.sne-journal.org), [www.eurosim.info](http://www.eurosim.info)

✉ [office@sne-journal.org](mailto:office@sne-journal.org)

Felix Breitenecker, [eic@sne-journal.org](mailto:eic@sne-journal.org)  
Anna Mathe, [Anna.Mathe@tuwien.ac.at](mailto:Anna.Mathe@tuwien.ac.at), [office@sne-journal.org](mailto:office@sne-journal.org)  
Nikolas Popper, [Niki.Popper@drahtwarenhandlung.at](mailto:Niki.Popper@drahtwarenhandlung.at)

If you have any information, announcement, etc. you want to see published, please contact a member of the editorial board in your country or the editorial office.



**EUROSIM**  
Federation of European  
Simulation Societies

**General Information.** EUROSIM, the Federation of European Simulation Societies, was set up in 1989. The purpose of EUROSIM is to provide a European forum for regional and national simulation societies to promote the advancement of modelling and simulation in industry, research, and development.

→ [www.eurosim.info](http://www.eurosim.info)

**Member Societies.** EUROSIM members may be national simulation societies and regional or international societies and groups dealing with modelling and simulation. At present EUROSIM has thirteen full members and three observer member:

ASIM	Arbeitsgemeinschaft Simulation <i>Austria, Germany, Switzerland</i>
CEA-SMSG	Spanish Modelling and Simulation Group <i>Spain</i>
CROSSIM	Croatian Society for Simulation Modeling <i>Croatia</i>
CSSS	Czech and Slovak Simulation Society <i>Czech Republic, Slovak Republic</i>
DBSS	Dutch Benelux Simulation Society <i>Belgium, Netherlands</i>
FRANCO-SIM	Société Francophone de Simulation <i>Belgium, France</i>
HSS	Hungarian Simulation Society <i>Hungary</i>
ISCS	Italian Society for Computer Simulation <i>Italy</i>
LSS	Latvian Simulation Society <i>Latvia</i>
PSCS	Polish Society for Computer Simulation <i>Poland</i>
SIMS	Simulation Society of Scandinavia <i>Denmark, Finland, Norway, Sweden</i>
SLOSIM	Slovenian Simulation Society <i>Slovenia</i>
UKSIM	United Kingdom Simulation Society <i>UK, Ireland</i>
ROMSIM	Romanian Society for Modelling and Simulation, <i>Romania, Observer Member</i>
RNSS	Russian National Simulation Society <i>Russian Federation, Observer Member</i>
LIOPHANT	LIOPHANT Simulation Club <i>Italy &amp; International, Observer Member</i>

EUROSIM Board / Officers. EUROSIM is governed by a board consisting of one representative of each member society, president and past president, and representatives for SNE Simulation notes Europe. The President is nominated by the society organising the next EUROSIM Congress. Secretary and Treasurer are elected out of members of the Board.

President	Khalid Al.Begain <i>kbegain@glam.ac.uk</i>
Past President	Mikuláš Alexík (CSSS), <i>alexik@frtk.fri.utc.sk</i>
Secretary	Borut Zupančič (SLOSIM) <i>borut.zupancic@fe.uni-lj.si</i>
Treasurer	Felix Breitenecker (ASIM) <i>felix.breitenecker@tuwien.ac.at</i>
SNE Repres.	Felix Breitenecker <i>felix.breitenecker@tuwien.ac.at</i>

SNE – Simulation Notes Europe. SNE is a scientific journal with reviewed contributions as well as a membership newsletter for EUROSIM with information from the societies in the *News Section*. EUROSIM societies are offered to distribute to their members the journal SNE as official membership journal. SNE Publishers are EUROSIM, ARGESIM and ASIM.

Editor-in-chief	Felix Breitenecker <i>felix.breitenecker@tuwien.ac.at</i>
-----------------	--

→ [www.sne-journal.org](http://www.sne-journal.org),

✉ [office@sne-journal.org](mailto:office@sne-journal.org)

EUROSIM Congress. EUROSIM is running the triennial conference series EUROSIM Congress. The congress is organised by one of the EUROSIM societies.

EUROSIM 2013 will be organised by UKSIM in Cardiff, Wales, UK, September 10-13, 2013.

**Chairs / Team EUROSIM 2013**

Khalid Al.Begain, *kbegain@glam.ac.uk*  
Richard Zobel, *r.zobel@ntlworld.com*  
David Al-Dabass, *david.al-dabass@ntu.ac.uk*  
Alessandra Orsoni, *a.orsoni@kingston.ac.uk*  
Richard Cant, *richard.cant@ntu.ac.uk*

→ [www.eurosim2013.info](http://www.eurosim2013.info)



## ASIM German Simulation Society Arbeitsgemeinschaft Simulation

ASIM (Arbeitsgemeinschaft Simulation) is the association for simulation in the German speaking area, servicing mainly Germany, Switzerland and Austria. ASIM was founded in 1981 and has now about 700 individual members, and 30 institutional or industrial members. Furthermore, ASIM counts about 300 affiliated members.

→ [www.asim-gi.org](http://www.asim-gi.org) with members' area

✉ [info@asim-gi.org](mailto:info@asim-gi.org), [admin@asim-gi.org](mailto:admin@asim-gi.org)

✉ ASIM – Inst. f. Analysis and Scientific Computing  
Vienna University of Technology  
Wiedner Hauptstraße 8-10, 1040 Vienna, Austria

### ASIM Officers

<b>President</b>	Felix Breitenecker <a href="mailto:felix.breitenecker@tuwien.ac.at">felix.breitenecker@tuwien.ac.at</a>
<b>Vice presidents</b>	Sigrid Wenzel, <a href="mailto:s.wenzel@uni-kassel.de">s.wenzel@uni-kassel.de</a> T. Pawletta, <a href="mailto:pawel@mb.hs-wismar.de">pawel@mb.hs-wismar.de</a>
<b>Secretary</b>	Anna Mathe, <a href="mailto:anna.mathe@tuwien.ac.at">anna.mathe@tuwien.ac.at</a>
<b>Treasurer</b>	I. Bausch-Gall, <a href="mailto:Ingrid@Bausch-Gall.de">Ingrid@Bausch-Gall.de</a>
<b>Membership Affairs</b>	S. Wenzel, <a href="mailto:s.wenzel@uni-kassel.de">s.wenzel@uni-kassel.de</a> W. Maurer, <a href="mailto:werner.maurer@zhwin.ch">werner.maurer@zhwin.ch</a> Ch. Deatcu, <a href="mailto:christina.deatcu@hs-wismar.de">christina.deatcu@hs-wismar.de</a> F. Breitenecker, <a href="mailto:felix.breitenecker@tuwien.ac.at">felix.breitenecker@tuwien.ac.at</a>
<b>Universities / Research Inst.</b>	S. Wenzel, <a href="mailto:s.wenzel@uni-kassel.de">s.wenzel@uni-kassel.de</a> W. Wiechert, <a href="mailto:W.Wiechert@fz-juelich.de">W.Wiechert@fz-juelich.de</a> J. Haase, <a href="mailto:Joachim.Haase@eas.iis.fraunhofer.de">Joachim.Haase@eas.iis.fraunhofer.de</a> Katharina Nöh, <a href="mailto:k.noeh@fz-juelich.de">k.noeh@fz-juelich.de</a>
<b>Industry</b>	S. Wenzel, <a href="mailto:s.wenzel@uni-kassel.de">s.wenzel@uni-kassel.de</a> K. Panreck, <a href="mailto:Klaus.Panreck@hella.com">Klaus.Panreck@hella.com</a>
<b>Conferences</b>	Klaus Panreck <a href="mailto:Klaus.Panreck@hella.com">Klaus.Panreck@hella.com</a> A. Gnauck, <a href="mailto:albrecht.gnauck@tu-cottbus.de">albrecht.gnauck@tu-cottbus.de</a>
<b>Publications</b>	Th. Pawletta, <a href="mailto:pawel@mb.hs-wismar.de">pawel@mb.hs-wismar.de</a> Christina Deatcu, <a href="mailto:christina.deatcu@hs-wismar.de">christina.deatcu@hs-wismar.de</a> F. Breitenecker, <a href="mailto:felix.breitenecker@tuwien.ac.at">felix.breitenecker@tuwien.ac.at</a>
<b>Repr. EuroSIM</b>	F. Breitenecker, <a href="mailto:felix.breitenecker@tuwien.ac.at">felix.breitenecker@tuwien.ac.at</a> N. Popper, <a href="mailto:niki.popper@drahtwarenhandlung.at">niki.popper@drahtwarenhandlung.at</a>
<b>Education / Teaching</b>	Ch. Deatcu, <a href="mailto:christina.deatcu@hs-wismar.de">christina.deatcu@hs-wismar.de</a> N. Popper, <a href="mailto:niki.popper@drahtwarenhandlung.at">niki.popper@drahtwarenhandlung.at</a> Katharina Nöh, <a href="mailto:k.noeh@fz-juelich.de">k.noeh@fz-juelich.de</a>
<b>International Affairs</b>	H. Szczerbicka, <a href="mailto:hsz@sim.uni-hannover.de">hsz@sim.uni-hannover.de</a> O. Rose, <a href="mailto:Oliver.Rose@tu-dresden.de">Oliver.Rose@tu-dresden.de</a>
<b>Editorial Board SNE</b>	T. Pawletta, <a href="mailto:pawel@mb.hs-wismar.de">pawel@mb.hs-wismar.de</a> Ch. Deatcu, <a href="mailto:christina.deatcu@hs-wismar.de">christina.deatcu@hs-wismar.de</a>
<b>Web EuroSIM</b>	Anna Mathe, <a href="mailto:anna.mathe@tuwien.ac.at">anna.mathe@tuwien.ac.at</a>

Last data update December 2012

ASIM Working Committee. ASIM, part of GI - Gesellschaft für Informatik, is organised in Working Committees, dealing with applications and comprehensive subjects in modelling and simulation:

### ASIM Working Committee

<b>GMMS</b>	Methods in Modelling and Simulation Th. Pawletta, <a href="mailto:pawel@mb.hs-wismar.de">pawel@mb.hs-wismar.de</a>
<b>SUG</b>	Simulation in Environmental Systems Wittmann, <a href="mailto:wittmann@informatik.uni-hamburg.de">wittmann@informatik.uni-hamburg.de</a>
<b>STS</b>	Simulation of Technical Systems H.T.Mammen, <a href="mailto:Heinz-Theo.Mammen@hella.com">Heinz-Theo.Mammen@hella.com</a>
<b>SPL</b>	Simulation in Production and Logistics Sigrid Wenzel, <a href="mailto:s.wenzel@uni-kassel.de">s.wenzel@uni-kassel.de</a>
<b>EDU</b>	Simulation in Education/Education in Simulation N. Popper, <a href="mailto:niki.popper@drahtwarenhandlung.at">niki.popper@drahtwarenhandlung.at</a>

Working Groups for Simulation in Business Administration, in Traffic Systems, for Standardisation, for Validation, etc.

## CROSSIM – Croatian Society for Simulation Modelling

CROSSIM-Croatian Society for Simulation Modelling was founded in 1992 as a non-profit society with the goal to promote knowledge and use of simulation methods and techniques and development of education. CROSSIM is a full member of EUROSIM since 1997.

→ [www.eurosim.info](http://www.eurosim.info)

✉ [vdusak@foi.hr](mailto:vdusak@foi.hr)

✉ CROSSIM / Vesna Dušak  
Faculty of Organization and Informatics Varaždin, University of Zagreb  
Pavlinska 2, HR-42000 Varaždin, Croatia

### CROSSIM Officers

<b>President</b>	Vesna Dušak, <a href="mailto:vdusak@foi.hr">vdusak@foi.hr</a>
<b>Vice president</b>	Jadranka Božikov, <a href="mailto:jbozikov@snz.hr">jbozikov@snz.hr</a>
<b>Secretary</b>	Vesna Bosilj-Vukšić, <a href="mailto:vbosilj@efzg.hr">vbosilj@efzg.hr</a>
<b>Executive board members</b>	Vlatko Čerić, <a href="mailto:vceric@efzg.hr">vceric@efzg.hr</a> Tarzan Legović, <a href="mailto:legovic@irb.hr">legovic@irb.hr</a>
<b>Repr. EuroSIM</b>	Jadranka Božikov, <a href="mailto:jbozikov@snz.hr">jbozikov@snz.hr</a>
<b>Edit. Board SNE</b>	Vesna Dušak, <a href="mailto:vdusak@foi.hr">vdusak@foi.hr</a>
<b>Web EuroSIM</b>	Jadranka Božikov, <a href="mailto:jbozikov@snz.hr">jbozikov@snz.hr</a>

Last data update December 2012



## CSSS – Czech and Slovak Simulation Society

CSSS -The *Czech and Slovak Simulation Society* has about 150 members working in Czech and Slovak national scientific and technical societies (*Czech Society for Applied Cybernetics and Informatics, Slovak Society for Applied Cybernetics and Informatics*). The main objectives of the society are: development of education and training in the field of modelling and simulation, organising professional workshops and conferences, disseminating information about modelling and simulation activities in Europe. Since 1992, CSSS is full member of EUROSIM.

→ [www.fit.vutbr.cz/CSSS](http://www.fit.vutbr.cz/CSSS)

✉ [snorek@fel.cvut.cz](mailto:snorek@fel.cvut.cz)

✉ CSSS / Miroslav Šnorek, CTU Prague  
FEE, Dept. Computer Science and Engineering,  
Karlovo nám. 13, 121 35 Praha 2, Czech Republic

### CSSS Officers

<b>President</b>	Miroslav Šnorek, <a href="mailto:snorek@fel.cvut.cz">snorek@fel.cvut.cz</a>
<b>Vice president</b>	Mikuláš Alexik, <a href="mailto:alexik@frtk.fri.utc.sk">alexik@frtk.fri.utc.sk</a>
<b>Treasurer</b>	Evžen Kindler, <a href="mailto:ekindler@centrum.cz">ekindler@centrum.cz</a>
<b>Scientific Secr.</b>	A. Kavička, <a href="mailto:Antonin.Kavicka@upce.cz">Antonin.Kavicka@upce.cz</a>
<b>Repr. EUROSIM</b>	Miroslav Šnorek, <a href="mailto:snorek@fel.cvut.cz">snorek@fel.cvut.cz</a>
<b>Deputy</b>	Mikuláš Alexik, <a href="mailto:alexik@frtk.fri.utc.sk">alexik@frtk.fri.utc.sk</a>
<b>Edit. Board SNE</b>	Mikuláš Alexik, <a href="mailto:alexik@frtk.fri.utc.sk">alexik@frtk.fri.utc.sk</a>
<b>Web EUROSIM</b>	Petr Peringer, <a href="mailto:peringer@fit.vutbr.cz">peringer@fit.vutbr.cz</a>

*Last data update December 2012*

## FRANCOSIM – Société Francophone de Simulation

FRANCOSIM was founded in 1991 and aims to the promotion of simulation and research, in industry and academic fields. Francosim operates two poles.

- Pole Modelling and simulation of discrete event systems. Pole Contact: *Henri Pierreval*, [pierre-va@imfa.fr](mailto:pierre-va@imfa.fr)
- Pole Modelling and simulation of continuous systems. Pole Contact: *Yskandar Hamam*, [y.hamam@esiee.fr](mailto:y.hamam@esiee.fr)

→ [www.eurosim.info](http://www.eurosim.info)

✉ [y.hamam@esiee.fr](mailto:y.hamam@esiee.fr)

✉ FRANCOSIM / Yskandar Hamam  
Groupe ESIEE, Cité Descartes,  
BP 99, 2 Bd. Blaise Pascal,  
93162 Noisy le Grand CEDEX, France

### FRANCOSIM Officers

<b>President</b>	Karim Djouani, <a href="mailto:djouani@u-pec.fr">djouani@u-pec.fr</a>
<b>Treasurer</b>	François Rocaries, <a href="mailto:f.rocaries@esiee.fr">f.rocaries@esiee.fr</a>
<b>Repr. EUROSIM</b>	Karim Djouani, <a href="mailto:djouani@u-pec.fr">djouani@u-pec.fr</a>
<b>Edit. Board SNE</b>	Karim Djouani, <a href="mailto:djouani@u-pec.fr">djouani@u-pec.fr</a>

*Last data update December 2012*

## DBSS – Dutch Benelux Simulation Society

The Dutch Benelux Simulation Society (DBSS) was founded in July 1986 in order to create an organisation of simulation professionals within the Dutch language area. DBSS has actively promoted creation of similar organisations in other language areas. DBSS is a member of EUROSIM and works in close cooperation with its members and with affiliated societies.

→ [www.eurosim.info](http://www.eurosim.info)

✉ [a.w.heemink@its.tudelft.nl](mailto:a.w.heemink@its.tudelft.nl)

✉ DBSS / A. W. Heemink  
Delft University of Technology, ITS - twi,  
Mekelweg 4, 2628 CD Delft, The Netherlands

### DBSS Officers

<b>President</b>	A. Heemink, <a href="mailto:a.w.heemink@its.tudelft.nl">a.w.heemink@its.tudelft.nl</a>
<b>Vice president</b>	W. Smit, <a href="mailto:smitnet@wxs.nl">smitnet@wxs.nl</a>
<b>Treasurer</b>	W. Smit, <a href="mailto:smitnet@wxs.nl">smitnet@wxs.nl</a>
<b>Secretary</b>	W. Smit, <a href="mailto:smitnet@wxs.nl">smitnet@wxs.nl</a>
<b>Repr. EUROSIM</b>	A. Heemink, <a href="mailto:a.w.heemink@its.tudelft.nl">a.w.heemink@its.tudelft.nl</a>
<b>Deputy</b>	W. Smit, <a href="mailto:smitnet@wxs.nl">smitnet@wxs.nl</a>
<b>Edit. Board SNE</b>	A. Heemink, <a href="mailto:a.w.heemink@its.tudelft.nl">a.w.heemink@its.tudelft.nl</a>

*Last data update April 2006*

## HSS – Hungarian Simulation Society

The Hungarian Member Society of EUROSIM was established in 1981 as an association promoting the exchange of information within the community of people involved in research, development, application and education of simulation in Hungary and also contributing to the enhancement of exchanging information between the Hungarian simulation community and the simulation communities abroad. HSS deals with the organization of lectures, exhibitions, demonstrations, and conferences.

→ [www.eurosim.info](http://www.eurosim.info)

✉ [javor@eik.bme.hu](mailto:javor@eik.bme.hu)

✉ HSS / András Jávör,  
Budapest Univ. of Technology and Economics,  
Sztoczek u. 4, 1111 Budapest, Hungary

**HSS Officers**

<b>President</b>	András Jávör, <a href="mailto:javor@eik.bme.hu">javor@eik.bme.hu</a>
<b>Vice president</b>	Gábor Szűcs, <a href="mailto:szucs@itm.bme.hu">szucs@itm.bme.hu</a>
<b>Secretary</b>	Ágnes Vigh, <a href="mailto:vigh@itm.bme.hu">vigh@itm.bme.hu</a>
<b>Repr. EUROSIM</b>	András Jávör, <a href="mailto:javor@eik.bme.hu">javor@eik.bme.hu</a>
<b>Deputy</b>	Gábor Szűcs, <a href="mailto:szucs@itm.bme.hu">szucs@itm.bme.hu</a>
<b>Edit. Board SNE</b>	András Jávör, <a href="mailto:javor@eik.bme.hu">javor@eik.bme.hu</a>
<b>Web EUROSIM</b>	Gábor Szűcs, <a href="mailto:szucs@itm.bme.hu">szucs@itm.bme.hu</a>

Last data update March 2008

**PSCS – Polish Society for Computer Simulation**

PSCS was founded in 1993 in Warsaw. PSCS is a scientific, non-profit association of members from universities, research institutes and industry in Poland with common interests in variety of methods of computer simulations and its applications. At present PSCS counts 257 members.

→ [www.ptsk.man.bialystok.pl](http://www.ptsk.man.bialystok.pl)✉ [leon@ibib.waw.pl](mailto:leon@ibib.waw.pl)✉ PSCS / Leon Bobrowski, c/o IBIB PAN,  
ul. Trojdena 4 (p.416), 02-109 Warszawa, Poland**PSCS Officers**

<b>President</b>	Leon Bobrowski, <a href="mailto:leon@ibib.waw.pl">leon@ibib.waw.pl</a>
<b>Vice president</b>	Andrzej Grzyb, Tadeusz Nowicki
<b>Treasurer</b>	Z. Sosnowski, <a href="mailto:zenon@ii.pb.bialystok.pl">zenon@ii.pb.bialystok.pl</a>
<b>Secretary</b>	Zdzisław Galkowski, <a href="mailto:Zdzislaw.Galkowski@simr.pw.edu.pl">Zdzislaw.Galkowski@simr.pw.edu.pl</a>
<b>Repr. EUROSIM</b>	Leon Bobrowski, <a href="mailto:leon@ibib.waw.pl">leon@ibib.waw.pl</a>
<b>Deputy</b>	Tadeusz Nowicki, <a href="mailto:tadeusz.nowicki@wat.edu.pl">tadeusz.nowicki@wat.edu.pl</a>
<b>Edit. Board SNE</b>	Zenon Sosnowski, <a href="mailto:z.sosnowski@pb.edu.pl">z.sosnowski@pb.edu.pl</a>
<b>Web EUROSIM</b>	Magdalena Topczewska <a href="mailto:m.topczewska@pb.edu.pl">m.topczewska@pb.edu.pl</a>

Last data update December 2012

**ISCS – Italian Society for Computer Simulation**

The Italian Society for Computer Simulation (ISCS) is a scientific non-profit association of members from industry, university, education and several public and research institutions with common interest in all fields of computer simulation.

→ [www.eurosim.info](http://www.eurosim.info)✉ [Mario.savastano@uniina.it](mailto:Mario.savastano@uniina.it)✉ ISCS / Mario Savastano,  
c/o CNR - IRSIP,  
Via Claudio 21, 80125 Napoli, Italy**ISCS Officers**

<b>President</b>	M. Savastano, <a href="mailto:mario.savastano@uniina.it">mario.savastano@uniina.it</a>
<b>Vice president</b>	F. Maceri, <a href="mailto:Franco.Maceri@uniroma2.it">Franco.Maceri@uniroma2.it</a>
<b>Repr. EUROSIM</b>	F. Maceri, <a href="mailto:Franco.Maceri@uniroma2.it">Franco.Maceri@uniroma2.it</a>
<b>Secretary</b>	Paola Provenzano, <a href="mailto:paola.provenzano@uniroma2.it">paola.provenzano@uniroma2.it</a>
<b>Edit. Board SNE</b>	M. Savastano, <a href="mailto:mario.savastano@uniina.it">mario.savastano@uniina.it</a>

Last data update December 2012

**SIMS – Scandinavian Simulation Society**

SIMS is the *Scandinavian Simulation Society* with members from the four Nordic countries Denmark, Finland, Norway and Sweden. The SIMS history goes back to 1959. SIMS practical matters are taken care of by the SIMS board consisting of two representatives from each Nordic country (Iceland one board member).

SIMS Structure. SIMS is organised as federation of regional societies. There are FinSim (Finnish Simulation Forum), DKSIM (Dansk Simuleringsforening) and NFA (Norsk Forening for Automatisering).

→ [www.scansims.org](http://www.scansims.org)✉ [esko.juuso@oulu.fi](mailto:esko.juuso@oulu.fi)

✉ SIMS / Esko Juuso, Department of Process and Environmental Engineering, 90014 Univ.Oulu, Finland

**SIMS Officers**

<b>President</b>	Esko Juuso, <a href="mailto:esko.juuso@oulu.fi">esko.juuso@oulu.fi</a>
<b>Vice president</b>	Erik Dahlquist, <a href="mailto:erik.dahlquist@mdh.se">erik.dahlquist@mdh.se</a>
<b>Treasurer</b>	Vadim Engelson, <a href="mailto:vadim.engelson@mathcore.com">vadim.engelson@mathcore.com</a>
<b>Repr. EUROSIM</b>	Esko Juuso, <a href="mailto:esko.juuso@oulu.fi">esko.juuso@oulu.fi</a>
<b>Edit. Board SNE</b>	Esko Juuso, <a href="mailto:esko.juuso@oulu.fi">esko.juuso@oulu.fi</a>
<b>Web EUROSIM</b>	Vadim Engelson

Last data update December 2012

**SLOSIM – Slovenian Society for Simulation and Modelling**

SLOSIM - Slovenian Society for Simulation and Modelling was established in 1994 and became the full member of EUROSIM in 1996. Currently it has 69



members from both slovenian universities, institutes, and industry. It promotes modelling and simulation approaches to problem solving in industrial as well as in academic environments by establishing communication and cooperation among corresponding teams.

→ [www.slosim.si](http://www.slosim.si)✉ [slosim@fe.uni-lj.si](mailto:slosim@fe.uni-lj.si)✉ SLOSIM / Rihard Karba, Faculty of Electrical Engineering, University of Ljubljana,  
Tržaška 25, 1000 Ljubljana, Slovenia



SLOSIM Officers	
<b>President</b>	B. Zupančič, <a href="mailto:borut.zupancic@fe.uni-lj.si">borut.zupancic@fe.uni-lj.si</a>
<b>Vice president</b>	Leon Žlajpah, <a href="mailto:leon.zlajpah@ijs.si">leon.zlajpah@ijs.si</a>
<b>Secretary</b>	Vito Logar, <a href="mailto:vito.logar@fe.uni-lj.si">vito.logar@fe.uni-lj.si</a>
<b>Treasurer</b>	Milan Simčič, <a href="mailto:milan.simcic@fe.uni-lj.si">milan.simcic@fe.uni-lj.si</a>
<b>Repr. EUROSIM</b>	B. Zupančič, <a href="mailto:borut.zupancic@fe.uni-lj.si">borut.zupancic@fe.uni-lj.si</a>
<b>Deputy</b>	Rihard Karba, <a href="mailto:rihard.karba@fe.uni-lj.si">rihard.karba@fe.uni-lj.si</a>
<b>Edit. Board SNE</b>	Rihard Karba, <a href="mailto:rihard.karba@fe.uni-lj.si">rihard.karba@fe.uni-lj.si</a>
<b>Web EUROSIM</b>	Vito Logar, <a href="mailto:vito.logar@fe.uni-lj.si">vito.logar@fe.uni-lj.si</a>

*Last data update December 2012*

## UKSIM - United Kingdom Simulation Society

UKSIM has more than 100 members throughout the UK from universities and industry. It is active in all areas of simulation and it holds a biennial conference as well as regular meetings and workshops.

→ [www.uksim.org.uk](http://www.uksim.org.uk)

✉ [david.al-dabass@ntu.ac.uk](mailto:david.al-dabass@ntu.ac.uk)

- ✉ UKSIM / Prof. David Al-Dabass  
Computing & Informatics,  
Nottingham Trent University  
Clifton lane, Nottingham, NG11 8NS  
United Kingdom

UKSIM Officers	
<b>President</b>	David Al-Dabass, <a href="mailto:david.al-dabass@ntu.ac.uk">david.al-dabass@ntu.ac.uk</a>
<b>Vice president</b>	A. Orsoni, <a href="mailto:A.Orsoni@kingston.ac.uk">A.Orsoni@kingston.ac.uk</a>
<b>Secretary</b>	Richard Cant, <a href="mailto:richard.cant@ntu.ac.uk">richard.cant@ntu.ac.uk</a>
<b>Treasurer</b>	A. Orsoni, <a href="mailto:A.Orsoni@kingston.ac.uk">A.Orsoni@kingston.ac.uk</a>
<b>Membership chair</b>	K. Al-Begain, <a href="mailto:kbegain@glam.ac.uk">kbegain@glam.ac.uk</a>
<b>Univ. liaison chair</b>	R. Cheng, <a href="mailto:rchc@maths.soton.ac.uk">rchc@maths.soton.ac.uk</a>
<b>Repr. EUROSIM</b>	Richard Zobel, <a href="mailto:r.zobel@ntlworld.com">r.zobel@ntlworld.com</a>
<b>Deputy</b>	K. Al-Begain, <a href="mailto:kbegain@glam.ac.uk">kbegain@glam.ac.uk</a>
<b>Edit. Board SNE</b>	Richard Zobel, <a href="mailto:r.zobel@ntlworld.com">r.zobel@ntlworld.com</a>

*Last data update December 2012*

## CEA-SMSG – Spanish Modelling and Simulation Group

CEA is the Spanish Society on Automation and Control. In order to improve the efficiency and to deep into the different fields of automation, the association is divided into thematic groups, one of them is named 'Modelling and Simulation', constituting the group.

→ [www.cea-ifac.es/wwwgrupos/simulacion](http://www.cea-ifac.es/wwwgrupos/simulacion)

→ [simulacion@cea-ifac.es](mailto:simulacion@cea-ifac.es)

- ✉ CEA-SMSG / María Jesús de la Fuente,  
System Engineering and Automatic Control department,  
University of Valladolid,  
Real de Burgos s/n., 47011 Valladolid, SPAIN

CAE - SMSG Officers	
<b>President</b>	M. À. Piera Eroles, <a href="mailto:MiquelAngel.Piera@uab.es">MiquelAngel.Piera@uab.es</a>
<b>Vice president</b>	Emilio Jimenez, <a href="mailto:emilio.jimenez@unirioja.es">emilio.jimenez@unirioja.es</a>
<b>Repr. EUROSIM</b>	Emilio Jimenez, <a href="mailto:emilio.jimenez@unirioja.es">emilio.jimenez@unirioja.es</a>
<b>Edit. Board SNE</b>	Emilio Jimenez, <a href="mailto:emilio.jimenez@unirioja.es">emilio.jimenez@unirioja.es</a>
<b>Web EUROSIM</b>	Mercedes Peres, <a href="mailto:mercedes.perez@unirioja.es">mercedes.perez@unirioja.es</a>

*Last data update December 2012*

## LSS – Latvian Simulation Society

The Latvian Simulation Society (LSS) has been founded in 1990 as the first professional simulation organisation in the field of Modelling and simulation in the post-Soviet area. Its members represent the main simulation centres in Latvia, including both academic and industrial sectors.

→ [briedis.itl.rtu.lv/imb/](http://briedis.itl.rtu.lv/imb/)

✉ [merkur@itl.rtu.lv](mailto:merkur@itl.rtu.lv)

- ✉ LSS / Yuri Merkuryev, Dept. of Modelling and Simulation Riga Technical University  
Kalku street 1, Riga, LV-1658, LATVIA

LSS Officers	
<b>President</b>	Yuri Merkuryev, <a href="mailto:merkur@itl.rtu.lv">merkur@itl.rtu.lv</a>
<b>Secretary</b>	Artis Teilans, <a href="mailto:Artis.Teilans@exigenservices.com">Artis.Teilans@exigenservices.com</a>
<b>Repr. EUROSIM</b>	Yuri Merkuryev, <a href="mailto:merkur@itl.rtu.lv">merkur@itl.rtu.lv</a>
<b>Deputy</b>	Artis Teilans, <a href="mailto:Artis.Teilans@exigenservices.com">Artis.Teilans@exigenservices.com</a>
<b>Edit. Board SNE</b>	Yuri Merkuryev, <a href="mailto:merkur@itl.rtu.lv">merkur@itl.rtu.lv</a>
<b>Web EUROSIM</b>	Oksana Sosho, <a href="mailto:oksana@itl.rtu.lv">oksana@itl.rtu.lv</a>

*Last data update December 2012*

## ROMSIM – Romanian Modelling and Simulation Society

ROMSIM has been founded in 1990 as a non-profit society, devoted to theoretical and applied aspects of modelling and simulation of systems. ROMSIM currently has about 100 members from Romania and Moldavia.

→ [www.ici.ro/romsim/](http://www.ici.ro/romsim/)

✉ [sflorin@ici.ro](mailto:sflorin@ici.ro)

- ✉ ROMSIM / Florin Stanculescu,  
National Institute for Research in Informatics, Avereșcu  
Av. 8 – 10, 71316 Bucharest, Romania

ROMSIM Officers	
<b>President</b>	Florin Stanculescu, <a href="mailto:sflorin@ici.ro">sflorin@ici.ro</a>
<b>Vice president</b>	Florin Hartescu, <a href="mailto:flory@ici.ro">flory@ici.ro</a> Marius Radulescu, <a href="mailto:mradulescu@ici.ro">mradulescu@ici.ro</a>
<b>Repr. EUROSIM</b>	Florin Stanculescu, <a href="mailto:sflorin@ici.ro">sflorin@ici.ro</a>
<b>Deputy</b>	Marius Radulescu, <a href="mailto:mradulescu@ici.ro">mradulescu@ici.ro</a>
<b>Edit. Board SNE</b>	Florin Stanculescu, <a href="mailto:sflorin@ici.ro">sflorin@ici.ro</a>
<b>Web EUROSIM</b>	Zoe Radulescu, <a href="mailto:radulescu@ici.ro">radulescu@ici.ro</a>

*Last data update December 2012*



## RNSS – Russian Simulation Society

NSS - The Russian National Simulation Society (Национальное Общество Имитационного Моделирования – НОИМ) was officially registered in Russian Federation on February 11, 2011. In February 2012 NSS has been accepted as an observer member of EUROSIM.

→ [www.simulation.su](http://www.simulation.su)

✉ [yusupov@ias.spb.su](mailto:yusupov@ias.spb.su)

✉ RNSS / R. M. Yusupov,  
St. Petersburg Institute of Informatics and Automation  
RAS, 199178, St. Petersburg, 14th lin. V.O, 39

### RNSS Officers

President	R. M. Yusupov, <a href="mailto:yusupov@ias.spb.su">yusupov@ias.spb.su</a>
Chair Man. Board	A. Plotnikov, <a href="mailto:plotnikov@sstc.spb.ru">plotnikov@sstc.spb.ru</a>
Secretary	M. Dolmatov, <a href="mailto:dolmatov@simulation.su">dolmatov@simulation.su</a>
Repr. EUROSIM	R. M. Yusupov, <a href="mailto:yusupov@ias.spb.su">yusupov@ias.spb.su</a>
Deputy	B. Sokolov, <a href="mailto:sokol@ias.spb.su">sokol@ias.spb.su</a>
Edit. Board SNE	Y. Senichenkov, <a href="mailto:sneyb@dcn.infos.ru">sneyb@dcn.infos.ru</a>

*Last data update February 2012*

## LIOPHANT Simulation

Liophant Simulation is a non-profit association born in order to be a trait-d'union among simulation developers and users; Liophant is devoted to promote and diffuse the simulation techniques and methodologies; the Association promotes exchange of students, sabbatical years, organization of International Conferences, organization of courses and stages in companies to apply the simulation to real problems.

→ [www.liophant.org](http://www.liophant.org)

✉ [info@liophant.org](mailto:info@liophant.org)

✉ LIOPHANT Simulation, c/o Agostino G. Bruzzone,  
DIME, University of Genoa, Polo Savonese,  
via Molinero 1, 17100 Savona (SV), Italy



### LIOPHANT Officers

President	A.G. Bruzzone, <a href="mailto:agostino@itim.unige.it">agostino@itim.unige.it</a>
Director	E. Bocca, <a href="mailto:enrico.bocca@liophant.org">enrico.bocca@liophant.org</a>
Secretary	A. Devoti, <a href="mailto:devoti.a@iveco.com">devoti.a@iveco.com</a>
Treasurer	Marina Masseimassei@itim.unige.it
Repr. EUROSIM	A.G. Bruzzone, <a href="mailto:agostino@itim.unige.it">agostino@itim.unige.it</a>
Deputy	F. Longo, <a href="mailto:f.longo@unical.it">f.longo@unical.it</a>
Edit. Board SNE	F. Longo, <a href="mailto:f.longo@unical.it">f.longo@unical.it</a>
Web EUROSIM	F. Longo, <a href="mailto:f.longo@unical.it">f.longo@unical.it</a>

*Last data update December 2012*

## SNE – Simulation Notes Europe

Simulation Notes Europe publishes peer reviewed *Technical Notes*, *Short Notes* and *Overview Notes* on developments and trends in modelling and simulation in various areas and in application and theory. Furthermore SNE documents the ARGESIM Benchmarks on *Modelling Approaches and Simulation Implementations* with publication of definitions, solutions and discussions (*Benchmark Notes*). Special *Educational Notes* present the use of modelling and simulation in and for education and for e-learning.

SNE is the official membership journal of EUROSIM, the Federation of European Simulation Societies. A *News Section* in SNE provides information for EUROSIM Simulation Societies and Simulation Groups. SNE also offers possibilities for post-conference publication of contributions to conferences of the EUROSIM member societies.

SNE is published in a printed version (Print ISSN 2305-9974) and in an online version (Online ISSN 2306-0271). With Online SNE the publisher ARGESIM follows the Open Access strategy, allowing download of published contributions for free. Since 2011 Online SNE contributions are identified by an DOI (Digital Object Identifier) assigned to the publisher ARGESIM (DOI prefix 10.11128). Print SNE, high-resolution Online SNE, source codes of the *Benchmarks* and other additional sources are available for subscription via membership in a EUROSIM society.

**Authors Information.** Authors are invited to submit contributions which have not been published and have not being considered for publication elsewhere to the SNE Editorial Office. SNE distinguishes different types of contributions (*Notes*):

- *Overview Note* – State-of-the-Art report in a specific area, up to 14 pages, only upon invitation
- *Technical Note* – scientific publication on specific topic in modelling and simulation, 6 – 8 (10) pages
- *Education Note* – modelling and simulation in / for education and e-learning; max. 6 pages
- *Short Note* – recent developments, max. 4 pages
- *Software Note* – development in simulators, max 4 pages
- *Benchmark Note* – Solution to an ARGESIM Benchmark; basic solution 2 pages, extended and commented solution 4 pages, comparative solutions on invitation

Interested authors may find further information at SNE's website → [www.sne-journal.org](http://www.sne-journal.org) layout templates for *Notes*, requirements for benchmark solutions, etc.).



# EUROSIM 2013

## 8<sup>th</sup> EUROSIM Congress on Modelling and Simulation

The City Hall, Cardiff, Wales, United Kingdom 10-13 September 2013

[www.eurosim2013.info](http://www.eurosim2013.info)



# EUROSIM 2013

## 8<sup>th</sup> EUROSIM Congress on Modelling and Simulation

The City Hall, Cardiff, Wales, United Kingdom 10-13 September 2013

[www.eurosim2013.info](http://www.eurosim2013.info)



# EUROSIM 2013

## 8<sup>th</sup> EUROSIM Congress on Modelling and Simulation

The City Hall, Cardiff, Wales, United Kingdom 10-13 September 2013

[www.eurosim2013.info](http://www.eurosim2013.info)



# EUROSIM 2016

9<sup>th</sup> EUROSIM Congress on Modelling and Simulation

City of Oulu, Finland, September 12 – 16, 2016



EUROSIM Congresses are the most important modelling and simulation events in Europe. For EUROSIM 2016, we are soliciting original submissions describing novel research and developments in the following (and related) areas of interest: Continuous, discrete (event) and hybrid modelling, simulation, identification and optimization approaches. Two basic contribution motivations are expected: M&S Methods and Technologies and M&S Applications. Contributions from both technical and non-technical areas are welcome.

**Congress Topics** The EUROSIM 2016 Congress will include invited talks, parallel, special and poster sessions, exhibition and versatile technical and social tours. The Congress topics of interest include, but are not limited to:

Intelligent Systems and Applications  
Hybrid and Soft Computing  
Data & Semantic Mining  
Neural Networks, Fuzzy Systems & Evolutionary Computation  
Image, Speech & Signal Processing  
Systems Intelligence and Intelligence Systems  
Autonomous Systems  
Energy and Power Systems  
Mining and Metal Industry  
Forest Industry  
Buildings and Construction  
Communication Systems  
Circuits, Sensors and Devices  
Security Modelling and Simulation

Bioinformatics, Medicine, Pharmacy and Bioengineering  
Water and Wastewater Treatment, Sludge Management and Biogas Production  
Condition monitoring, Mechatronics and maintenance  
Automotive applications  
e-Science and e-Systems  
Industry, Business, Management, Human Factors and Social Issues  
Virtual Reality, Visualization, Computer Art and Games  
Internet Modelling, Semantic Web and Ontologies  
Computational Finance & Economics

Simulation Methodologies and Tools  
Parallel and Distributed Architectures and Systems  
Operations Research  
Discrete Event Systems  
Manufacturing and Workflows  
Adaptive Dynamic Programming and Reinforcement Learning  
Mobile/Ad hoc wireless networks, mobicast, sensor placement, target tracking  
Control of Intelligent Systems  
Robotics, Cybernetics, Control Engineering, & Manufacturing  
Transport, Logistics, Harbour, Shipping and Marine Simulation

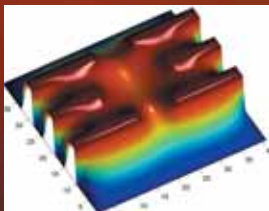
**Congress Venue / Social Events** The Congress will be held in the City of Oulu, Capital of Northern Scandinavia. The main venue and the exhibition site is the Oulu City Theatre in the city centre. Pre and Post Congress Tours include Arctic Circle, Santa Claus visits and hiking on the unique routes in Oulanka National Park.

**Congress Team:** The Congress is organised by SIMS - Scandinavian Simulation Society, FinSim - Finnish Simulation Forum, Finnish Society of Automation, and University of Oulu. Esko Juuso EUROSIM President, Erik Dahlquist SIMS President, Kauko Leiviskä EUROSIM 2016 Chair

**Info:** [eurosims2016.automaatioseura.fi](http://eurosims2016.automaatioseura.fi), [office@automaatioseura.fi](mailto:office@automaatioseura.fi)

# Parlez-vous MATLAB?

Über eine Million Menschen weltweit sprechen MATLAB. Ingenieure und Wissenschaftler in allen Bereichen – von der Luft- und Raumfahrt über die Halbleiterindustrie bis zur Biotechnologie, Finanzdienstleistungen und Geo- und Meereswissenschaften – nutzen MATLAB, um ihre Ideen auszudrücken. Sprechen Sie MATLAB?



*Modellierung eines elektrischen Potentials in einem Quantum Dot.*

*Dieses Beispiel finden Sie unter:  
[www.mathworks.de/lc](http://www.mathworks.de/lc)*

**MATLAB**<sup>®</sup>  
The language of technical computing

